COO-3060-3
MITNE-129

INSTRUMENTAL METHODS FOR NEUTRON SPECTROSCOPY IN THE MIT BLANKET TEST FACILITY

by

N.R. Ortiz, I.C. Rickard, M.J. Driscoll
and N.C. Rasmussen

May, 1972

Massachusetts Institute of Technology
Department of Nuclear Engineering
Cambridge, Massachusetts 02139
AEC Research and Development Report
UC-34 Physics

Contract AT(11-1)-3060
U.S. Atomic Energy Commission

MASSACHUSETTS INSTITUTE OF TECHNOLOGY
DEPARTMENT OF NUCLEAR ENGINEERING

Cambridge, Massachusetts

INSTRUMENTAL METHODS FOR NEUTRON SPECTROSCOPY IN THE MIT BLANKET TEST FACILITY

by

N.R. Ortiz, I.C. Rickard, M.J. Driscoll and N.C. Rasmussen

May, 1972

COO-3060-3

MITNE-129

AEC Research and Development Report

UC-34 Physics

Contract AT(11-1)-3060

U.S. Atomic Energy Commission

DISTRIBUTION LIST

Contract AT(11-1)-3060

U.S. Atomic Energy Commission, Headquarters
Division of Reactor Development and Technology
Reactor Physics Branch (3 copies)

U.S. Atomic Energy Commission (2 copies)
Cambridge Office

Dr. Paul Greebler, Manager
Nuclear Energy Division
Breeder Reactor Department
General Electric Company
310 DeGuigne Drive
Sunnyvale, California 94086 (1 copy)

Dr. Harry Morewitz, Manager
LMFBR Physics and Safety Projects
Atomics International
P.O. Box 309
Canoga Park, California 91305 (1 copy)

Mr. Malcolm Dyos, Manager
Nuclear Development, LMFBR Project
Westighouse Electric Corporation
Advanced Reactors Division
Waltz Mill Site
P.O. Box 158
Madison, Pennsylvania 15663 (1 copy)

Dr. Robert Avery, Director
Reactor Physics Division
Argonne National Laboratory
9700 South Cass Avenue
Argonne, Illinois 60539 (1 copy)

Dr. Charles A. Preskitt, Jr.
Mgr., Atomic and Nuclear Department
Gulf Radiation Technology
P.O. Box 608
San Diego, California 02112 (1 copy)

ABSTRACT

The energy spectrum of the neutron flux in a realistic mockup of the blanket region of a large liquid-metal-cooled fast breeder reactor was measured using three different spectrometers: He-3 and Li-6 semiconductor detectors and a Proton-Recoil proportional counter. The He-3 detector was operated in the sum and difference modes, and the Li-6 detector in the sum, difference and triton modes. The experimental data was unfolded using direct, integral and derivative techniques.

Methods were developed or perfected to enable use of the He-3 detector over the neutron energy range from 10 keV to 1.3 MeV and the Li-6 detector from 10 keV to 3.1 MeV; the Proton-Recoil detector was operated in the region from 2 keV to 1.5 MeV. In general, good agreement was found between the experimental measurements for all detector types, modes of operation and methods of unfolding, except for the low-energy He-3 data.

The present experimental results and previously reported data obtained using a method based on gamma line-broadening are in relatively good agreement in the high energy region above 0.8 MeV. The measured neutron spectrum is also similar in shape to neutron spectra measured at ANL in critical assembly mockups of large LMFBR cores, but systematically softer, as expected. However, there is a large discrepancy in the energy region from 10 keV to 50 keV between the present results and either spectra unfolded from foil data or those numerically calculated using the 1-D ANISN code in the S_8 option with 26 energy groups.

ACKNOWLEDGMENTS

The success of the MIT Fast Reactor Blanket Research Project is due to the support of the U.S. Atomic Energy Commission and to the contribution of a number of individuals. The work described in this report has been performed primarily by the principal author, N.R. Ortiz who has submitted substantially the same report in partial fulfillment of the requirements for the Sc.D. degree at MIT.

TABLE OF CONTENTS

Page

LIST OF FIGURE

Page

LIST OF TABLES

Chapter 1

INTRODUCTION

1.1 BACKGROUND

The United States Atomic Energy Commission has given high priority to the development of the liquid metal cooled fast breeder reactor (LMFBR) because of the almost universal consensus that this system is best suited to insure a reliable and economical source of electrical power for the foreseeable future. The economic attractiveness of the LMFBR stems from its ability to breed more fissible fuel than it consumes. Since the blanket region of the LMFBR core accounts for a large fraction of the breeding, M.I.T. has undertaken under AEC contract a detailed program of blanket physics analysis, of which the present research is a part.

The central objective of reactor physics analysis is an accurate description of neutron interaction rates, which can be represented as the product of a target material property, the cross section, and a projectile flux-the neutron flux. Both of these properties are energy dependent. It is the second of these two factors, the energy spectrum of the neutron flux, which is the subject of the present research. More specifically, the objective of the work reported here has been the application and evaluation of instrumental methods for neutron spectroscopy to the determination of an accurate ambient spectrum in Blanket Test Facility Mockup No. 2, a simulation of the blanket region of a large LMFBR designed for

central station power generation.

The energy range of interest is from a few keV to several MeV. Over this energy range instrumental methods can compete favorably with non-instrumental methods such as nuclear emulsions and foil activation. Nuclear emulsions (N1,D2) are generally used to detect high energy neutrons (0.5 to 20 MeV) but the process of analyzing the necessary number of tracks is time consuming. Also it is difficult to find high energy events among low energy background. Foil activation has been used extensively (D3,H3,P2) to study reaction rates and to obtain integral measurements of fast neutron spectra. The applications of this technique to the physics analysis of Blanket Mockup No. 2 is covered in reference (L1). A review of instrumental methods is presented in the next section.

1.2 REVIEW OF INSTRUMENTAL METHODS

Some of the existing techniques used to measure fast neutron spectra, their characteristics and limitations are discussed in the following paragraphs as a prelude to focusing upon those systems best suited to the present task. A survey of instrumental methods is found in references (R4,P1,F2,D1).

a) Time-of-Flight Method

This is one of the most direct methods for neutron spectroscopy. The neutron energy is related to the time-of-flight and the flight distance by the following relation (R4):

$$E\ (\text{MeV}) = \frac{72.3\ L\ (\text{m})}{t\ (\text{ns})}^{2} \qquad (1.1)$$

The time-of-flight is measured by recording the time at which neutrons leave the initial point and the time at which they arrive at the terminal point of the flight path. The latter can be determined by a neutron counter at the end of the path. The starting time is determined by one of the following methods: (1) detection of gamma radiation emitted at the same time as the neutron (2) detection of scattered source neutrons in a counter placed close to the origin of the flight path, (3) use of a pulsed neutron source.

The characteristics of a typical time-of-flight system are (F2):

Resolution	Efficiency	Useful Energy Range
1% at 10 keV		0.01 MeV
3.5% at 0.5 MeV	2×10^{-5}	to
14% at 140 MeV	2×10^{-7}	140 MeV

A typical setup uses a time-to-pulse-height converter combined with a multichannel pulse-height analyzer to record the events. The flight path usually varies from 0.2 to 26 meters.

b) Scintillation Detectors

Some of the reactions used for fast neutron scintillation include (n,p), (n,α) and (n,f) processes (P1). The proton-recoil process has also been used extensively (D1,T2). The lithium iodide crystal is an example of a detector whose operation is based on the (n,α) process.

Scintillation media may be gaseous, liquid or solid. Solid and liquid media are the most commonly used for neutron spectroscopy.

The solid scintillator is usually placed on top of a photomultiplier tube which observes scintillations from the crystal. In a well designed system the photomultiplier output is directly proportional to the luminous output of the crystal. However, the luminous output of the crystal is not directly proportional to the energy deposited by the charged particle in the crystal. Therefore, to unfold the pulse-height spectrum (the amplitude of pulses at the output of the photomultiplier) it is necessary to take into account the nonlinear response of the scintillator (B11).

The principal advantage of scintillation detectors is their high efficiency for neutron detection. Some of their characteristics (P1) are as follows:

Resolution	Efficiency	Useful Energy Range
22% at 2 MeV	10% at 2 MeV	
12.5% at 4 MeV	(2 cm long stilbene crystal)	0.1 MeV to 10 MeV
7% at 8 MeV		

Their shortcomings are high sensitivity to gamma radiation and limited resolution. Pulse shape discrimination techniques have been used to discriminate against gamma background (F3). Winyard, Lutkin and McBeth have described a versatile pulse shape discrimination system which is compatible with most scintillation counters (W2).

c) Proportional Counters

The most widely used proportional counter for detection of fast neutrons is based on neutron-proton scattering. In an elastic scattering event, neutrons give at least part of their energy to the struck proton, and the ionization that the latter produces can be measured. The (n,p) scattering has the advantage that the cross section is relatively large and its energy dependence well known. Bennett (B2,B3) has developed a proton-recoil system with the following characteristics:

Resolution	Efficiency	Useful Energy Range
60% at 1 keV	10^{-2} at	1 keV to 2 MeV
10% at 1 MeV	500 keV	

The system uses pulse shape discrimination to reject gamma radiation. This technique is based upon the larger specific ionization (ion pairs per cm of track) of a recoiling proton compared to a fast electron of the same total ionization.

d) Lithium-6 Semiconductor Detector

This detector consists of a lithium-6 foil placed between two silicon semiconductor crystals in a sandwich configuration. Detection is based on the reaction:

$$ {}_0n^1 + {}_3Li^6 \longrightarrow {}_1H^3 + {}_2He^4 + Q \qquad (1.2) $$

In this reaction the neutron and the nucleus interact to form two product particles. An energy Q is released; this

energy plus the energy of the incident neutron appears as kinetic energy of the product particles.

$$E_n + Q \longrightarrow E_T + E_\alpha \qquad (1.3)$$

The neutron energy is therefore obtained with no ambiguity from a measurement of the total energy released. The unfolding of the measured spectrum is straightforward and simple.

The rejection of gamma radiation is improved by counting only those pulses that occur in coincidence in both detectors. The background from the interaction of neutrons with the silicon is measured using another detector without the lithium-6 foil. This spectrum is then subtracted from the spectrum measured with the lithium-6 foil in place (J1). Pertinent properties are:

Resolution	Efficiency	Useful Energy Range
300 keV at thermal	10^{-2} for thermal	0.4 MeV to 8 MeV
470 keV at 3 MeV	10^{-6} for 5 MeV	

The main disadvantage of the detector is that the high Q value (4.78 MeV) makes it difficult to measure low energy neutrons. In Chapter 3 two different techniques to improve this low energy limitation are discussed.

e) Helium-3 Semiconductor Detector

This system consists of two silicon semiconductor detectors in a sandwich configuration; the space between the two detectors is filled with He-3 gas. The operation of the He-3

detector is very similar to that of the Li-6 detector.

The Q value for the reaction is 764 keV and the characteristics of the system are (J1):

Resolution	Efficiency	Useful Energy Range
100 keV at thermal	10^{-2} for thermal	0.2 MeV to 4 MeV
130 keV at 3 MeV (at 5 atm operating pressure)	10^{-6} for 5 MeV	

The advantages of the Helium-3 spectrometer are: (1) the He-3 (n,p) reaction cross section starts with a large value for thermal neutrons and varies smoothly with energy, having no known resonances, unlike Li-6; (2) as for Li-6 there are no excited daughter products, therefore the reaction products, the triton and proton, contain the total energy of the reaction.

The main disadvantage of the spectrometer is that the high Q value makes the measurement of neutron energies below 100 keV difficult.

Measurement of the neutron spectrum from a few keV to several MeV is a challenging problem. Despite the usefulness of the neutron-detection methods mentioned above, improvements and new methods are necessary.

1.3 INSTRUMENTS AND TECHNIQUES USED IN THIS WORK

Three of the instrumental methods discussed in the previous section were selected to measure the neutron spectrum in the M.I.T. Blanket Test Facility. These are the Li-6

semiconductor detector, the He-3 semiconductor detector and the proton-recoil proportional counter.

The Li-6 semiconductor detector was used in three different modes of operation, denoted as the Sum, Difference and Triton Methods. The last two methods were used in an attempt to improve the useful energy range and the resolution of the spectrometer.

The He-3 solid state detector was used in the Sum and Difference Modes. The latter mode improves the resolution, useful energy range and gamma discrimination of the detector.

The proton-recoil proportional counter selected was similar to that developed by Bennett (B2,B3), and extensively applied to fast critical experiments at ANL.

Detailed descriptions of the detectors and techniques are given in the following chapters.

1.4 DESCRIPTION OF THE BLANKET TEST FACILITY AND TEST ASSEMBLY

A detailed description of the experimental facility is given in references (F1) and (L2). Only a brief description will be presented here. The Blanket Test Facility (BTF) is at the rear of the graphite-lined cavity comprising the MITR hohlraum; Figure 1.1 shows the cross section of the facility. The key component in the BFT is a converter lattice made up of graphite and slightly enriched uranium fuel rods, which converts the incident hohlraum thermal spectrum into a spectrum of fast neutrons typical of that leaking from a large LMFBR core. The total power of the converter lattice is about

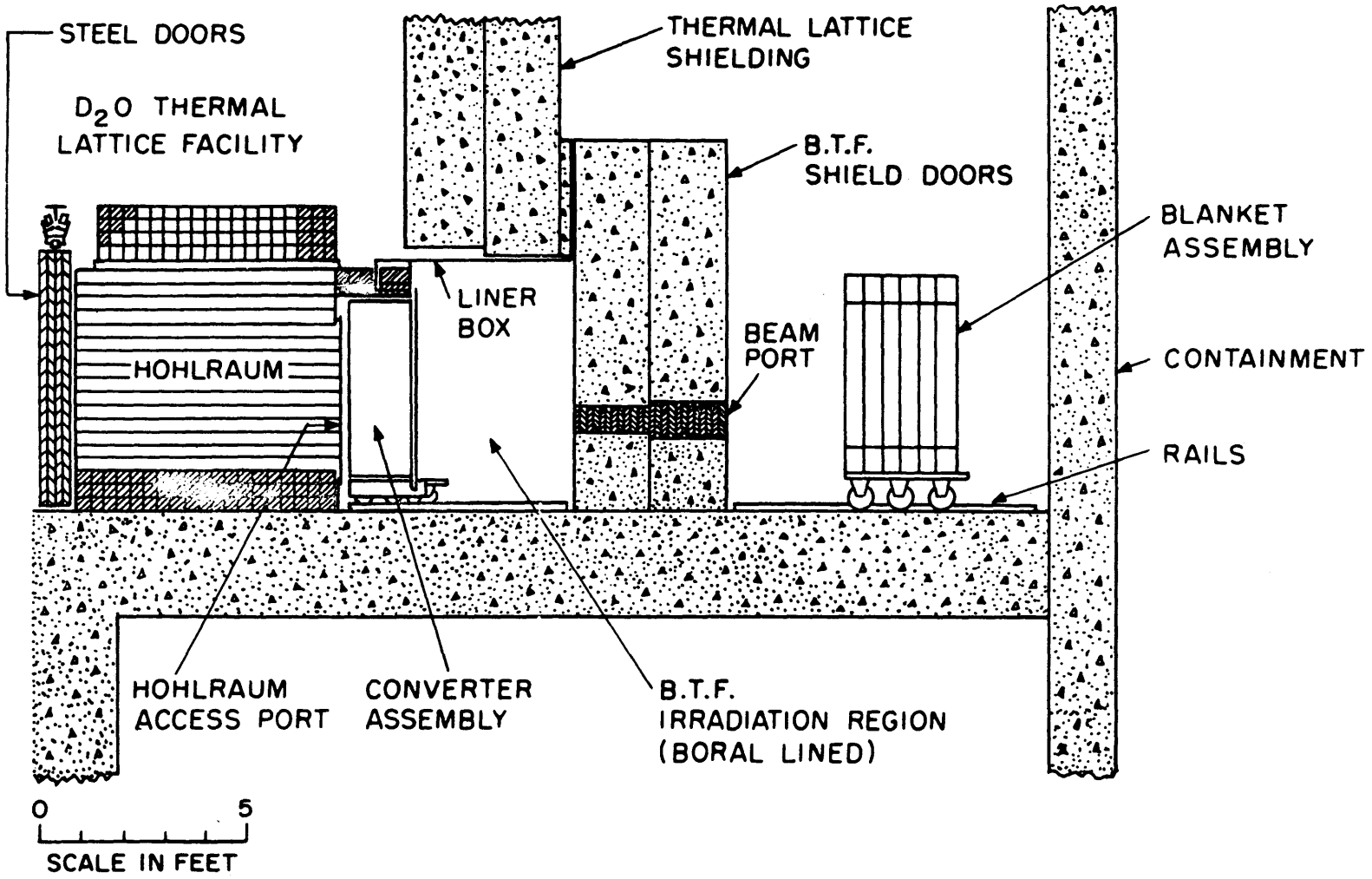

FIG. 1.1 SCHEMATIC CROSS SECTION VIEW OF HOHLRAUM AND BLANKET TEST FACILITY

50 watts and the fast neutron flux approximately 10^9 n/cm^2-sec.

Blanket Assembly No. 2 is a mockup of a representative large LMFBR blanket. It consists of three rows of subassemblies containing steel-clad uranium metal fuel rods and anhydrous sodium chromate powder (Fig. 1.2). The relative proportion of the various constituents has been chosen to correctly simulate the UO_2 fuel, stainless steel clad and sodium coolant of a real LMFBR blanket (see Table 1.1). The blanket has an 18 inch thick reflector of mild steel plate.

The blanket subassembly boxes are 5.92 in. square, 60 in. high and have an approximate wall thickness of 3/32 in. Each subassembly contains 121 fuel rods arranged in an eleven by eleven square lattice with a pitch of 0.511 in. The fuel rods have a mean U-235 enrichment of 1.08%.

Figure 1.3 shows the position of the test subassembly used to hold the instruments to measure the neutron flux. The subassembly is within the 30 in. center region which has been shown to have reached spectral equilibrium (L2). The test subassembly is similar to the subassemblies described above except that a 1.75 X 1.75 in. center section has been removed and replaced by a hollow steel channel (see Fig. 1.4). Figure 1.5 shows the inner subassembly insert which fits into the center of the test subassembly. The insert consists of two sections, a bottom section and a top section. The bottom section is a 1.5 X 1.5 X 21 in. long square box, with nine uranium metal fuel elements, carbon steel-clad, 5/16 in O.D.

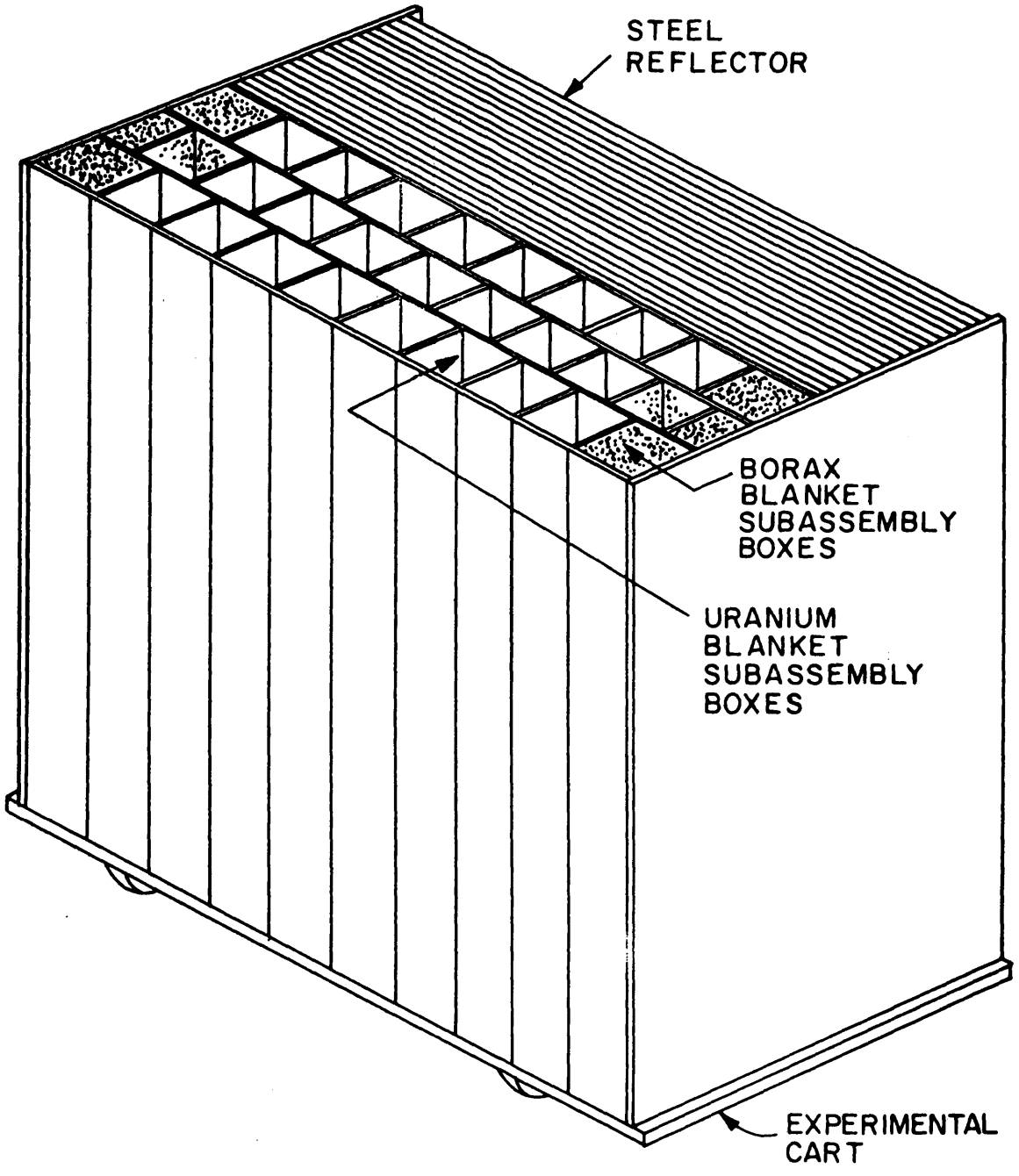

FIG. 1.2 SCHEMATIC VIEW OF BLANKET ASSEMBLY NO. 2

TABLE 1.1

Homogenized Atom Densities in B.T.F. Blanket No. 2

Nuclide	Blanket No. 2		Equivalent Realistic Blanket*	
U^{235}	0.000088		0.000016	
U^{235}	0.008108		0.008131	
O	0.016293		0.016293	
Na	0.008128		0.008128	
Cr	0.004064	0.017814	0.003728	0.017814
Fe	0.013750		0.012611	
Ni	0.000000		0.001475	
H	0.000073		0.000000	
C	0.000096		0.000082	

*Composed of 37.0 v/o depleted UO_2 (at 90% of theoretical density), 20.7 v/o Type 316 stainless steel, 32 v/o sodium and 10.3 v/o void.

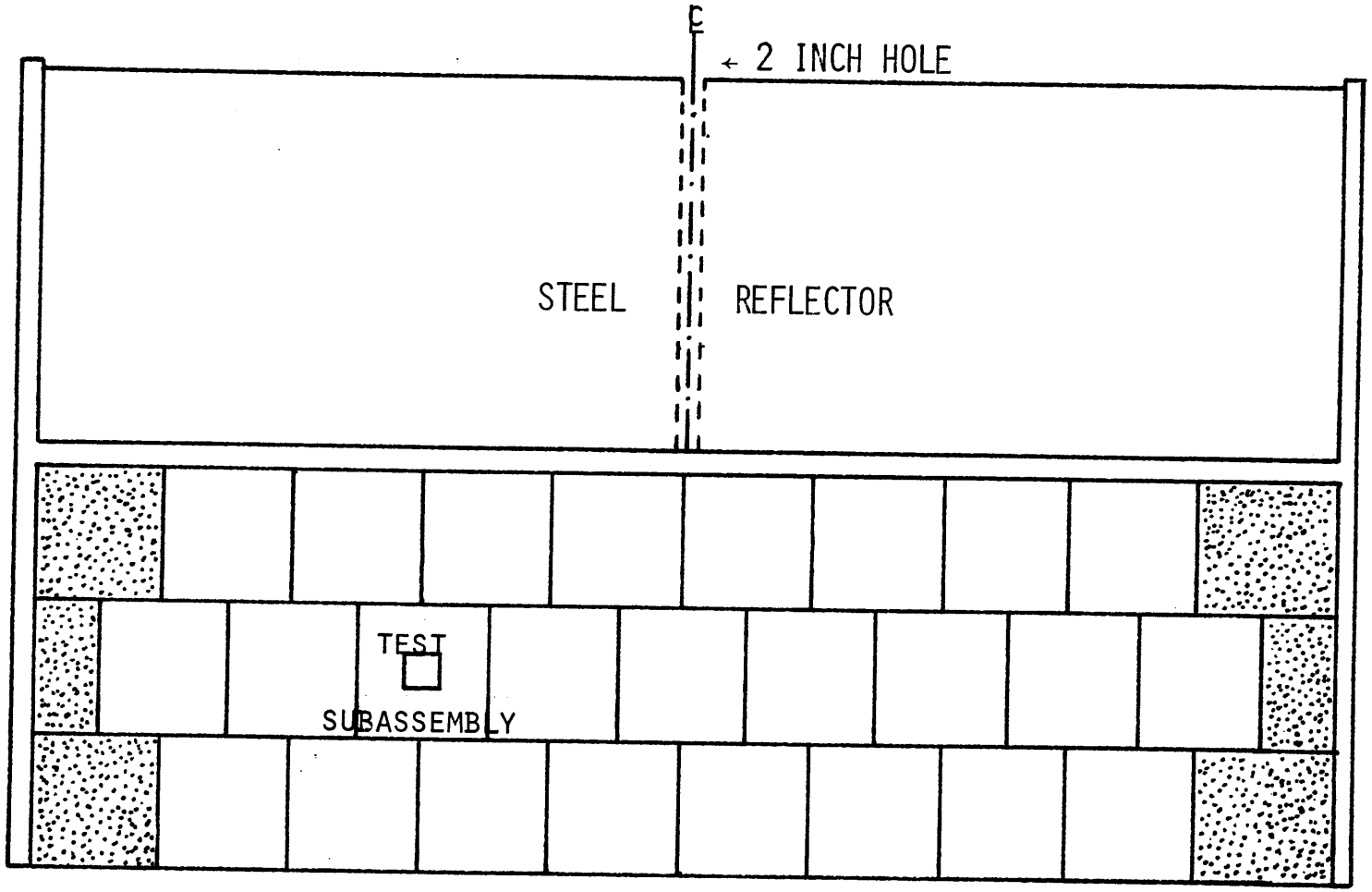

FIG. 1.3 PLAN VIEW OF BLANKET ASSEMBLY SHOWING THE TEST SUBASSEMBLY POSITION

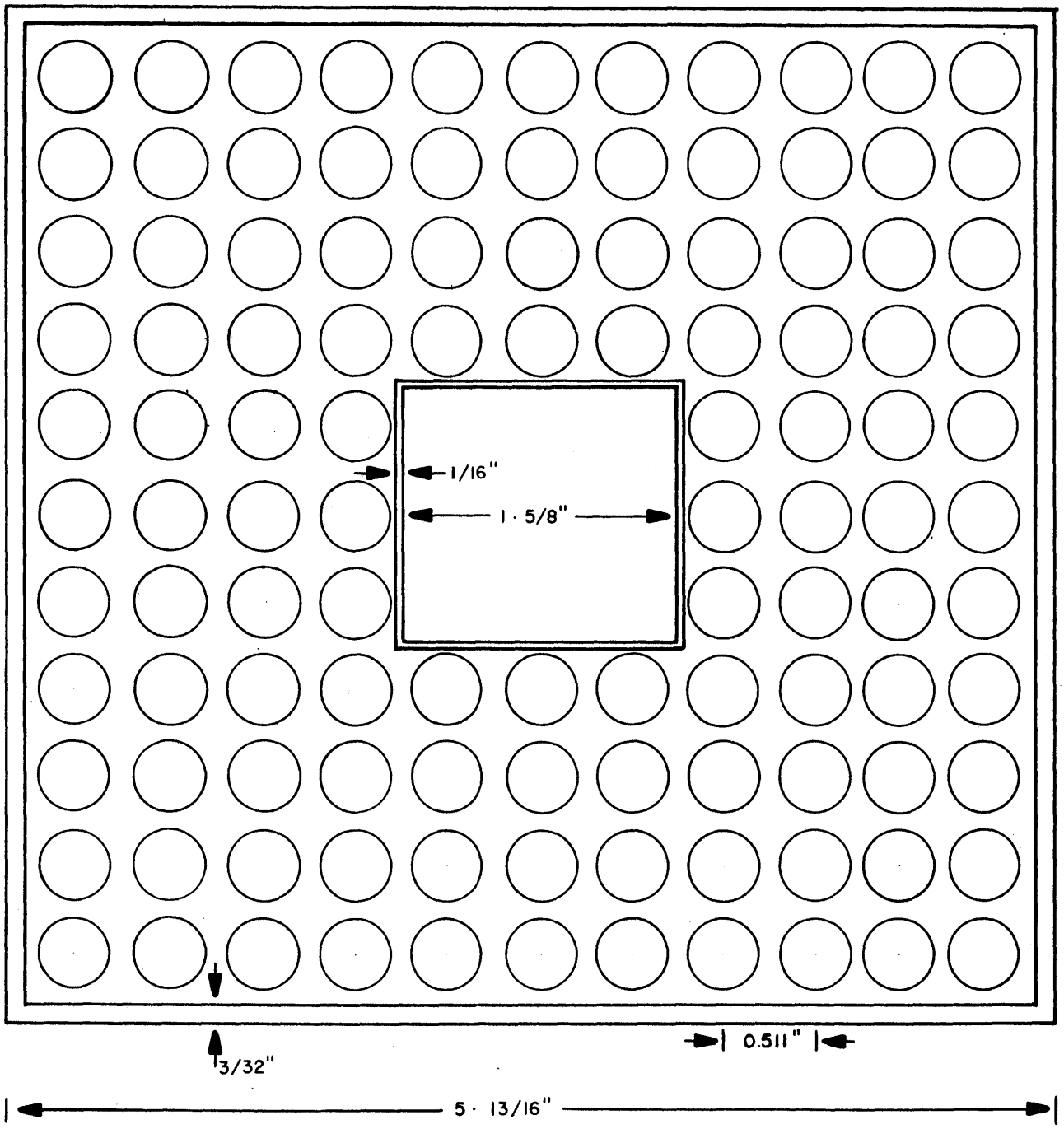

CROSS SECTION THROUGH B T F TEST SUBASSEMBLY

FIGURE 1.4

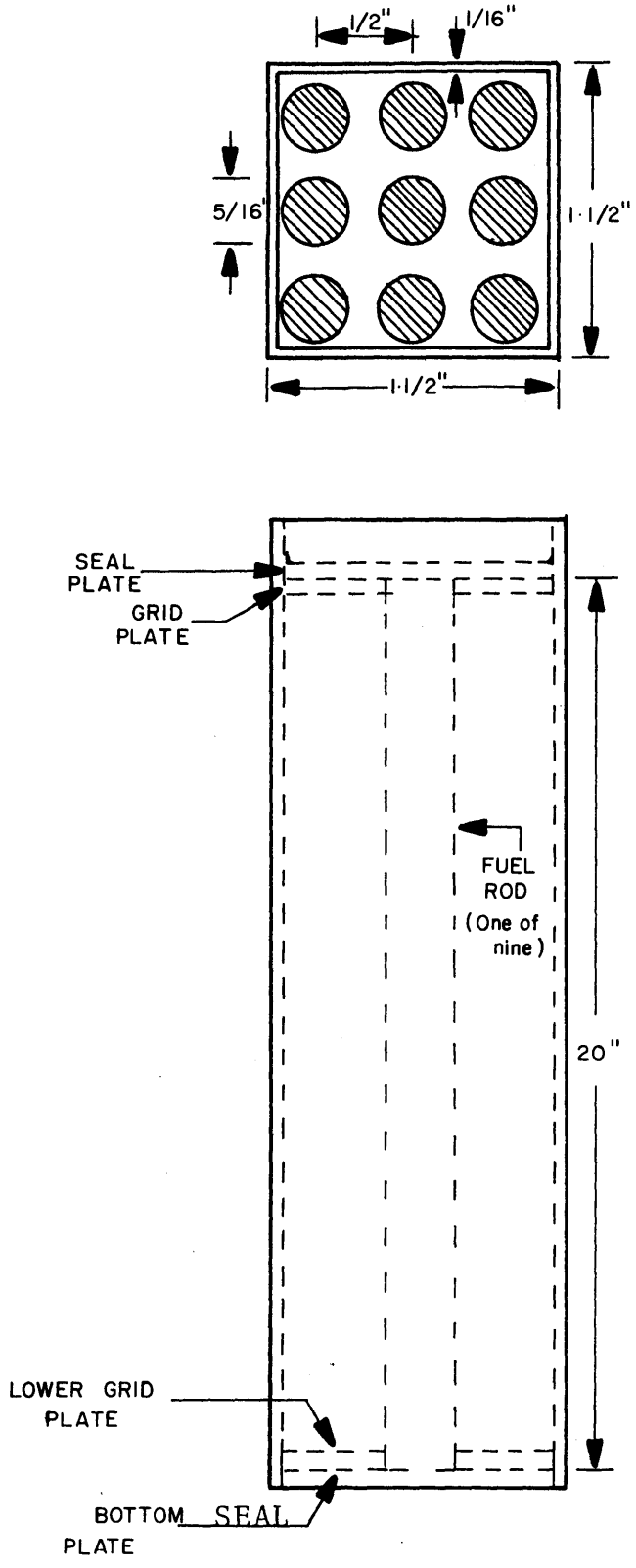

FIG. 1.5 Bottom Inner Subassembly Insert

The top section is similar to the one described above, but two fuel elements in opposite corners have been removed to leave space for instrument cables. The detector (e.g. Li-6, He-3, proton-recoil) is placed between the two sections of the inner subassembly insert, in a cavity 1.5 X 1.5 inches in cross section and 8 in. long. With the exception of the thin steel channel walls, the special subassembly has been designed to have a composition similar to the other standard subassemblies to avoid creation of large flux perturbations (see Table 1.2). The same experimental setup was used with the He-3 semiconductor detector, the Li-6 semiconductor detector, and the proton-recoil detector. Figure 1.6 shows a schematic of the upper section of the inner subassembly with the proton-recoil detector installed.

1.5 FORMAT OF THE REPORT

Chapter 2, which follows, presents the basic equations for the kinematics of the nuclear reactions involved. These equations are applied to the interaction of neutrons with the He-3 nucleus, which is the basis of the He-3 Semiconductor Detector. The two methods of operation, i.e., the Sum and Difference Method are described in detail. The experimental procedures, analysis and results of neutron spectrum measurements in the Blanket Test Facility are discussed.

In Chapter 3, the Li-6 detector and its different modes of operation are explained in detail. Included are the results of neutron spectrum measurements with the detector operating

TABLE 1.2

SUBASSEMBLY COMPONENT WEIGHTS

	Standard Subassembly	Test Subassembly
Uranium Metal	89.30 kg	87.58 kg
Na_2CrO_4	31.11 kg*	29.46 kg
Cladding	13.00 kg	12.75 kg
Subassembly box	26.55 kg	26.60 kg
Inner Subassembly		4.48 kg
Grid plate support tubes	0.91 kg	0.92 kg
Grid plates	0.36 kg	0.38 kg
Total	161.26 kg	162.17 kg
*The loadings vary from	30.51 kg to	31.80 kg

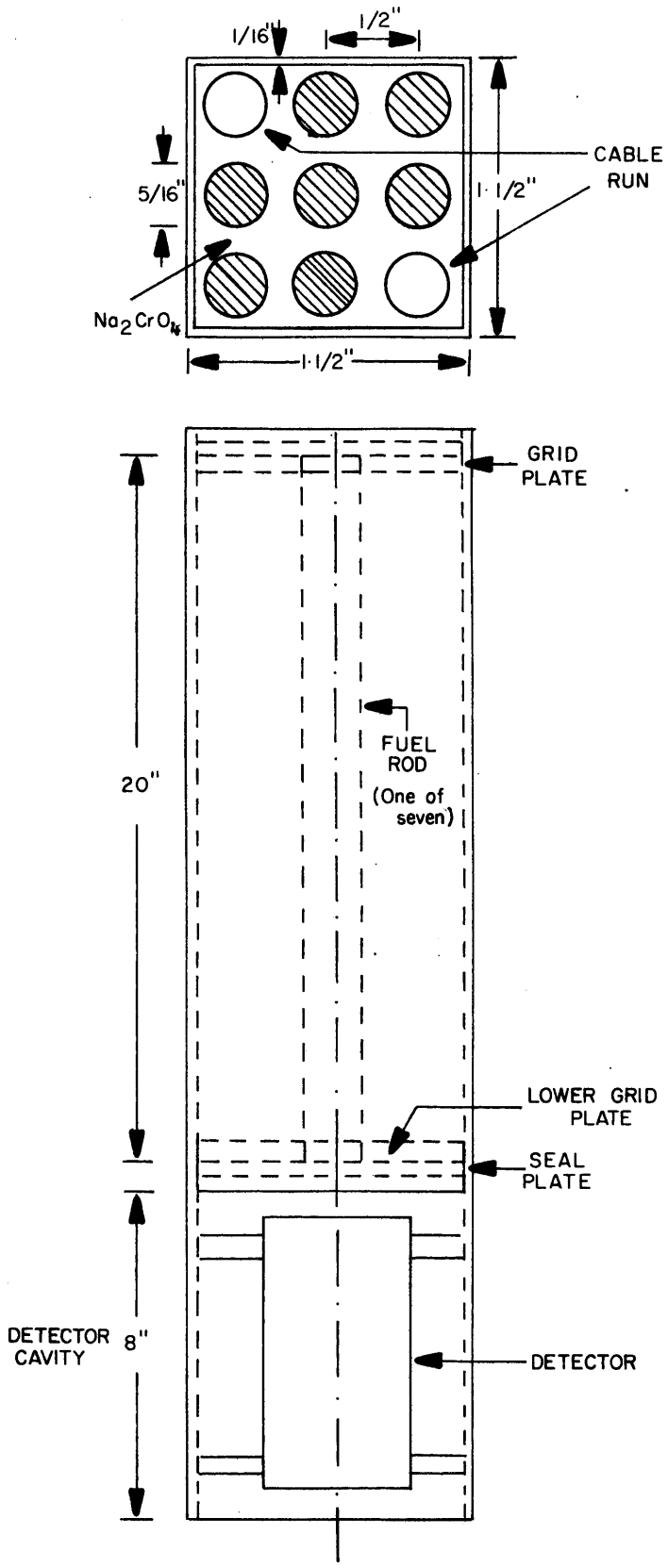

FIG. 1.6 Top Inner Subassembly Showing Detector Installed In Cavity

in the Sum, Difference and Triton Modes. The unfolding techniques used for each of the three methods are also described.

Chapter 4 contains a description of the Proton-Recoil System and the results of neutron spectrum measurements using this device. These results and the results from previous chapters and other work on the Blanket Test Facility are compared in Chapter 5 which also includes the conclusions and recommendations for future work.

Chapter 2

HELIUM-3 SEMICONDUCTOR DETECTOR

2.1 INTRODUCTION

In this chapter the basic equations for the kinematics of the reaction of a neutron with a nucleus of mass M_2 are discussed. These equations are applied to the $^3He(n,p)T$-reaction, and in the next chapter to the $^6L_i(n,\alpha)T$-reaction. The operation of the He-3 semiconductor detector in the Sum and Difference Modes to measure the neutron spectrum in the Blanket Test Facility and the analysis of the experimental data are described in detail.

The operating principle underlying several types of neutron spectrometers derives from the general neutron-induced reaction (F2);

$$n + M_2 \longrightarrow M_3 + M_4 + Q \qquad (2.1)$$

In this reaction the neutron and nucleus react to form product particles M_3 and M_4, accompanied by the release of the energy Q. To be of use for a neutron spectrometer, the reaction must satisfy several requirements:

1) The cross section must be large to insure adequate sensitivity, and a smoothly varying function of the neutron energy, since any sharp resonances make the analysis of data more difficult.

2) Within reasonable limits there must be no alternative reactions, including those in which one of the product particles is left in a different state of excitation. In other words, all energy must be accounted for as kinetic energy of the charged particles produced.

3) If the low-energy range is to be covered, Q must be positive. Also the value of Q should be reasonably small since the resolution of the spectrometer improves as Q decreases. On the other hand too small a value of Q will not suffice to produce a signal above low-energy background events.

4) The material containing the target nuclei M_2 must be obtainable in a form which is convenient to use either in or on the surface of an energy-sensitive nuclear detector.

Unfortunately there is no neutron-induced reaction known which completely satisfies all these requirements. Because of the first two requirements the choice is limited to reactions with light nuclei such as:

$$ {}_0n^1 + {}_2He^3 \rightarrow {}_1H^1 + {}_1H^3 \qquad Q = 0.764 \text{ MeV} $$

$$ {}_0n^1 + {}_3Li^6 \rightarrow {}_2He^4 + {}_1H^3 \qquad Q = 4.78 \text{ MeV} $$

$$ {}_0n^1 + {}_5B^{10} \rightarrow {}_2He^4 + {}_3Li^7 \qquad Q = 2.79 \text{ MeV} $$

$$ {}_0n^1 + {}_7N^{14} \rightarrow {}_1H^1 + {}_6C^{14} \qquad Q = 0.615 \text{ MeV} $$

The kinematics of the first reaction is discussed in detail in the next section.

2.2 KINEMATICS OF THE REACTION

Referring to Fig. 2.1, the capture of a neutron of mass M_1 by a target nucleus of mass M_2 forms the compound nucleus, M_c, with subsequent emission of the charged particles M_3 and M_4. For the non-relativistic case in which the kinetic energy of the projectile particle is small compared with its rest energy, M_1c^2, the equation for the conservation of mass-energy is (E1).

$$E_1 + Q = E_3 + E_4 \quad , \tag{2.2}$$

The equation for the conservation of linear momentum in the direction of the incident particle is

$$\sqrt{2M_1E_1} = \sqrt{2M_3E_3}\cos\theta + \sqrt{2M_4E_4}\cos\phi \quad , \tag{2.3}$$

and that for the linear momentum in the direction perpendicular to the direction of the incident particle is

$$0 = \sqrt{2M_3E_3}\sin\theta - \sqrt{2M_4E_4}\sin\phi \cdot \tag{2.4}$$

By a simultaneous solution of Eqs. (2.2), (2.3) and (2.4)

$$\sqrt{E_3} = V \pm \sqrt{V^2 + W} \tag{2.5}$$

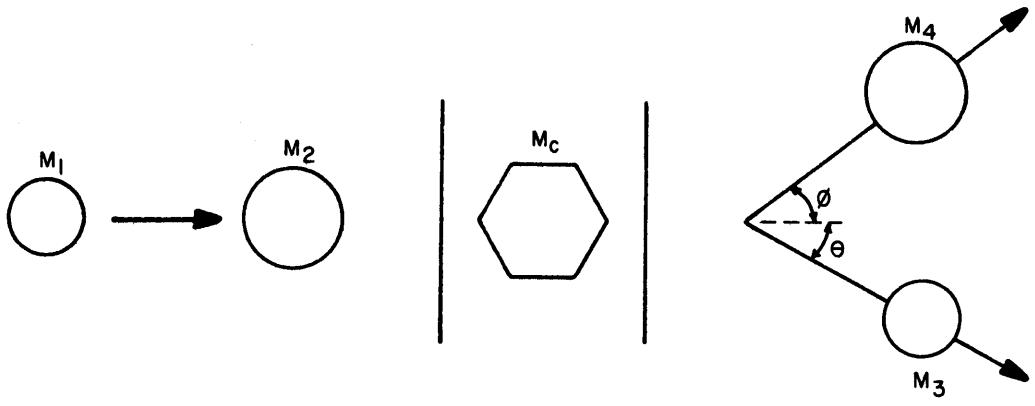

Notation, In Laboratory System

BEFORE COLLISION		AFTER COLLISION
Rest Mass	M_1, M_2	M_3, M_4
Velocity	V_1 ; $V_2=0$	V_3, V_4
Kinetic Energy	E_1; $E_2=0$	E_3, E_4
Angle	0 , 0	θ , Ø

FIG. 2.1 Schematic Of Reaction Kinematics

where $$V = a\sqrt{E_1}\cos\theta \tag{2.6}$$

$$W = b\,Q + C\,E_1 \tag{2.7}$$

$$a = \frac{M_1 M_3}{M_3+M_4}\,; \quad b = \frac{M_4}{M_3+M_4}, \quad c = \frac{M_4 - M_1}{M_3+M_4} \tag{2.8}$$

The energetically possible reactions are those for which E_3 is real and positive.

2.3 DESCRIPTION OF THE DETECTOR AND ELECTRONICS

Figure 2.2 is a schematic drawing of the commercially available Helium-3 detector head (Ortec 780 Neutron Spectrometer) used in this work (I1). It utilizes two closely matched silicon semiconductor detectors mounted with a separation of 1 mm between faces. The volume between the detectors is filled with high-purity Helium-3 gas. A small tank of He-3 gas is provided to fill the detector to the desired operating pressure. The absorption of a neutron by a He-3 nucleus will result in the emission of a triton and a proton. The arrangement of the two silicon detectors is such that for favorable emergence angles, the triton will be detected in one detector and the proton in the other.

The energy resolution and efficiency of the detector depend on the Helium-3 pressure in the sensitive volume. High gas pressure will increase the efficiency and decrease the resolution. The detector is operated at 16 psig; the resolution at this pressure is about 65 keV for thermal neutrons.

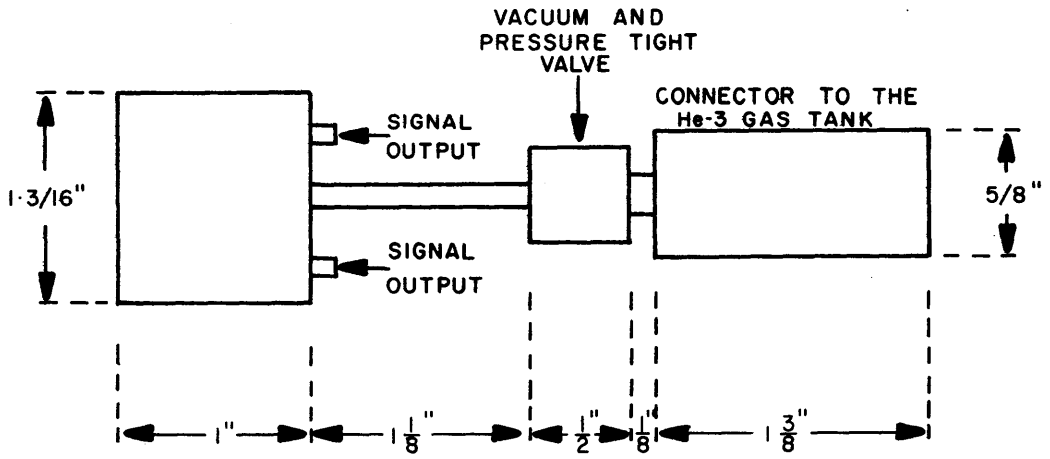

FIG. 2.2 He-3 Detector Head

The detector bias is 135 volts.

Figure 2.3 shows the block diagram of the neutron spectrometer electronic system. The output of each silicon detector is analyzed in a separate channel, and time discrimination is applied, i.e., a pulse in one channel must be in coincidence with that in the other channel to be accepted; all other signals are rejected. This reduces the gamma background, pulses due to parasitic reactions in the silicon detectors, and the random signals due to He-3 recoil events. The output of the timing single channel analyzer (TSCA) is fed to a fast coincidence unit with a narrow resolving time (70 ns.). The logic shaper and delay unit reshape and delay the output of the fast-coincidence unit to meet the specifications of the multichannel analyzer gate input. In the present research only 512 channels of the 4096-channel multichannel-pulse-height analyzer (PHA) were used to accumulate the spectrum.

2.4 SUM METHOD

2.4.1 Description of the Method

In the Sum Method the output of both detectors is added and only those which fulfill the coincidence requirements are accumulated in the multichannel pulse-height analyzer. According to Eq. (2.2) the height of the sum pulse is proportional to the energy of the neutron plus the Q value of the reaction. Therefore if the detector head is exposed to a thermal neutron flux ($E_n \sim 0$) and both outputs are added

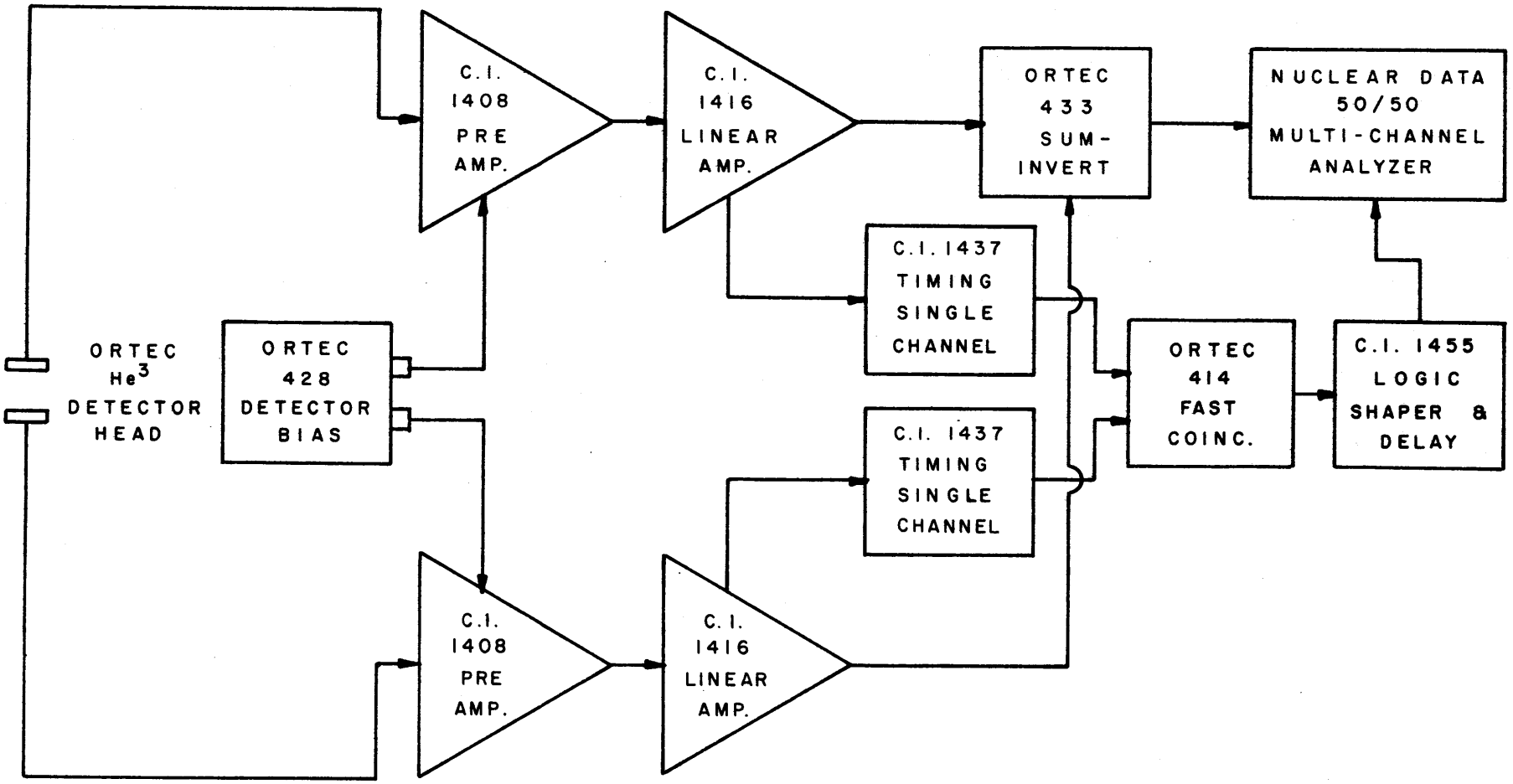

FIG. 2.3 Electronic System For He-3 Neutron Spectrometer

in coincidence, a peak is observed in the channel corresponding to the Q value (764 keV). If only one output of the detector is analyzed, Eq. (2.5) gives

$$E_3 = \frac{3}{4} Q, \tag{2.9}$$

and a second peak is obtained in the channel corresponding to the proton energy of 573 keV (Fig. 2.4). It is important to adjust the gain of the amplifiers such that each detector will produce the peak in the same channel. A linear relationship between channel number and energy is then assumed to provide the energy calibration of each channel. A precision pulser, Ortec 448, was used to check the linearity of the system (see Fig. 2.5).

2.4.2 Effect of the Discriminator Settings

To discriminate against the noise inherent in the electronic system and to reduce the number of small gamma-ray induced pulses reaching the coincidence unit, a baseline setting equivalent to 150 keV was selected for the TSCA. The application of this energy discrimination will cause the rejection of some real events in which one of the emitted particles does not carry away enough kinetic energy. Figure 2.6 shows that the proton will always carry an energy higher than the discriminator level of 150 keV. However, for all but the lowest neutron energies a proportion of the tritons will have an energy less than 150 keV. The probability that reaction products will satisfy the discriminator level

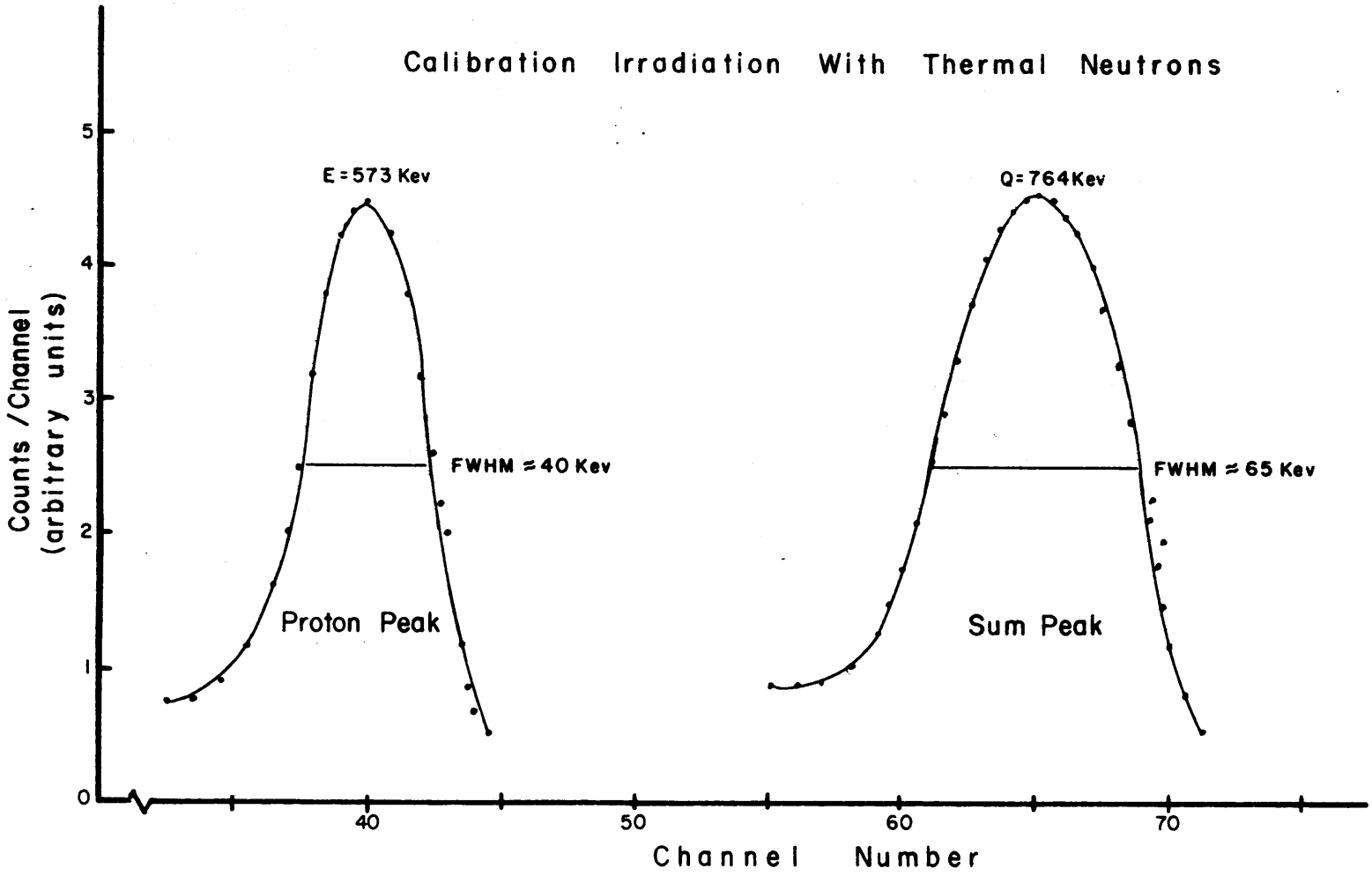

FIG. 2.4 Proton And Sum Peak - He-3 System

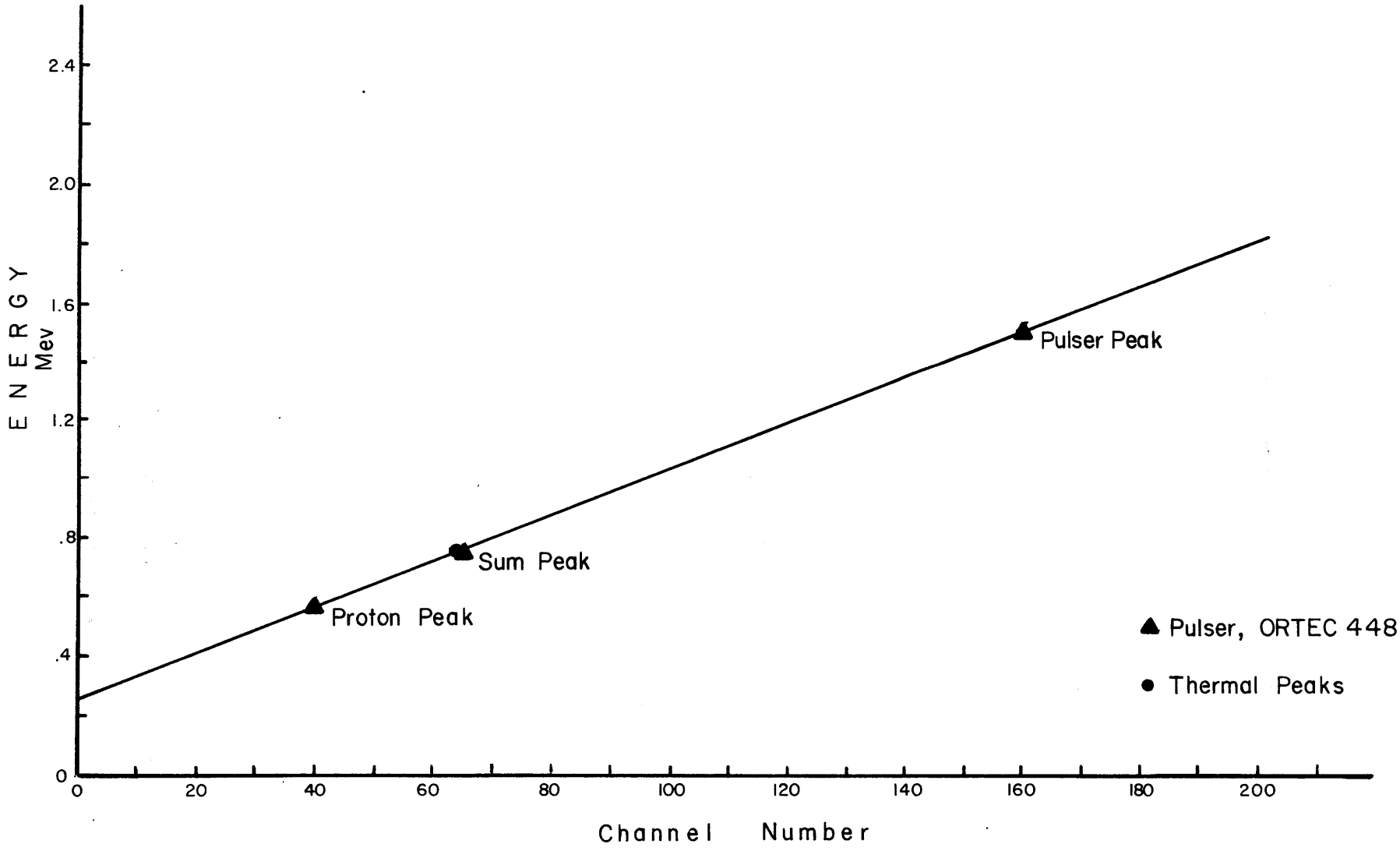

FIG. 2.5 He-3 System Energy Calibration

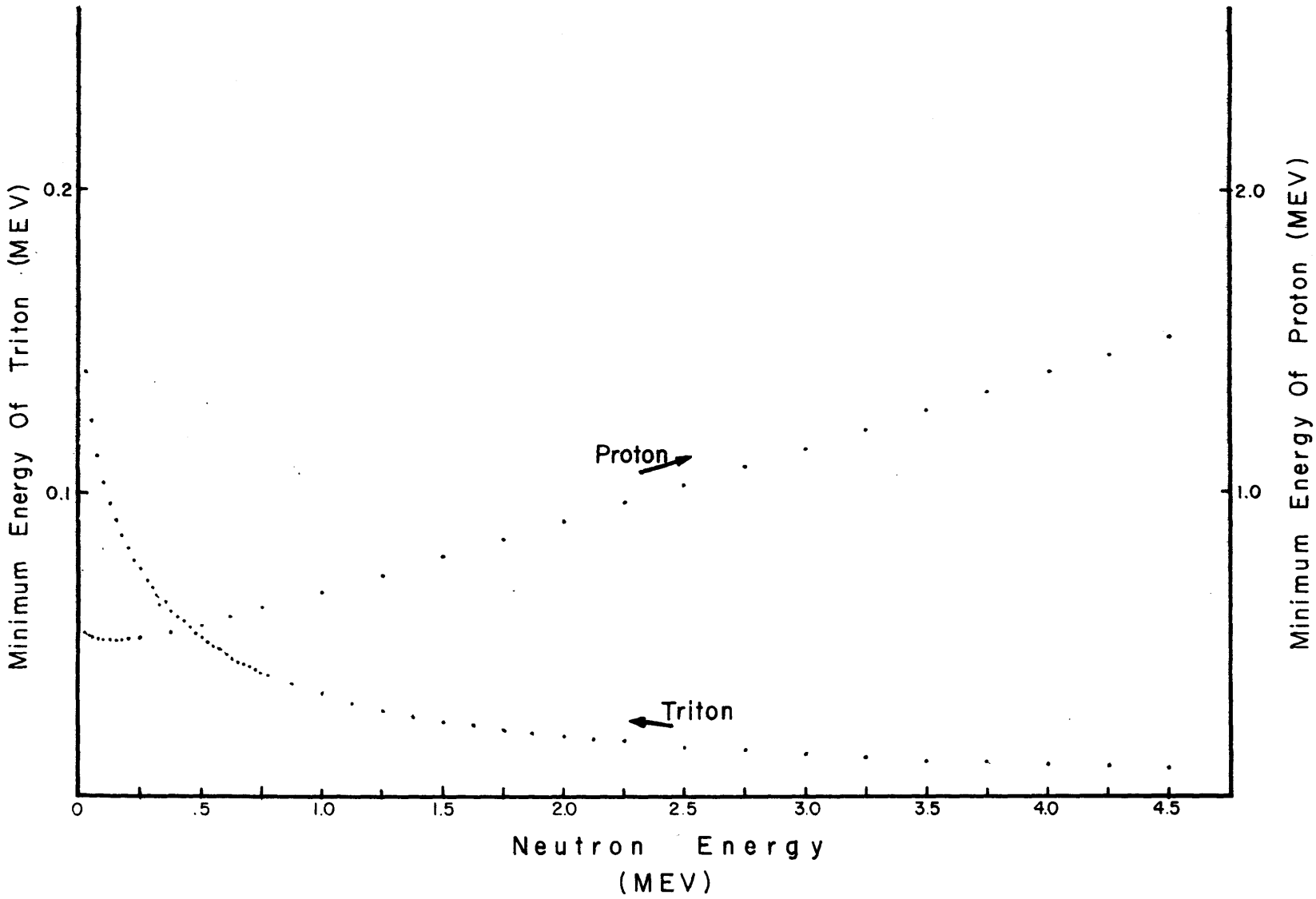

FIG. 2.6 Minimum Energy Carried By The Reaction Products Of The He-3 Neutron Interaction

is plotted as a function of the neutron energy in Fig. (2.7). This curve is used in the unfolding of the measured spectrum which is discussed in the next section.

2.4.3 Unfolding of the Measured Spectrum

The integral equation that relates the measured charged particles' spectrum to the incident neutron flux is

$$M(E) = N \int_{0}^{\infty} \varepsilon(E')R(E' \rightarrow E)\sigma(E')\phi(E')dE' \qquad (2.10)$$

where

$M(E)$ = Measured charged particle energy spectrum

$\varepsilon(E')$ = Efficiency of the detector

$R(E' \rightarrow E)$ = Resolution function; probability that a reaction which takes place at a neutron energy E' contributes to the counting rate at E.

N = Number of He-3 atoms in the detector

$\sigma(E')$ = Absorption cross section

$\phi(E')$ = Incident neutron flux

It is assumed that the distribution $R(E' \rightarrow E)$ is a function only of the difference between E' and E; this allows us to write (J1):

$$R(E' \rightarrow E) = R(E-E')$$

It is convenient to change the energy variable:

$$\eta = E-E_o, \text{ where } E_o = Q \text{ value of the reaction.} \qquad (2.11)$$

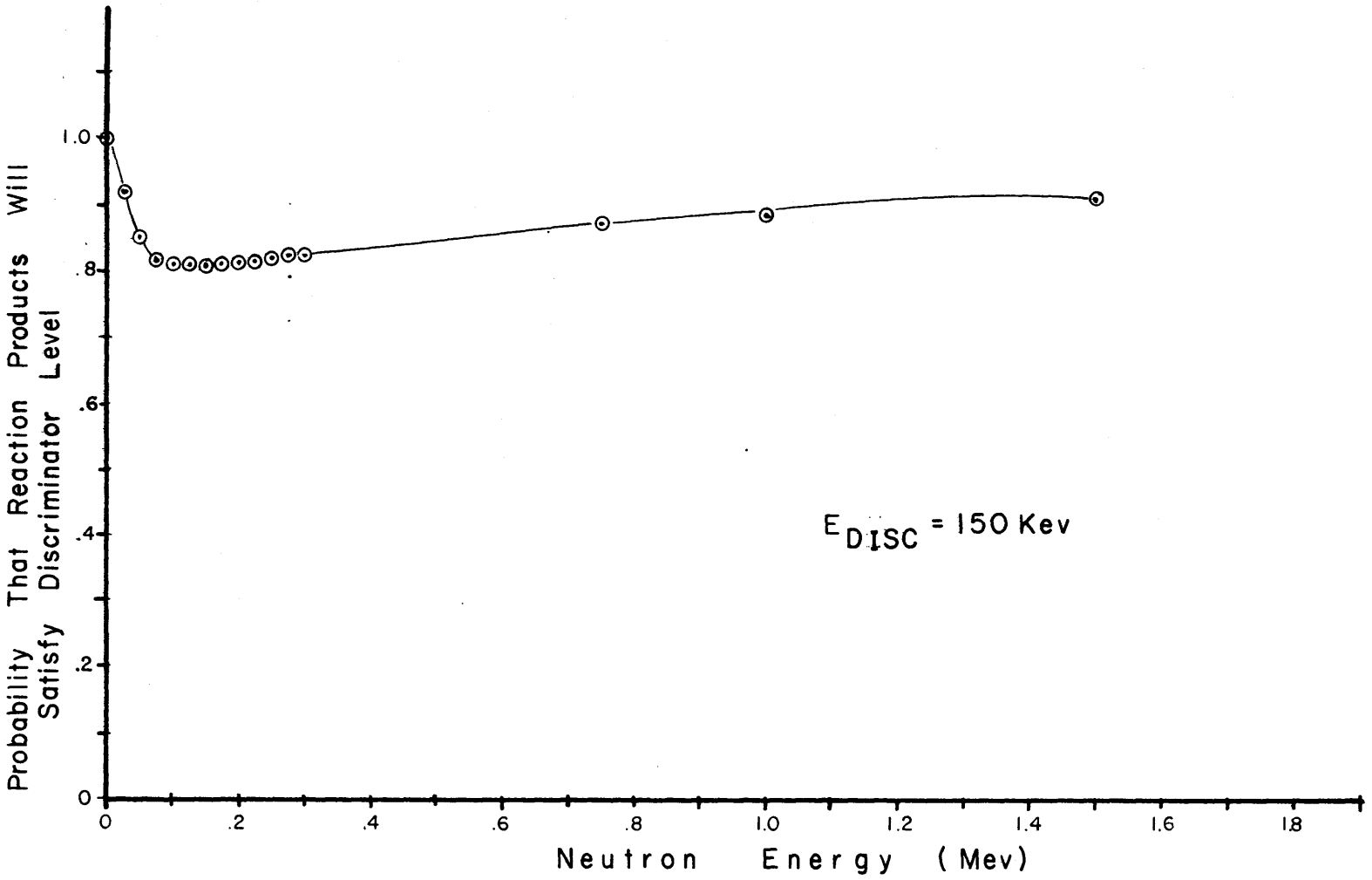

FIG. 2.7 Efficiency Curve For A Discriminator Setting Of 150 Kev

Then, Eq. (2.10) becomes

$$M\ (\eta+E_o) = N \int_o^\infty \varepsilon(E')R(\eta-E')\sigma(E')\phi(E')dE' \qquad (2.12)$$

The function $R(\eta-E')$ is determined by measuring the resolution for monoenergetic neutrons. If the detector is exposed to a thermal flux, Eq. (2.12) gives

$$M(\eta+E_o)\alpha R(\eta) \qquad (2.13)$$

$R(\eta)$ is proportional in this case to $M(\eta+E_o)$; therefore it can be measured (within a multiplicative constant) in a thermal neutron flux. The distribution curve for the resolution is more or less Gaussian in shape for events around the value E', but it is slightly dissymmetrical towards the low-energy region mainly because of electronic noise and detector edge effects. The points at which $R(\eta)$ is approximately equal to zero are denoted by (-d,e). To solve Eq. (2.12) the resolution is assumed to be a Gaussian distribution between points (-d,e). The equation is then rewritten as:

$$M(\eta+E_o) = \int_{-d}^{e} R(u)\cdot F(\eta-u)du; \quad , \qquad (2.14)$$

where $\eta-E' = u$

and $F(\eta-u)\ \cdot = N\phi(\eta-u)\sigma(\eta-u)\cdot\varepsilon(\eta-u)$

The derivation which follows is adapted from reference

(B6). It is assumed that the function $F(\eta-u)$ is a smooth function which can be approximated in the interval (-d,e) by a polynomial of order n. The Taylor's series representing $F(\eta-u)$ about the value of η in the interval (-d,e) is

$$F(\eta-u) = F(\eta) - u\cdot F'(\eta) + \frac{u^2}{2} F''(\eta) - \frac{u^3}{3}\cdot F'''(\eta) + \frac{u^4}{24} F''''(\eta)+\cdots+ \qquad (2.15)$$

Substituting Eq. (2.15) into Eq. (2.14)

$$M(\eta+E_o) = F(\eta)\int_{-d}^{e} R(u)du - F'(\eta)\int_{-d}^{e} uR(u)du + F''(\eta)\int_{-d}^{e} \frac{u^2}{2}R(u)du - F'''(\eta)\int_{-d}^{e} \frac{u^3}{6}R(u)du + F''''(\eta)\int_{-d}^{e} \frac{u^4}{24}R(u)du \qquad (2.16)$$

But $\int_{-d}^{e} R(u)du = \underline{1}$

and defining:

$$\int_{d}^{e} uR(u)du = A \ , \qquad (2.17)$$

$$\int_{d}^{e} u^3R(u)du = C \ , \qquad (2.18)$$

$$\int_{d}^{e} u^4R(u)du = D \ , \qquad (2.19)$$

then

$$B^2 = \int_d^e u^2 R(u)du - A^2 \quad . \tag{2.20}$$

This gives

$$M(\eta+E_o) = F(\eta) - A\cdot F'(\eta) + \frac{A^2+B^2}{2} F''(\eta) -$$

$$\frac{C}{6} F'''(\eta) + \frac{D}{24} F''''(\eta) \tag{2.21}$$

or

$$M(\eta+E_o) = (I - Aq + \frac{A^2+B^2}{2} q^2 - \frac{C}{6} q^3 + \frac{D}{24} q^4)F(\eta) \tag{2.22}$$

where

I = unity operator

q = difference operator such that

$$q^n M(\eta+E_o) = \frac{d^n}{d\eta} M(\eta+E_o) \tag{2.23}$$

If $$S = (I - Aq + \frac{A^2+B^2}{2}q^2 - \frac{C}{6} q^3 + \frac{D}{24} q^4) \tag{2.24}$$

then

$$F(\eta) = S^{-1}\cdot M(\eta+E_o) \tag{2.25}$$

It is known that (H1):

$$\frac{1}{1-X} = (1-X)^{-1} = \sum_{n=o}^{\infty} X^n \text{ if } | X | < 1 \tag{2.26}$$

If $$X = (Aq - \frac{A^2+B^2}{2} q^2 + \frac{C}{6} q^3 - \frac{D}{24} q^4) \ , \tag{2.27}$$

then

$$S^{-1} = I + X + X^2 + X^3 + X^4 + \ldots + \ldots \quad . \tag{2.28}$$

Limiting the series to a polynomial of order four

$$S^{-1} = 1 + Aq + \frac{A^2-B^2}{2} q^2 + \frac{C-6AB^2}{6} q^3 +$$

$$\frac{-D+BA(C-3AB^2)+6(B^4-A^4)q^4}{24} \tag{2.29}$$

Using standard difference equation formulation (K2) the derivatives of the measured spectrum are calculated in an energy interval, h, on each side of the value of η as:

$$M'_i = \frac{M_{i+1}-M_{i-1}}{2h} \tag{2.30}$$

$$M''_i = \frac{1}{h^2} (M_{i+1} - 2M_i + M_{i-1}) \tag{2.31}$$

$$M'''_i = \frac{1}{2h^3} (M_{i+2} - 2M_{i+1} + 2M_{i-1} - M_{i-2}) \tag{2.32}$$

$$M''''_i = \frac{1}{4h^4} (M_{i+3} - 2M_{i+2} - M_{i+1} + 4M_i - M_{i-1} - 2M_{i-2} + M_{i-3}) \tag{2.33}$$

For simplification let:

$$D_1 = \frac{A}{2h}; \quad D_2 = \frac{A^2-B^2}{2h^2}; \quad D_3 = \frac{C-6AB^2}{12h^3}$$

$$D_4 = \frac{-D+8A(C-3AB^2)+6(B^4-A^4)}{96h^4}$$

so that

$$F_i = M_i+D_1(M_{i+1}-M_{i-1})+D_2(M_{i+1}-2M_i+M_{i-1})+$$

$$D_3(M_{i+2}-2M_{i+1}+2M_{i-1}-M_{i-2})+D_4(M_{i+3}-2M_{i+2}-$$

$$M_{i+1}+4M_i-M_{i-1}-2M_{i-2}+M_{i-3}) \qquad (2.34)$$

Equation 2.34 is the desired relation between the collision density and the multichannel analyzer data points M_i. A computer program SUMMA was written to calculate the coefficients D_1, D_2, D_3, D_4 and the collision density F_i for each channel, i, based on Eq. (2.34). It also calculates the neutron flux using Eq. (2.15). The values of the cross section for the $He^3(n,p)T$-reaction as a function of energy were obtained from reference (B10). The cross section data was divided into five energy regions: 1 to 10 keV, 10 to 100 keV, 100 to 200 keV and 200 to 2000 MeV. Each region was fitted with a polynomial of fifth order to provide continous data as a function of energy (see Appendix B).

2.4.4 Experimental Results

The He-3 detector was placed in the test subassembly located in the second row of Blanket Mockup No. 2 (see Fig. 1.3), to measure the ambient fast neutron flux. The steel doors controlling the thermal neutron flux incident on the

converter cart were opened only two and a half (of a normal 30) turns to limit the converter power and thereby avoid the pile-up of events at the output of the detector preamplifier. The same experimental conditions were used in all the experiments performed with the He-3 semiconductor detector, Li-6 semiconductor detector and proton-recoil proportional counter. The detector was operated at a count rate of 180 counts/sec in coincidence. The background count rate was about 50 counts/sec, mainly due to the interaction of neutrons with the silicon detectors and gamma-ray events. Figures 2.8 and 2.9 show the raw data and the results after unfolding, respectively. The experimental data was collected in 260 channels. One flux point per channel was obtained from the computer program SUMMA. The unfolded neutron spectrum, plotted per unit lethargy in Fig. 2.9 ($\phi(u)=E\phi(E)$), shows a broad peak around 350 keV. Only the region above a neutron energy of about 200 keV was measured with the Sum Method just described, since the large value of the absorption cross section for low-energy neutrons, produces a large background peak which affects the measurements below 200 keV.

2.4.5 Error Analysis

As shown in Eq. 2.34, the collision density can be represented as a linear combination of a certain number of measured data points

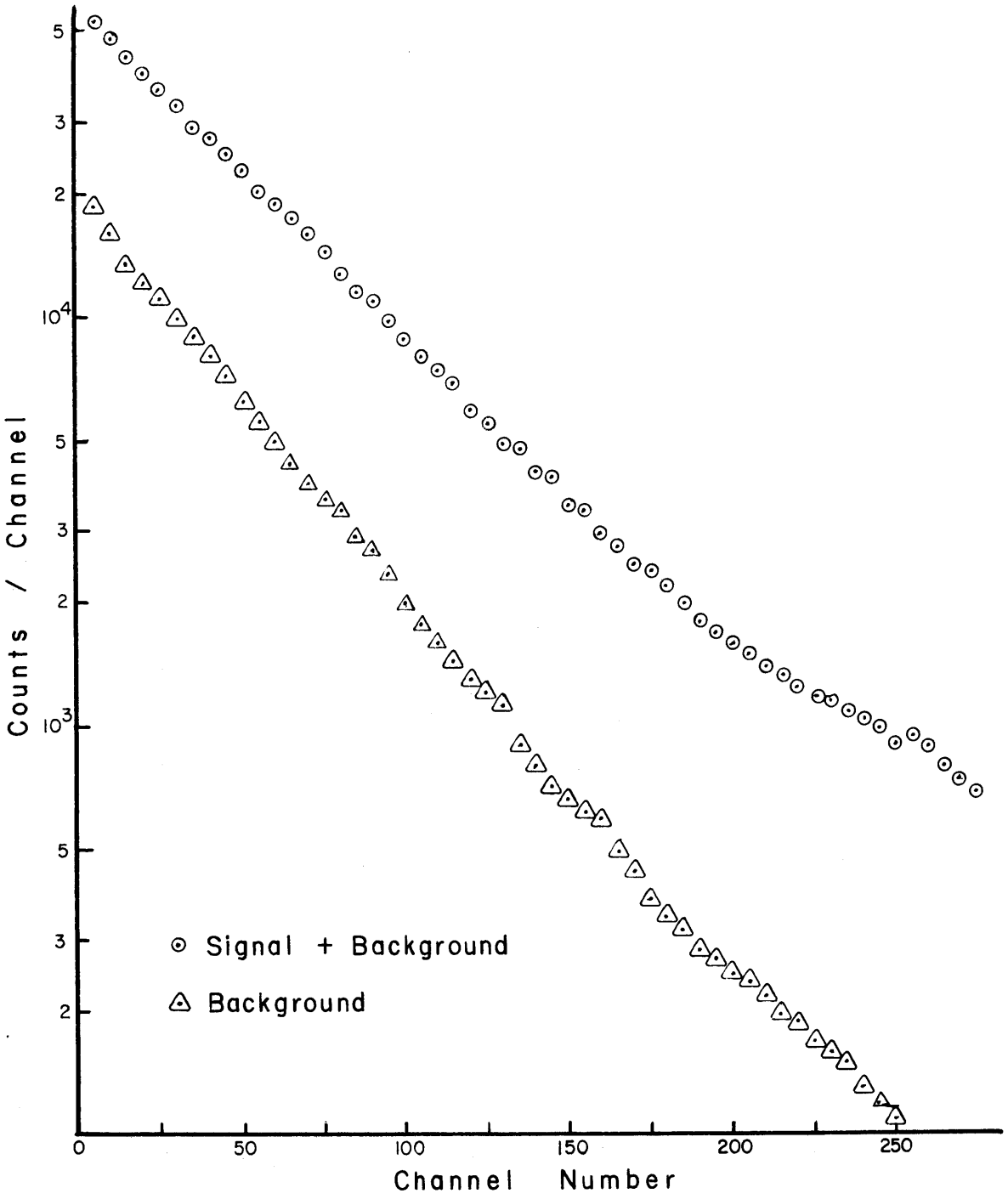

FIG. 2.8 Signal Plus Background Measurements Using The He-3 Detector Operating In The Sum Mode

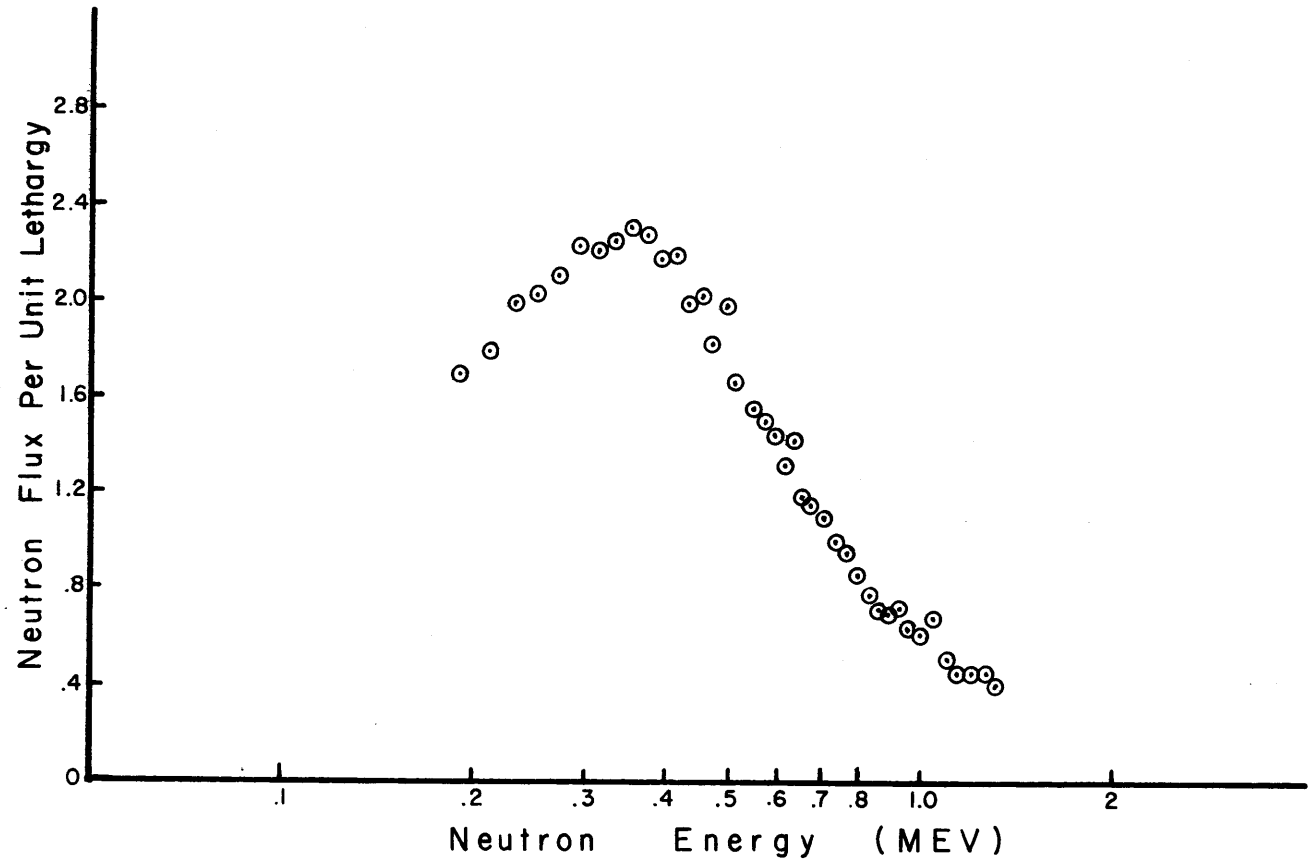

FIG. 2.9 Neutron Spectrum In Blanket Mockup NO.2 Using The He-3 System Sum Method

$$F_i = \sum_k C_k^i \cdot M_k$$

The neutron flux measurement is done in two steps

(1) A measurement of the signal plus background M_{s+b}

(2) A measurement of the background M_b

The net number of counts is

$$M = M_{s+bi} - M_{bi} \tag{2.35}$$

If M_{s+b} has a standard deviation σ_{s+b}, and M_b, σ_b, the variance of the difference of the measurements is

$$\sigma_i^2 = \sigma_{s+b}^2 + \sigma_b^2 = M_{s+bi} + M_{bi} \quad . \tag{2.36}$$

If the collision density, F(E), is represented by a fourth order polynomial

$$F_i = \sum_{k=i-3}^{i+3} C_k^i \cdot M_k \quad , \tag{2.37}$$

the variance is given by

$$\sigma^2 F_i = \sum_{k=i-3}^{i+3} C_k^{i2} \sigma^2 M_k \quad . \tag{2.38}$$

since

$$\sigma^2 M_k = M_k \quad , \tag{2.39}$$

$$\sigma F_i = \sum_{k=i-3}^{i+3} C_k^{i\,2} \cdot M_k \qquad (2.40)$$

The coefficients C_k^i are obtained from Eq. (2.34) which can be written as:

$$F_i = D_4 M_{i-3} + (-D_3-2D_4)\cdot M_{i-2} + (-D_1+D_2+2D_3-D_4)M_{i-1} +$$

$$(1-2D_2+4D_4)M_i + (D_1+D_2-2D_3-D_4)M_{i+1} + (D_3-2D_4)M_{i+2} +$$

$$D_4 M_{i+3} \quad . \qquad (2.41)$$

Comparison of Eqs. (2.41) and (2.37) gives

$$C_{i-3} = D_4$$

$$C_{i-2} = -D_3-2D_4$$

$$C_{i-1} = -D_1+D_2+2D_3-D_4$$

$$C_i = 1-2D_2+4D_4$$

$$C_{i+1} = D_1+D_2-2D_3-D_4$$

$$C_{i+2} = D_3-2D_4$$

and

$$\sigma F_i = (C_{i-3}^2 M_{i-3} + C_{i-2}^2 M_{i-2} + C_{i-1}^2 M_{i-1} + C_i^2 M_i + C_{i+1}^2 M_{i+1} + C_{i+2}^2 M_{i+2} + C_{i+3}^2 M_{i+3})^{\frac{1}{2}} \qquad (2.42)$$

Equation 2.42 is the desired relation between the standard deviation of the collision density and the multichannel analyzer data points M_i. The probable error is defined in terms of the standard deviation as follows (E1):

$$rF_i = 0.6745\sigma F_i$$

To calculate the neutron flux the collision density has to be divided by the cross section of the $He^3(n,p)T$-reaction, therefore the error in the values of the latter will affect the accuracy of the results. The cross section values and associated errors were obtained from reference (B10).

The estimated errors for the neutron flux range from about 9% to 13% in the energy region from 200 keV to 1.3 MeV; they are listed in Table 2.1.

2.4.6 Advantages and Limitations

The main advantage of the Sum Method is the simplicity of the spectrum unfolding process. There is a unique relationship between the measured total energy of the reaction and the energy of the incident neutron. Only the resolution

TABLE 2.1

ESTIMATED ERRORS IN He-3 SUM METHOD SPECTROMETRY

Neutron Energy (keV)	Calibration Error	Statistical Error	Cross Section Error	Total Error
200 to 400	±2%	±2.4%	±8.9%	±9.4%
410 to 600	±1.5%	±4.5%	±10.0%	±11.1%
610 to 800	±1.5%	±6.3%	±10.0%	±11.2%
810 to 1,300	±1%	±8.4%	±10.0%	±13.1%

function $R(E' \rightarrow E)$ and the efficiency curve $\varepsilon(E')$, which accounts for the effect of the energy discriminator setting, need to the taken into account to unfold the neutron spectrum from the measured charged particle sum spectrum.

The disadvantages are: first, there is a limitation on the measurement of the energy of low-energy neutrons because of the relatively poor resolution of the system; and second, a high gamma background or noisy environment will affect the measurements. This latter effect arises for low values of the discriminator setting.

2.5 DIFFERENCE METHOD

2.5.1 General Considerations

The Difference Method is used in an attempt to improve the low-energy resolution of the system and to improve the rejection of gamma and noise background. This technique was first used with Li-6 semiconductor detectors in a beam geometry experiment (M2). In this technique the signals of both detectors are fed into a C.I. 1417 Amplier operating in the difference mode; the amplified output is then fed in coincidence with the output of the logic shaper and delay to the multichannel analyzer. The rest of the electronic system is similar to the Sum Method electronics (see Fig. 2.10).

This method has the advantage that any equal-amplitude noise common to both detectors is cancelled in the

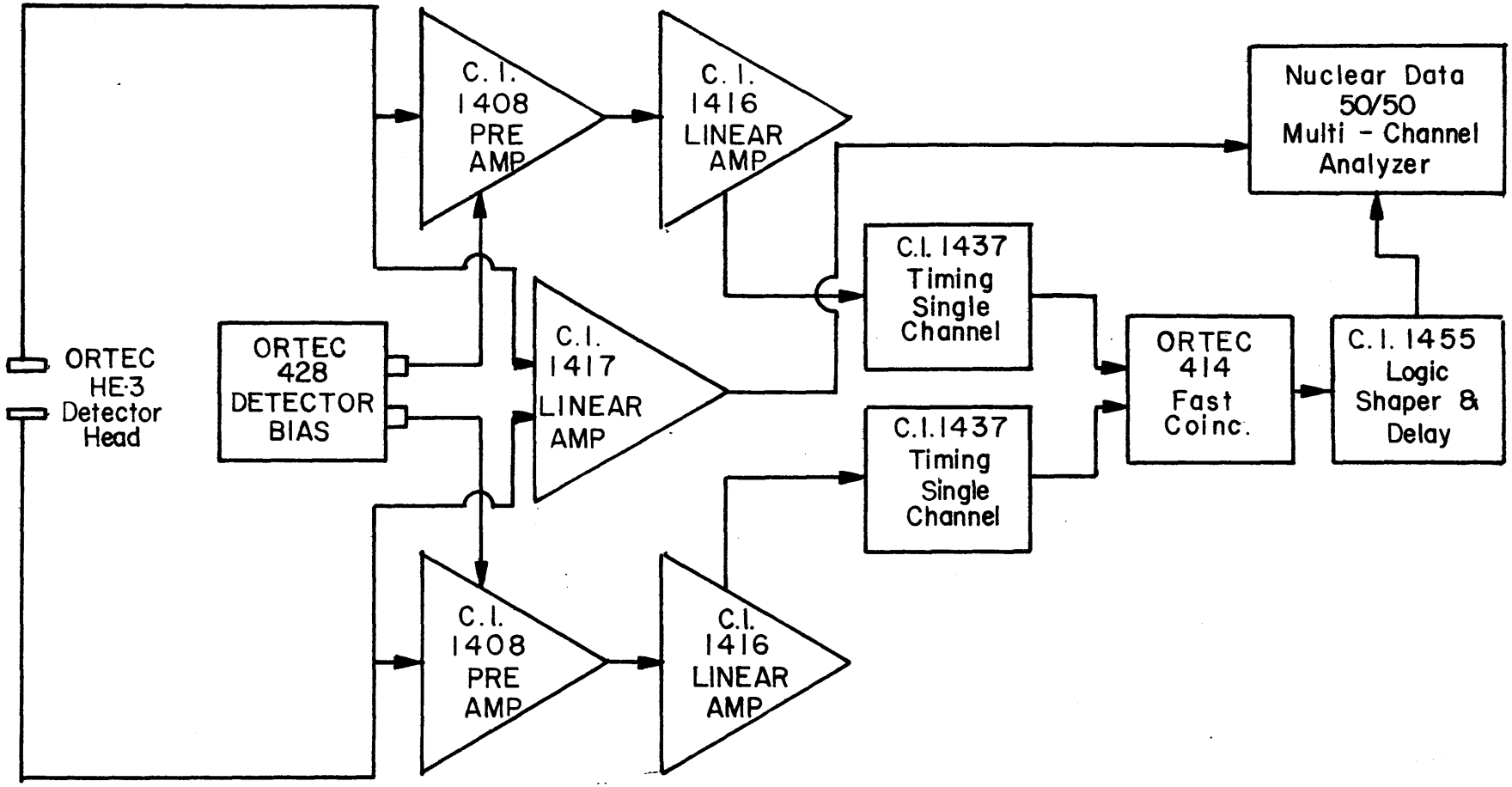

FIG. 2.10 He-3 Neutron Spectrometer, Difference Method Electronic System

subtraction process. Similarly, those gamma events which cause the same or nearly the same ionization in both detectors are rejected, improving the gamma discrimination. In the present work the cables that bring the signals from the preamplifiers to the amplifier were about 200 meters long; but since they share a common cable run they pick up the same noise, which is eliminated with the difference technique.

2.5.2 Improvements in Resolution

The equations for the kinematics of the reaction show that the difference between the product energies changes much more rapidly at neutron energies in the low keV region than does the sum of the product energies. Replacement of the sum amplifier by a difference amplifier should therefore improve the energy resolution. The difference energy is defined as

$$\Delta = E_3 - E_4 = Q + E_1 - 2E_4 \cdot \qquad (2.43)$$

Since

$$E_3 = 2V^2 + W + 2V\sqrt{V^2 + W} \quad ,$$

$$\Delta = (4a^2\cos^2\Theta + 2C - 1)\, E_1 +$$

$$4a\cos\Theta\sqrt{E_1}\ \sqrt{(a^2\cos^2\Theta + C)\, E_1 + bQ}$$

$$+ (2b - 1)\ Q \qquad (2.44)$$

For the $_2He^3(n,p)T$-reaction, E_3 and E_4 represent the proton and triton kinetic energy, respectively. Table (2.2) shows a comparison of the sum and the maximum difference energy ($\theta = 0^o$) of the charged particles for different neutron energies.

The difference energies shown in Table (2.2) are for a system with no energy discriminator. With a discriminator setting (E_{Disc}) the difference energy becomes

$$\Delta_{max} = Q + E_1 - 2E_{Disc} \tag{2.45}$$

Table (2.3) shows the effect of the discriminator level on the maximum difference energy of the charged particles for different neutron energies. It is important to observe that the value of Δ_{max} for $E_4 = E_{Disc}$ does not correspond to $\theta = 0^o$, but to that angle at which the triton particle has enough kinetic energy to satisfy the discriminator setting. This produces smaller values for Δ_{max} than with no discriminator. Therefore, the case with discriminator setting is less sensitive to low-energy neutrons, since the change in Δ with respect to the neutron energy is smaller than with no discriminator.

2.5.3 Derivation of the Response Function

The equation relating the measured difference spectrum to the incident neutron flux is

$$M(\Delta) = N \int_0^\infty \varepsilon(E)P(E,\Delta)\sigma(E)\phi(E)dE \tag{2.46}$$

TABLE 2.2

He-3 SYSTEM - COMPARISON OF DIFFERENCE METHOD AND SUM METHOD

E_1 (keV)	E_3 (keV)	E_4 (keV)	Δ^*_{max} E_3-E_4 (keV)	E_3+E_4 (keV)
0	573.	191.	382.	764.
0.5	582.	182.5	399.5	764.5
1.0	586.	179.	407.	765.
2.0	591.	175.	416.	766.
3.0	595.	172.	423.	767.
10.0	617.	157.	460.	774.
25.0	649.	140.	509.	789.
50.0	691.	123.	568.	814.
100.0	761.	103.	658.	864.
200.0	883.	81.	802.	964.
500.0	1212.	52.	1160.	1264.
750.0	1474.	40.	1434.	1514.
1000.0	1731.	33.	1698.	1764.
1500.0	2239.	25.	2214.	2264.

*For observation of products at $\Theta = 0^o$, $\phi = 180^o$

TABLE 2.3

He-3 SYSTEM - EFFECT OF THE DISCRIMINATOR ON THE DIFFERENCE ENERGY

E_1 (keV)	E_3 (keV)	E_4 (keV)	Δ^*_{max} E_3-E_4 (keV)	Without Disc. E_3-E_4 (keV)
0	573.	191.	382.*	382.
0.5	582.	182.5	399.5	399.5
1.0	586.	179.	407.*	407.
2.0	591.	175.	416.*	416.
3.0	595.	172.	423.*	423.
10.0	617.	157.	460.*	460.
25.0	639.	150.**	489.	509.
50.0	664.	150.	514.	568.
100.0	714.	150.	564.	658.
200.0	814.	150.	664.	802.
500.0	1114.	150.	964.	1168.
750.0	1364.	150.	1214.	1434.
1000.0	1614.	150.	1464.	1698.
1500.0	2114.	150.	1964.	2214.

**E_{Disc} = 150 keV

*For observation of products at $\Theta = 0^o$, $\phi = 180^o$

where

$M(\Delta)$ = Measured charged particle spectrum at a difference energy Δ

$\varepsilon(E)$ = detector efficiency

$P(E,\Delta)$ = Probability function: probability that a reaction which takes place at a neutron energy E contributes to the counting rate at Δ.

$\sigma(E)$ = Absorption cross section at energy E

$\phi(E)$ = Incident neutron flux

To unfold the measured spectrum it is necessary to obtain the probability function $P(E,\Delta)$.

$$P(E,\Delta)\, d\Delta = P(E,\Psi)\, d\Omega \qquad (2.47)$$

where

Ψ = Angle of emission of the particle M_3, in the center of mass coordinates.

$P(E,\Psi)$ = Probability that from a reaction which takes place at energy E there will emerge a particle M_3, in a solid angle $d\Omega$ about Ψ.

We have

$$P(E,\Delta)\, d\Delta = 2\pi d(\cos\Psi)\sigma_{\Omega}(E,\cos\Psi) \quad , \qquad (2.48)$$

where

$\sigma_{\Omega}(E,\cos\Psi)$ = Differential cross section of the reaction for neutrons of energy E.

If the reaction is isotropic in the center of mass a simpler expression is obtained for the probability function.

$$P(E,\Delta)\ d\Delta = \xi(E_3)dE_3 \tag{2.49}$$

or

$$P(E,\Delta) = \xi(E_3)\ \frac{dE}{d\Delta} = 0.5\xi(E_3) \tag{2.50}$$

where

$\xi(E_3)$ = Probability that the particle M_3 will carry away an energy dE, about E_3.

One also has

$$d\sigma = \sigma_\Omega(E,\cos\Psi)\ d_\Omega = \xi(E_3)dE_3 \tag{2.51}$$

If isotropic in the center of mass, $d\sigma/d\Omega$ is constant, as is $\sigma_\Omega(E,\cos\Psi)$; thus $\xi(E_3)$ is also constant (E1).

It is required that:

$$\int_{E_{3min}}^{E_{3max}} \xi(E_3)dE_3 = 1\ ,$$

or

$$\xi(E_3) = \text{const.} = \frac{1}{E_{3max}-E_{3min}}\ , \tag{2.52}$$

therefore

$$P(E,\Delta) = \frac{1/2}{E_{3max}-E_{3min}} \tag{2.53}$$

For $\Theta = 0^o$ in Eq. (2.5):

$$E_{3max} = 2a^2E_1 + bQ + cE_1 + 2a\sqrt{E_1}\sqrt{a^2E_1+bQ+cE_1}\ , \tag{2.54}$$

at $\Theta = 180^o$:

$$E_{3min} = 2a^2E_1 + bQ + cE_1 - 2a\sqrt{E_1}\sqrt{a^2E_1+bQ+cE_1}\ , \tag{2.55}$$

and

$$E_{3max}-E_{3min} = 4a\sqrt{E_1}\sqrt{a^2E_1+bQ+cE_1}\ , \tag{2.56}$$

or

$$P(E,\Delta) = \frac{1}{8a\sqrt{E_1}\sqrt{(a^2+c)E_1+bQ}} \tag{2.57}$$

For the $_2He^3(n,p)T$-reaction:

$$a = \frac{1}{4}, \quad b = \frac{3}{4}, \quad c = \frac{1}{2},$$

therefore

$$P(E,\Delta) = \frac{2/3}{\sqrt{E_1(E_1+0.75Q)}} \tag{2.58}$$

This probability distribution has a rectangular shape,

independent of the Δ energy.

Equation (2.53) can also be expressed as:

$$P(E,\Delta) = \frac{1}{\Delta_{max} - \Delta_{min}} \quad ,$$

where

$$\Delta_{max} = (4a^2 + 2c - 1)\, E_1 + 4a\sqrt{E_1}\,\sqrt{(a^2 + c)E_1 + bQ} + (2b - 1)Q \qquad (2.59)$$

$$\Delta_{min} = (4a^2 + 2c - 1)\, E_1 - 4a\sqrt{E_1}\,\sqrt{(a^2 + c)E_1 + bQ} + (2b - 1)Q \qquad (2.60)$$

and

$$\Delta_{max} - \Delta_{min} = 8a\sqrt{E_1}\,\sqrt{(a^2 + c)E_1 + bQ} \qquad (2.61)$$

For the $He^3(n,p)T$-reaction the cross section is assumed to be isotropic in the center of mass, since no evidence exists of any anisotropy in the energy range from 1 keV to 2 Mev (B10,R5,S4).

2.5.4 Effect of the Discriminator on the Probability Function

The discriminator settings of the TSCA described in section 2.5.2 will also affect the probability function. Those events for which the minimum kinetic energy ($\Theta = 180°$) of the triton product is less than E_{Disc} will not be registered. This means that the maximum proton energy will not correspond to the condition $\Theta = 0°$, but to the complement of the angle at wich $E_{4min} = E_{Disc}$. Figure (2.11) shows the magnitude of $P(E,\Delta)$ as a function of neutron energy for both cases (i.e. with and without discriminator). The use of the discriminator tends to increase the magnitude of the probability function and decrease the energy range of the distribution.

2.5.5 Effect of the Electronics on the Probability Function

So far only the difference (E_3-E_4) has been considered, but the electronics are unable to distinguish the case (E_4-E_3) for (E_4-E_3) positive. This affects the probability function.

The range of the probability function depends on the neutron energy. For thermal neutrons the function shrinks to a delta function ($\Delta_{max}=\Delta_{min}$). As the neutron energy increases the range of the function also increases. For neutron energies greater than 1.18 Q the absolute value of Δ_{min} becomes greater than Q/2. The electronics will register these events as if their difference energy were in effect greater than Q/2 instead of less than (-Q/2). The magnitude of the probability will therefore be twice the value given by Eq. (2.58) over the interval (Δ_{min} - Q/2), as shown in Fig. (2.12).

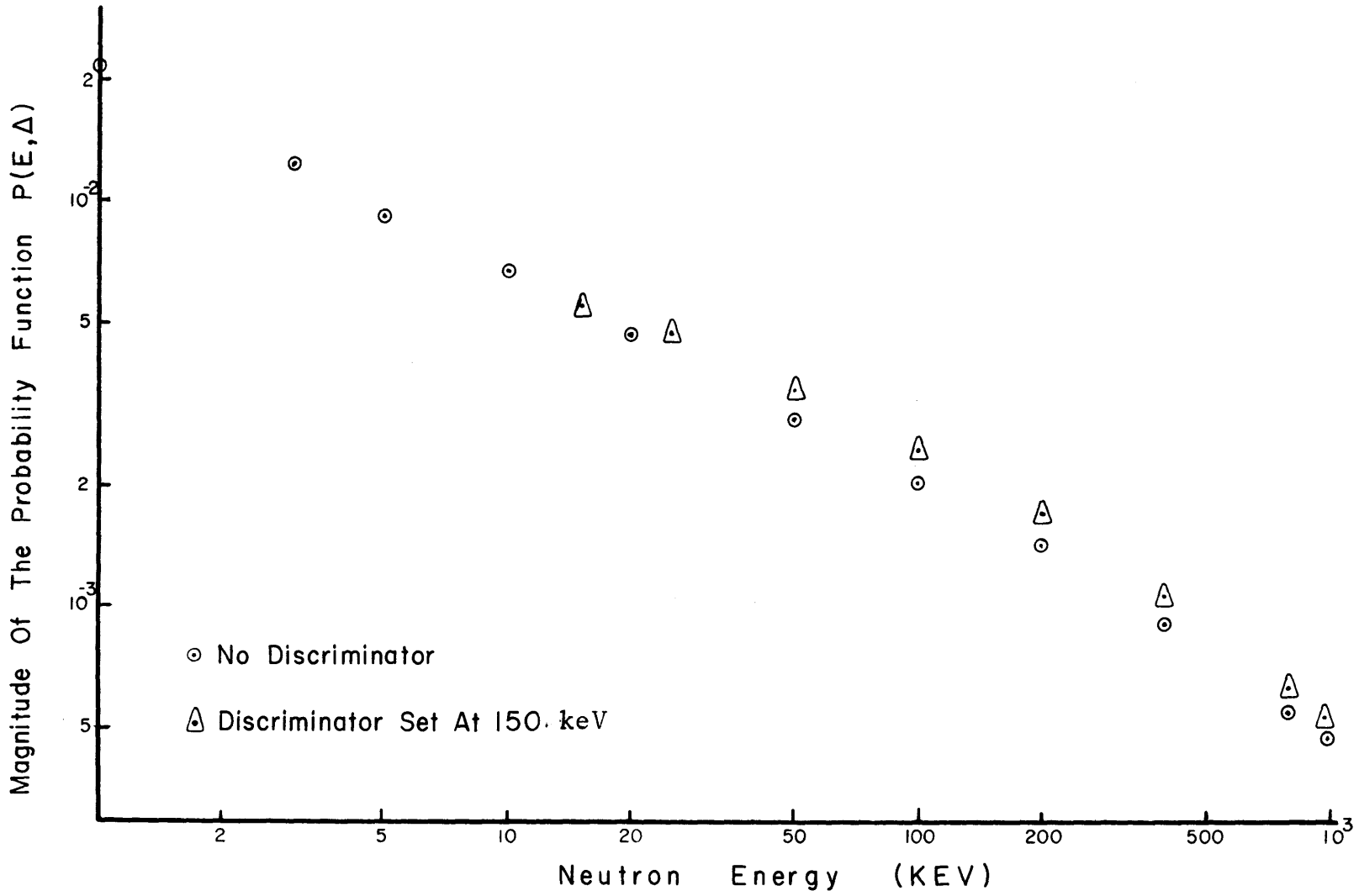

FIG. 2.11 Magnitude Of The Probability Function P(E,Δ) For The He-3 System Operating In The Difference Mode

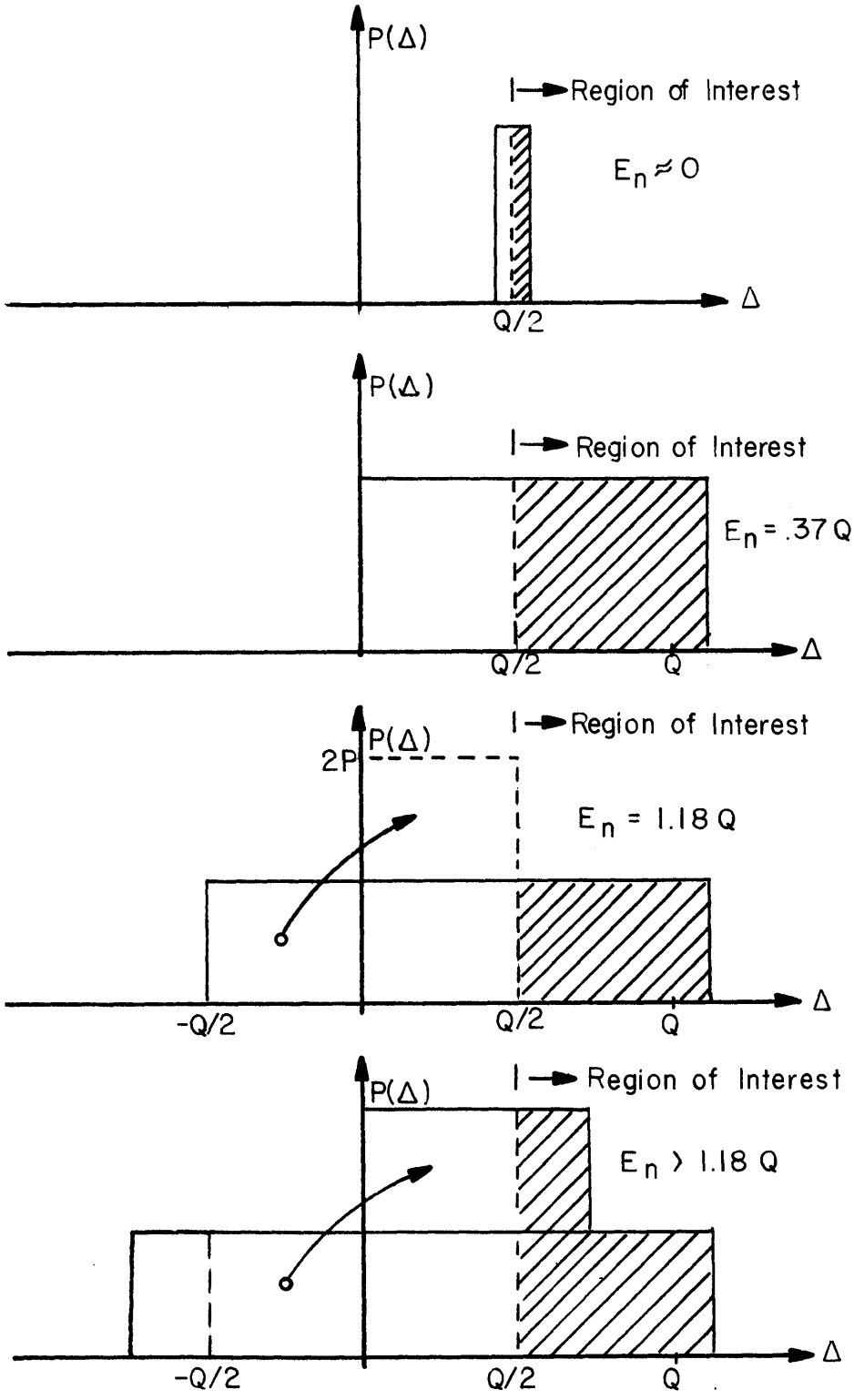

FIG. 2.12 The Construction Of The Detector Probability Function (He −3, Difference Technique)

2.5.6 Energy Calibration

The channel-energy calibration was obtained by exposing the detector to a thermal flux in the MITR Thermal Facility Port 2CH1. When only one detector is connected to the amplifier operating in the difference mode, a peak is obtained in the channel corresponding to the proton energy of 573 keV. The variable resistance in one of the amplifier inputs is adjusted such that each detector will produce a peak in the same channel of the multichannel analyzer. This will compensate for any small difference in the detector or in the preamplifiers before further processing of the signal. If both detectors are connected to the amplifier a peak is obtained corresponding to a difference energy of Q/2 or 382 keV. A linear relationship is assumed to provide the energy calibration of each channel. A precision pulser (Ortec 448) was used to check the linearity assumption.

The transformation from difference energy to neutron energy is derived from Eq. (2.59):

$$a_1 E_1^2 + b_1 E_1 + c_1 = 0 \quad , \tag{2.62}$$

where

$$a_1 = (2c-1)^2 - 8a^2 \tag{2.63}$$

$$b_1 = -2(4a^2+2c-1)\,(\Delta_{max}+Q) + 4(2c-1)bQ \tag{2.64}$$

$$c_1 = (\Delta_{max} - (2b-1)Q)^2 \tag{2.65}$$

For the $_2He^3(n,p)T$-reaction, Eq. (2.62) becomes

$$E_1^2 + (\Delta_{max}+Q)\ E_1 - \frac{(2\Delta_{max}-Q)^2}{2} = 0 \tag{2.66}$$

Those neutron energies at which the minimum kinetic energy of the triton is less than the discriminator level are related to the difference energy by Eq. (2.45).

2.5.7 Unfolding Using the Derivative Technique

The integral equation that relates the measured difference spectrum and the incident neutron flux is

$$M(\Delta) = N_o \int_o^\infty \varepsilon(E^1)\ P(E^1,\Delta)\sigma(E^1)\ \phi(E^1)dE^1 \tag{2.67}$$

In preceeding sections expressions for $\varepsilon(E)$ and $P(E,\Delta)$ have been discussed. The cross section $\sigma(E)$ for the $_2He^3(n,p)T$-reaction was obtained from reference (B10).

Now that all the terms of the expression are known, Eq. (2.67) can be solved for $\phi(E)$. Two ways of solving it will be considered: the derivative method, and the integral method. The first method is discussed in this section; and the latter is explained in the next section.

To take into account the effect of the electronics,

Eq. (2.67) is written as:

$$M(\Delta) = \int_{E^1=E}^{E^1=E_L} \varepsilon(E^1)\ P(E^1,\Delta)\ \sigma(E^1)dE^1 +$$

$$\int_{E^1=E_L}^{E_{max}} \varepsilon(E^1)\ P_o(E^1,\Delta)\ \Sigma(E^1)\ \phi(E^1)dE^1 \quad ,$$

where

E_L = Neutron energy at which the effect of the electronics will double the value of the probability function.

E_{max} = Maximum neutron energy.

$P_o\ (E^1,\Delta) = 2P(E^1,\Delta)$ = Probability function.

Applying Leibnitz's Rule:

$$\frac{dM(\Delta)}{dE} = + \varepsilon(E_L)\ P(E_L,\Delta)\ \Sigma(E_L)\ \phi(E_L)\ \frac{dE}{dE}L$$

$$- \varepsilon(E)\ P(E,\Delta)\ \Sigma(E)\ \phi(E)$$

$$- \varepsilon(E_L)\ P_o(E_L,\Delta)\ \Sigma(E_L)\ \phi(E_L)\ \frac{dE}{dE}L \quad ,$$

$$\frac{dM(\Delta)}{dE} = - \varepsilon(E_L)\ P(E_L,\Delta)\ \Sigma(E_L)\ \phi(E_L)\ \frac{dE}{dE}_L$$

$$+ \varepsilon(E)\ P(E,\Delta)\ \Sigma(E)\ \phi(E) \quad , \tag{2.68}$$

or

$$\phi(E) = - \frac{dM(\Delta)}{dE} \quad \frac{1}{\varepsilon(E)P(E,\Delta)\Sigma(E)}$$

$$+ \frac{P(E_L,\Delta)\Sigma(E_L)\phi(E_L)}{\varepsilon(E)P(E,\Delta)\Sigma(E)} \quad \frac{dE}{dE}_L \tag{2.69}$$

At high neutron energies the second term vanishes and the expression becomes

$$\phi(E) = - \frac{dM(\Delta)}{dE} \quad \frac{1}{P(E,\Delta)\Sigma(E)\varepsilon(E)} \tag{2.70}$$

The neutron flux is calculated first at high neutron energies (E > 1 MeV) using Eq. (2.70). In other words, the measured data is unfolded starting with the highest channel. As the energy is decreased the second term of Eq. 2.69 becomes important and Eq. 2.69 is used to continue the unfolding down to the lowest neutron energy. A computer program called DIFFE was written to perform the unfolding

of the measured spectrum (Appendix C).

2.5.8 Unfolding Using the Integral Technique

The integral equation (2.67) can be replaced by the (approximate) Matrix equation

$$M_i(\Delta) = \sum_{j=1}^{n} K_{ij} \; P_{ij} \; \phi_j \qquad (2.71)$$

or

$$\bar{M} = \bar{A} \; \bar{\phi} \qquad (2.72)$$

where

K_{ij} is a square n x n matrix

$$A_{ij} = \sum_j K_{ij} \; P_{ij} \qquad (2.73)$$

$\bar{A}$ is known as the detector response matrix. The first task is to determine the elements of the matrix $\bar{A}$ for a particular problem. In this case they are calculated from the kinematics equations of the reaction discussed in section 2.2. The second portion of the analysis is common to all problems of this type, i.e. the solution of Eq. (2.72) for $\bar{\phi}$, the neutron flux. The equation cannot be

solved by simply inverting matrix $\bar{A}$ because of the instability of the solutions obtained (for example negative fluxes with large oscillations). The Gold unfolding technique is used; this is discussed in detail in reference (G1).

A set of evenly spaced (Δ_{max}) is chosen to construct a triangular detector response matrix based on the probability function. This matrix is used to unfold the distribution $M(\Delta)$; the equation (2.72) is multiplied by the transpose of the detector response matrix.

$$\bar{A}^T\bar{M} = \bar{A}^T\bar{A}\bar{\phi} \qquad (2.74)$$

It has been found that for a diagonally dominant response matrix, A^TA is better suited for unfolding than is $\bar{A}$, the response matrix itself. A trial solution is estimated (any reasonable guess), and the result checked against the arresting condition. The arresting condition is defined as the square root of the sum of the variance of each measurement. In other words, convergence is achieved when the test solution and the measured distribution agree within the statistical uncertainty of the measurements. If the arresting condition is not satisfied the result is used as a second guess. An iterative loop is followed until the criterion for convergence is satisfied or the maximum

number of iterations is reached. A computer program MATRIX was written to solve the problem and is discussed in Appendix A.

2.5.9 Neutron flux Measurements

The He-3 semiconductor detector operating in the difference mode was placed in the second row of Blanket Mockup No. 2 to measure the neutron flux. The experimental conditions are the same as described in section 2.4.4. Figure 2.13 shows the signal plus background and background measurements prior to analysis.

The measured spectrum was unfolded using both the Integral Technique and the Derivative Technique. The results are in good agreement (see Fig. 2.14). The derivative technique provides an output flux per unit lethargy at a sequence of energies having a fixed fractional spacing. The spacing is input as DINC in the DIFFE program (Appendix C). The integral technique provides an output flux per unit lethargy at fifty energy values fixed by the MATRIX Program (Appendix A). The measured neutron spectrum shows a small fraction of low energy neutrons and then rises steadily to reach a broad peak around 300 keV. It is important to recall that the existence of a discriminator setting affects the capability of the system to measure low energy neutrons accurately.

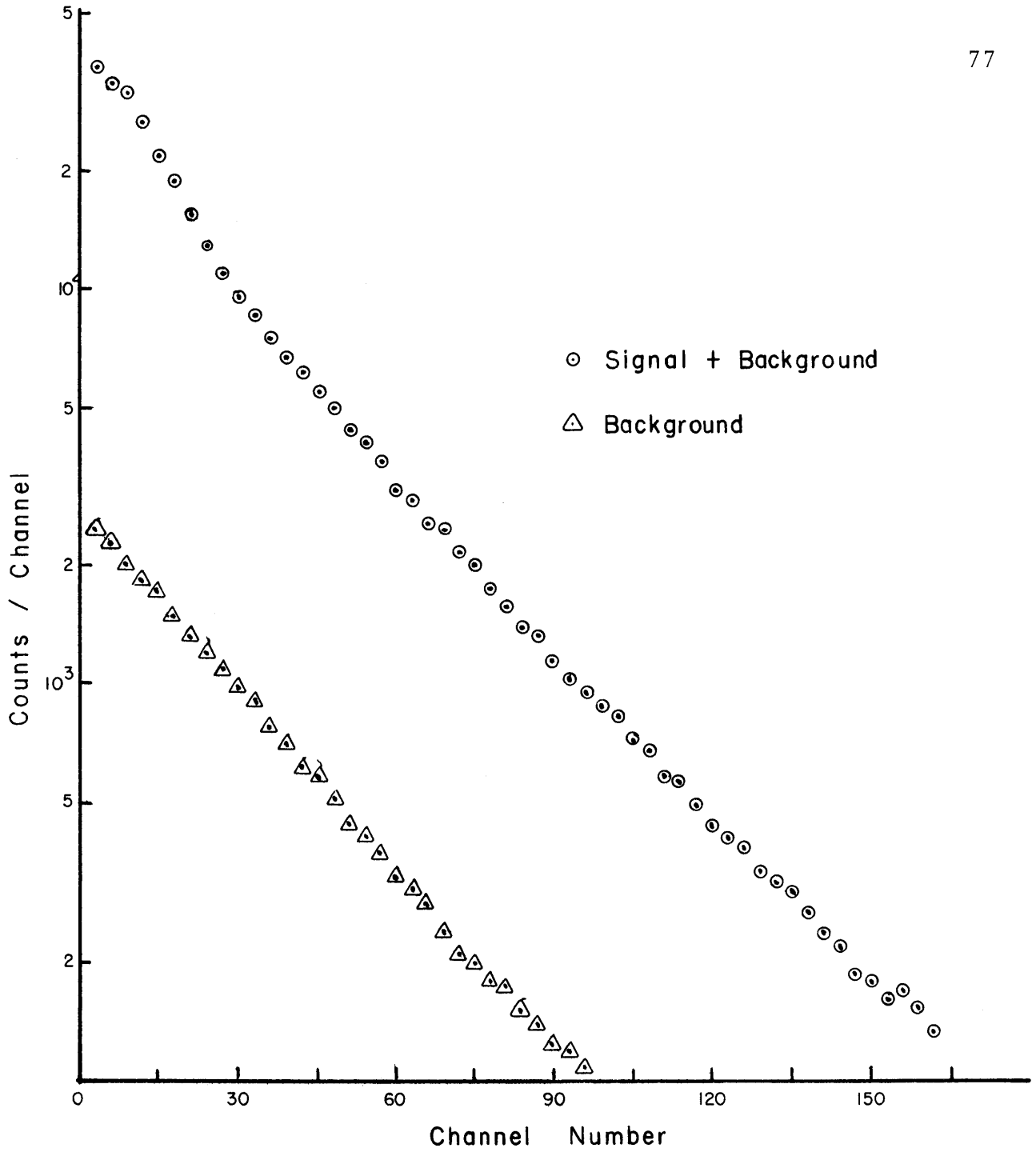

FIG. 2.13 Signal Plus Background And Background Measurements Using He-3 System Operating In The Difference Method

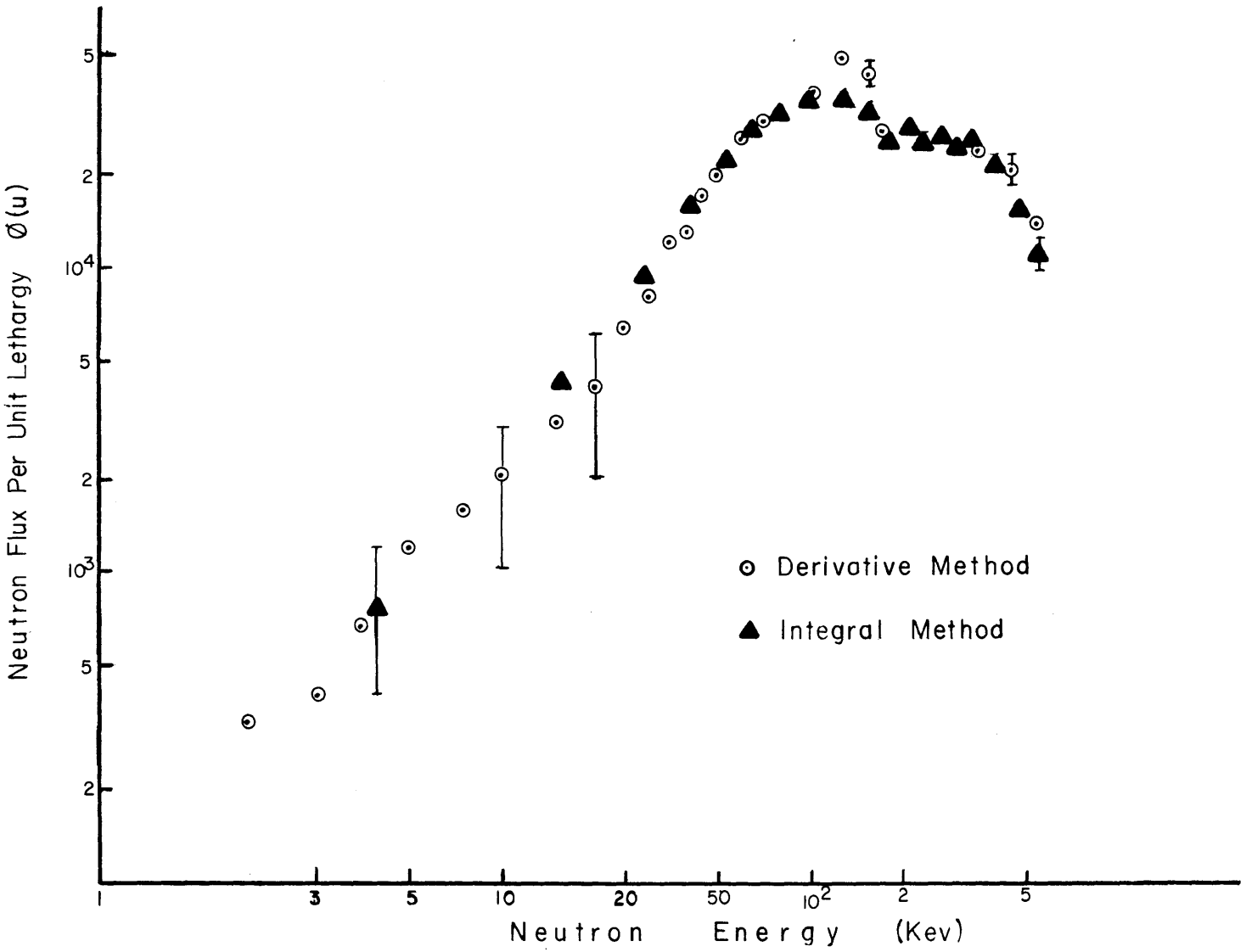

FIG. 2.14 Neutron Spectrum In The Blanket Mockup NO. 2 - He-3 System Difference Method

2.5.10 Improvement in Gamma Discrimination

An experiment was set up in the irradiation facility which uses the neutron beam port 4TH1 of the M.I.T. Research Reactor (H2), to compare the gamma discrimination of the Difference Method and the Sum Method. A uranium metal sample 1/4 in. diameter, and 4 in. long having 1.016 w% U-235 enrichment was placed in the thermal neutron beam. A lead collimator 1.75 feet long with a 0.5 in. hole was placed between the sample and the detector. The detector was shielded with cadmium and boron to absorb scattered thermal neutrons.

The signal produced in the detector by the uranium prompt capture gammas was recorded in a multichannel analyzer using the Sum Method and the Difference Method. The results show that with the Difference Method the counts/channel in the region of interest were reduced by a factor of eight to ten (Fig. 2.15). The quantitative interpretation of these results is difficult because fast neutrons from U-235 fission are also present, thus not all is spurious gamma signal. Also for a given neutron energy the Sum Method tends to concentrate the counts around a few channels, since there is a unique relationship between neutron energy and measured energy; on the other hand, the Difference Method tends to spread the counts over a larger number of channels.

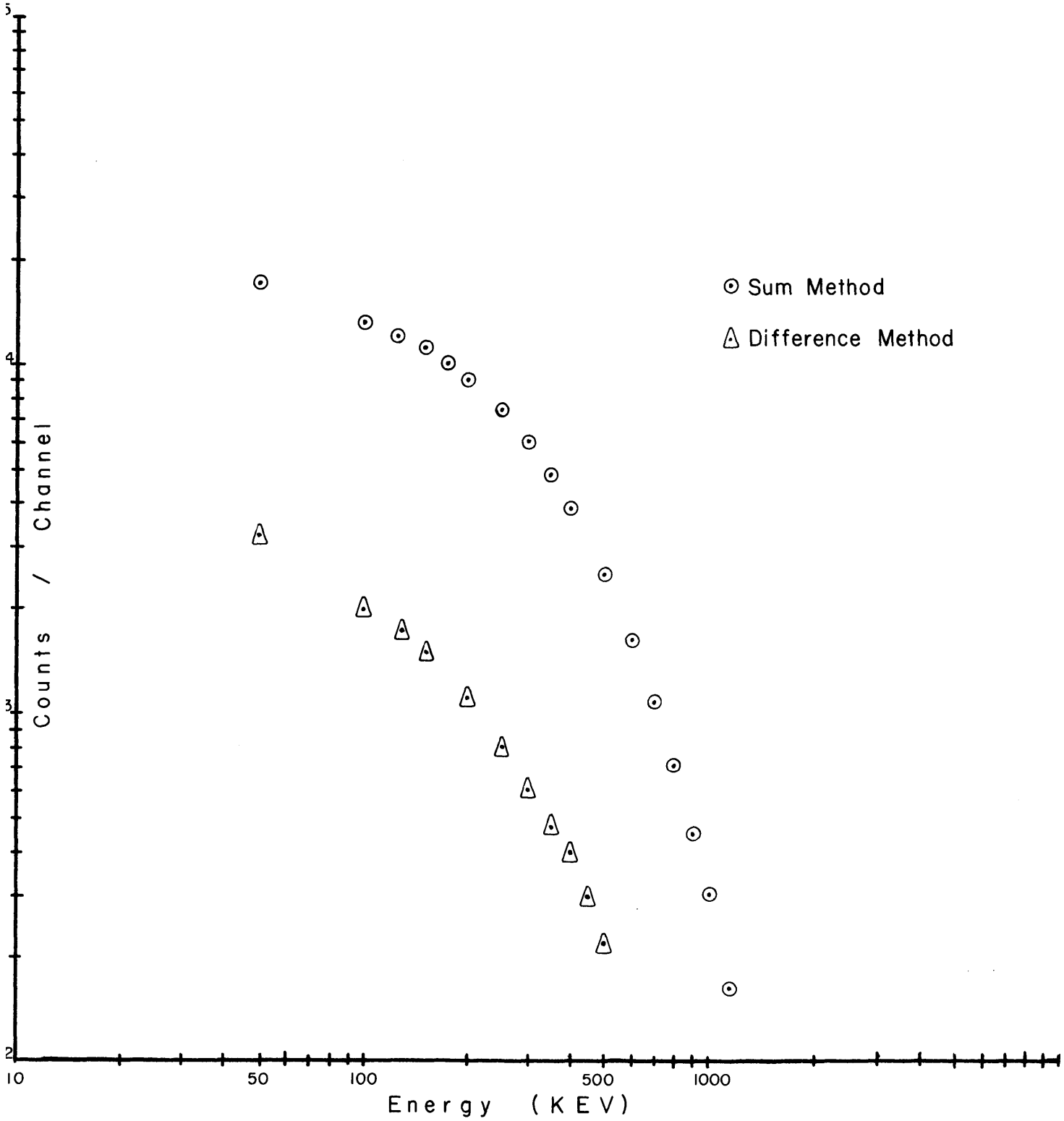

FIG. 2.15 Prompt γ Background From Uranium Sample

A similar experiment was done with a 5.2 mci Co-60 source. In this case the Difference Method showed a decrease in the counts/channel in the region of interest by a factor of four to five.

The experimental data taken in Blanket Mockup No. 2 using the Sum and Difference Method can also be used to assess the improvement in rejection of unwanted signal. Define the ratio SN, for a given neutron energy as

$$SN = \frac{\text{foreground - background}}{\text{background}}$$

where

foreground = measurement taken with He-3 gas in the detector head

background = measurement taken without He-3 gas in the detector head.

In the Sum Method the signal-to-background ratio, SN, varies from 2.2 to 5 in the energy region from 200 keV to 1 MeV. For the Difference Method SN changes from 8.6 to 10.0 over the same energy region. This clearly shows an improvement in the gamma and noise rejection.

2.5.11 Error Analysis

The errors associated with this method for energies higher than 200 keV are essentially the same as for the

Sum Method. There are minor differences; the better signal-to-background ratio and the fact that the counting errors are averaged over an energy interval give a slight improvement. The estimated errors for the low energy region range from 10% to 55%. The energy region below 50 keV has a large error (55%) because of the uncertainty in the discriminator level (±20 keV).

2.6 SUMMARY

The He-3 semiconductor detector operating in the Sum and Difference Modes was used to measure the neutron spectrum in Blanket Mockup No. 2. The Sum Method covers an energy range from 200 keV to 1.3 MeV. The Difference Method extends the low energy limit and covers an energy range from 10 keV to 1.1 MeV. The overlap region for both techniques (200 keV to 1.1 MeV) shows good agreement between the two neutron flux measurements (Fig. 2.16). The Difference Method improves the gamma and noise discrimination.

The integral technique and differential technique used to unfold the difference spectrum are in good agreement over the entire energy range of the measurements. This consistency gives confidence in the procedures applied to each technique.

The uncertainty in the discriminator settings affects

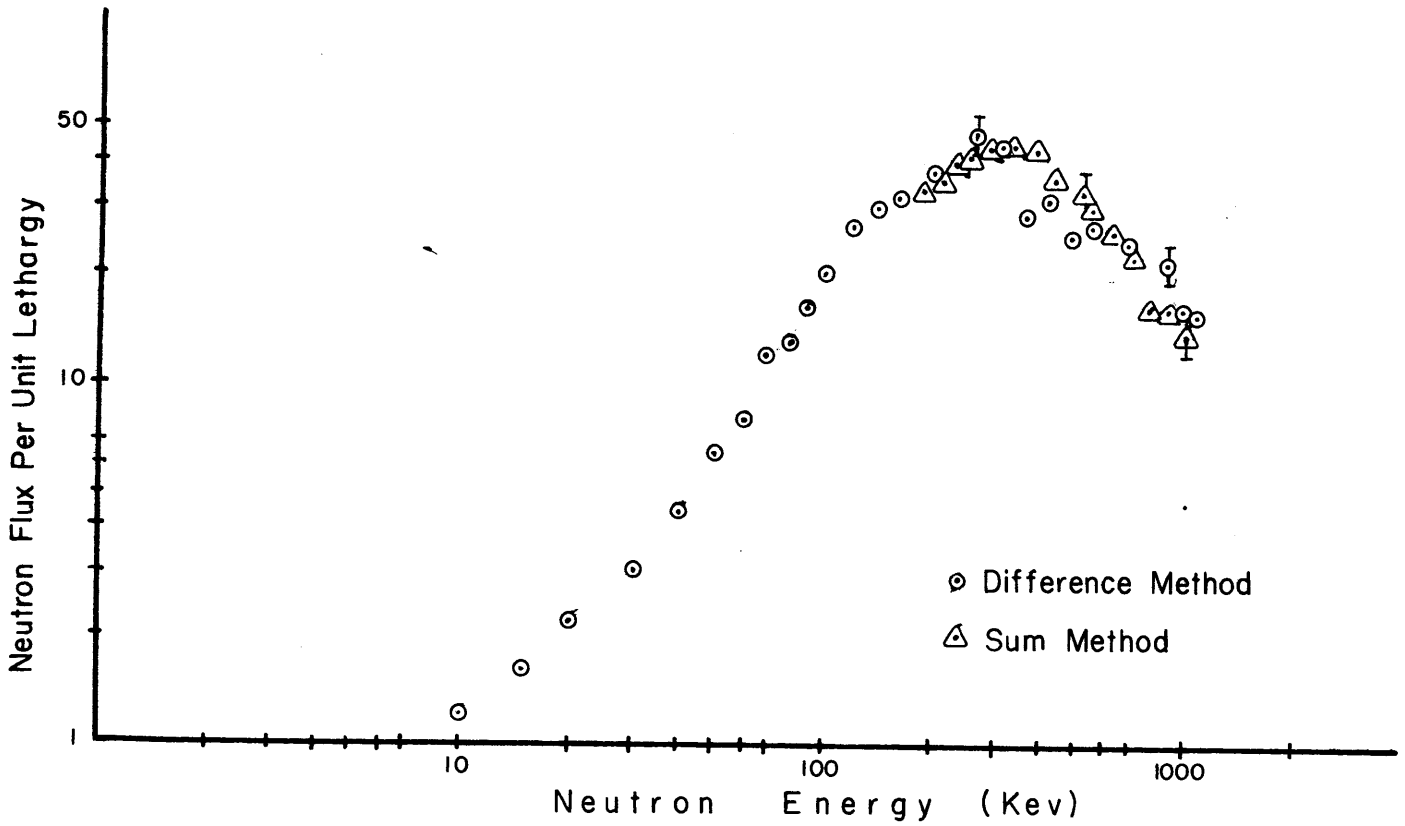

FIG. 2.16 Neutron Flux Measurement In The Blanket Mockup NO. 2 - He-3 System

the accuracy of the measurements in the low-energy region and reduces the sensitivity of the detector to low-energy neutrons.

Chapter 3

LITHIUM-6 SEMICONDUCTOR DETECTOR

3.1 INTRODUCTION

The compact and relatively simple design of the Li-6 Semiconductor sandwich spectrometer makes it well suited for in-pile measurements of fast neutron spectra. It has been used to measure fast neutron spectra in several low power reactors (B7,S2,W1) and it has produced reliable results from 0.5 MeV to about 8 MeV.

In this detector neutrons react with Li-6 nuclei to produce two charged particles, a triton and an alpha. If these particles are absorbed by the semiconductor detectors, each produces a pulse whose height is proportional to the energy deposited by the particle.

In this chapter, three different methods of operation of the detector are described to cover the energy range from 10 keV to 3 MeV: The Sum Method from 500 keV to 3 MeV, the Triton Method from 10 keV to 600 keV and the Difference Method from 10 keV to 600 keV.

A Cf-252 neutron source was used as a standard to calculate the response function of the detector. The corrections obtained with this source allow one to extend the low energy limit of the Sum Method down to 160 keV.

Finally, it should be noted that the high Q value of

the $^{6}L_{i}(n,\alpha)T$-reaction improves the gamma discrimination of the system in comparison with the He-3 system.

3.2 DETECTOR AND ELECTRONICS

The Li-6 Neutron Spectrometer consists of a sandwich configuration of two closely spaced (0.002 in.) surface barrier detectors (400 microns sensitive thickness and 240 mm^2 active area) with a thin layer (150 $\mu gm/cm^2$) of ^{6}LiF located between the detectors (I1). The size and shape of the detector head is similar to the Helium-3 system (Fig. 2.1), except that no vacuum valve is needed.

The system also includes a matched sandwich pair of silicon detectors without a Li-6 coating for determination of background. This permits subtraction of the majority of the coincident background events. The background is largely due to fast neutron reactions in the silicon.

The electronics associated with this system is similar to the electronics used with the He-3 system. Only the settings of the linear amplifiers and the timing single channel analyzers are different.

3.3 SUM METHOD

3.3.1 Description of the Technique

The Li-6 semiconductor detector is based on the reaction

$$ {}_{0}n^{1} + {}_{3}Li^{6} \longrightarrow {}_{1}H^{3} + {}_{2}He^{4} + Q \qquad (3.1) $$

The alpha and triton are detected in the two semiconductor

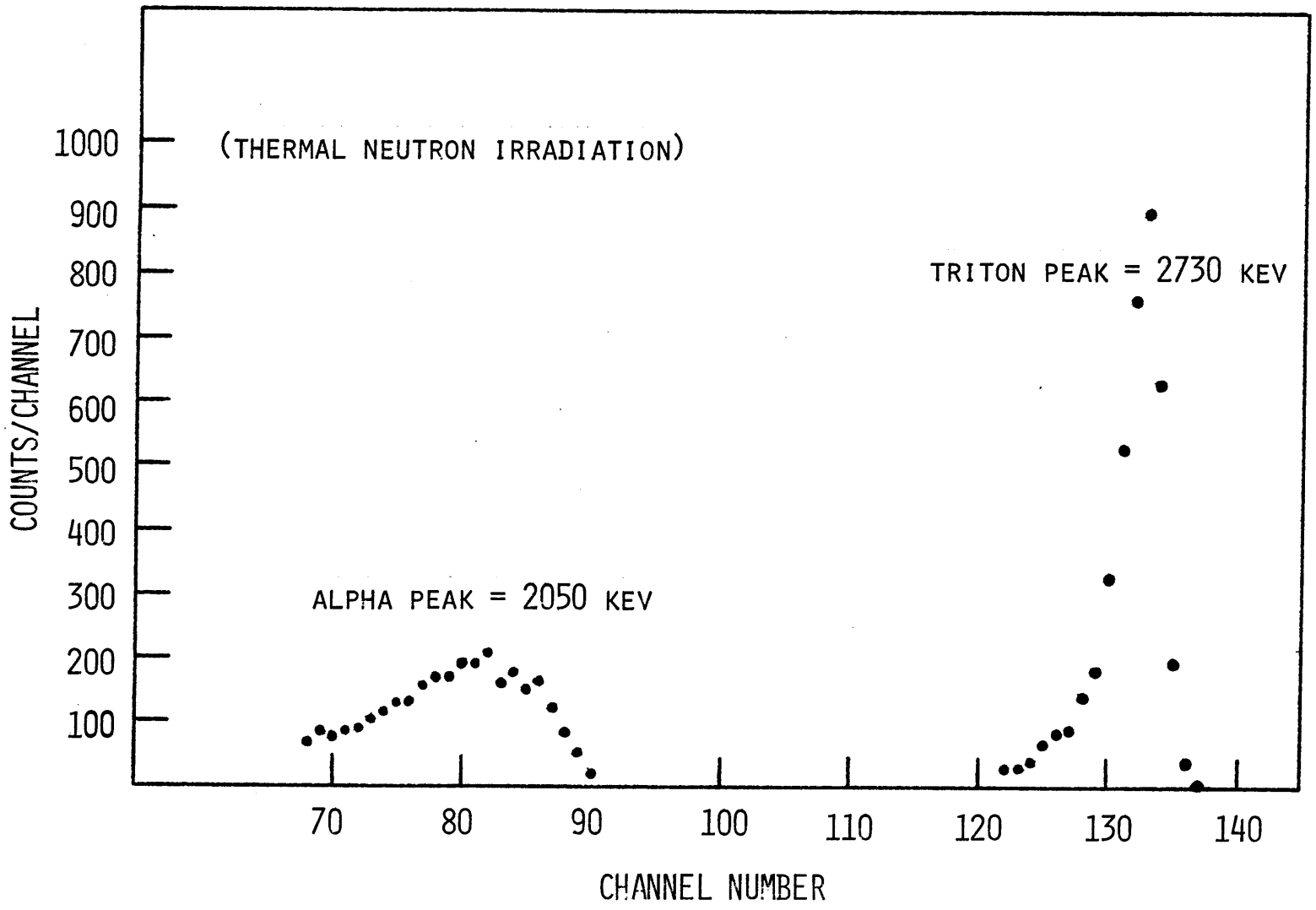

FIG. 3.1 ALPHA AND TRITON PEAKS FOR THE $^{6}Li(n,\alpha)_{1}H^{3}$ REACTION

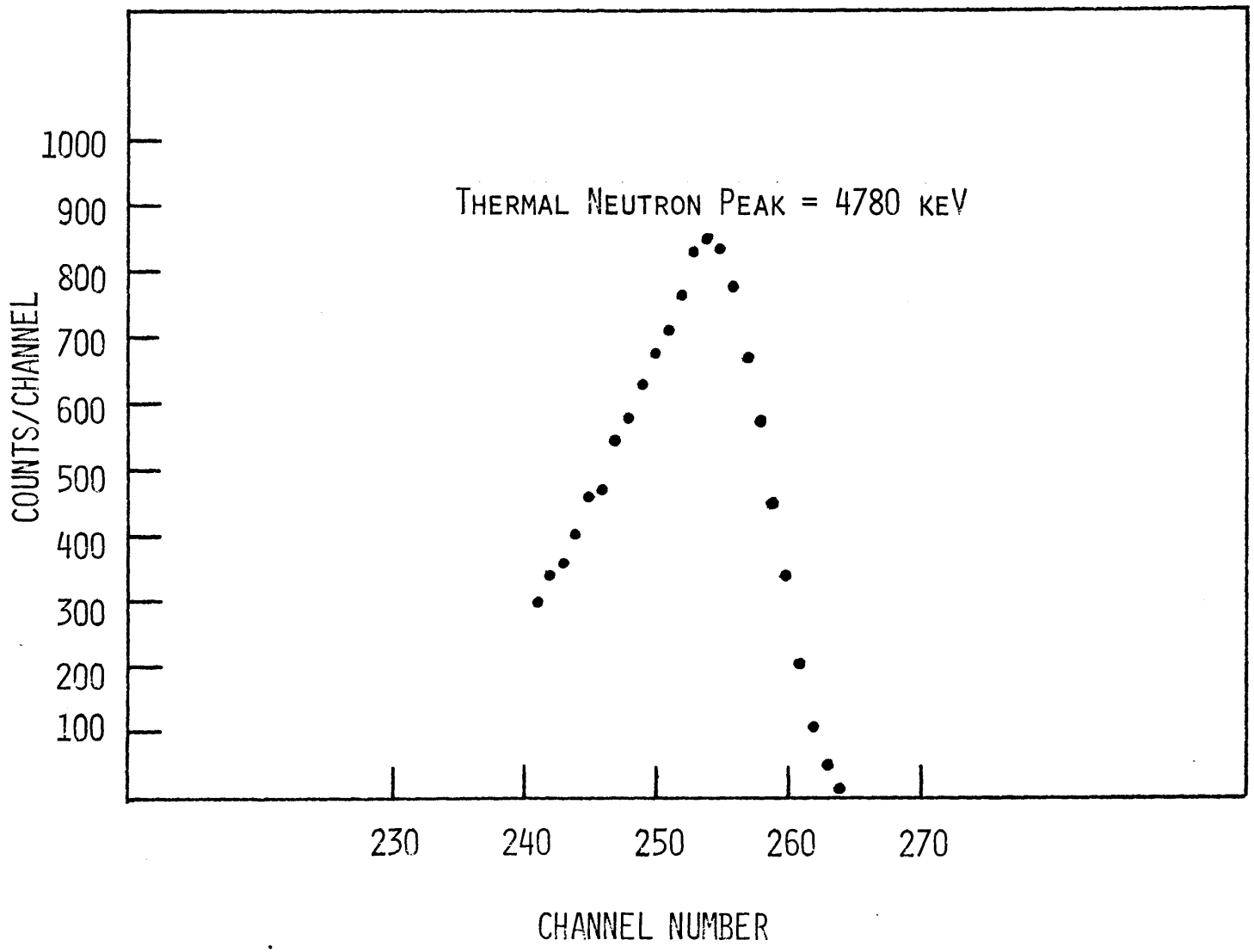

FIG. 3.2 THERMAL NEUTRON PEAK FROM THE $^{6}Li(n,\alpha)_{1}H^{3}$ REACTION

detectors and the total energy shared by these particles is indicated by summing in coincidence the output pulse from the two detectors. The amplitude of the sum pulse thus has a one-to-one correspondence with the energy of the incident neutron. The neutron energy is equal to the total energy minus the Q value of the reaction (4.78 MeV).

The detector was calibrated in the thermal column facility of the MITR, port 2CH1. Each individual detector was tested in turn to establish its response to the alpha and triton particles. Figure 3.1 shows the alpha and triton peaks obtained for a single detector. The gain of the linear amplifiers was then adjusted so that the pulse heights for the triton peaks were the same for both detectors.

The triton peak corresponds to 2.730 MeV and the alpha peak to 2.050 MeV. The full coincidence circuit was then connected to obtain the thermal neutron peak shown in Fig. 3.2, which corresponds to 4.78 MeV. These three points then allowed construction of the linear relationship between channel and energy shown in Fig. 3.3. A correction was applied to the first and last points to take into account the average energy lost by the alpha particle in the Li-6 foil, which is about 125 keV for this detector.

The kinetic equations discussed in section 2.4 apply to the above reaction with the following substitutions:

$$a = \sqrt{\frac{3}{7}} \quad b = \frac{4}{7} \quad c = \frac{3}{7} \quad Q = 4.78 \text{ MeV} \qquad (3.2)$$

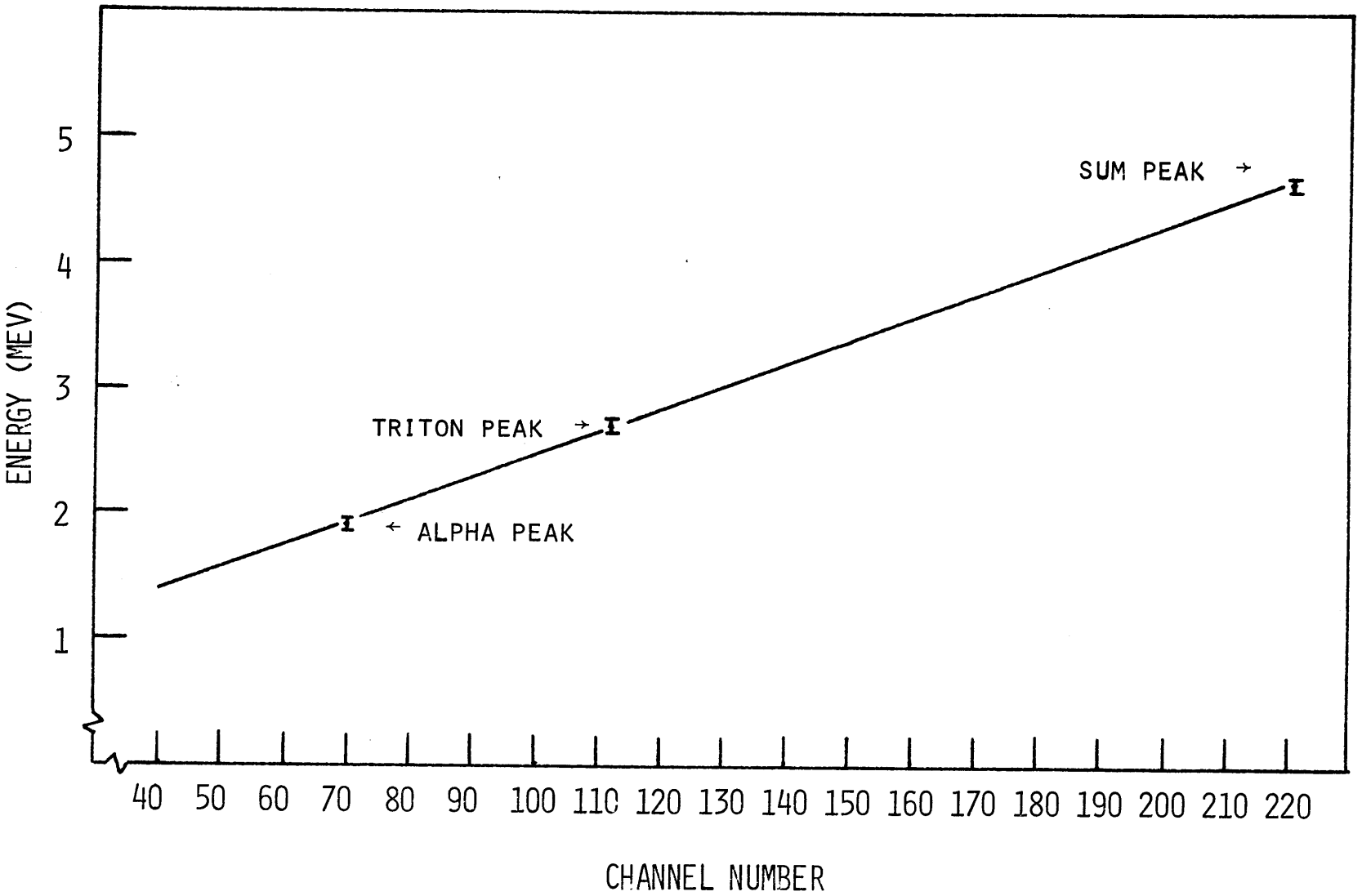

FIG. 3.3 Li-6 DETECTOR ENERGY CALIBRATION

3.3.2 Consideration of the Energy Discriminator Setting

To discriminate against low-energy gamma radiation and electronic noise, the baseline of the TSCA was set at 1.2 MeV. Considering the kinetics of the neutron reaction, it is found that the minimum alpha energy is 1.6 MeV. In Fig. 3.4, the minimum energy of both secondaries is shown as a function of neutron energy. It can be seen that the energy of neither of the products from the $^{6}Li(n,\alpha)T$-reaction falls below 1.2 MeV, which is the level of energy discrimination. Therefore, the discriminator settings do not reject any of the events of interest.

3.3.3 Unfolding Technique

The unfolding techniques described in section 2.4.3 also apply to the Li-6 semiconductor detector. The resolution function $R(E \rightarrow E')$ was calculated by exposing the detector to a thermal neutron flux, just as with the He-3 detector.

The neutron cross section for the $^{6}Li(n,\alpha)T$-reaction reported by different authors shows considerable discrepancies. The most recent set of cross sections, measured by I.C. Rickard (R2), was used in the energy range from 150 keV to 3.8 MeV. In the low-energy region the cross section is relatively well known, the data of Bame and Cubitt (B1) and Schwartz (S1) being in reasonable agreement. The latter was selected for the energy region from 1 keV to 150 keV. Tables (3.1) and (3.2) summarize the data used for the cross section.

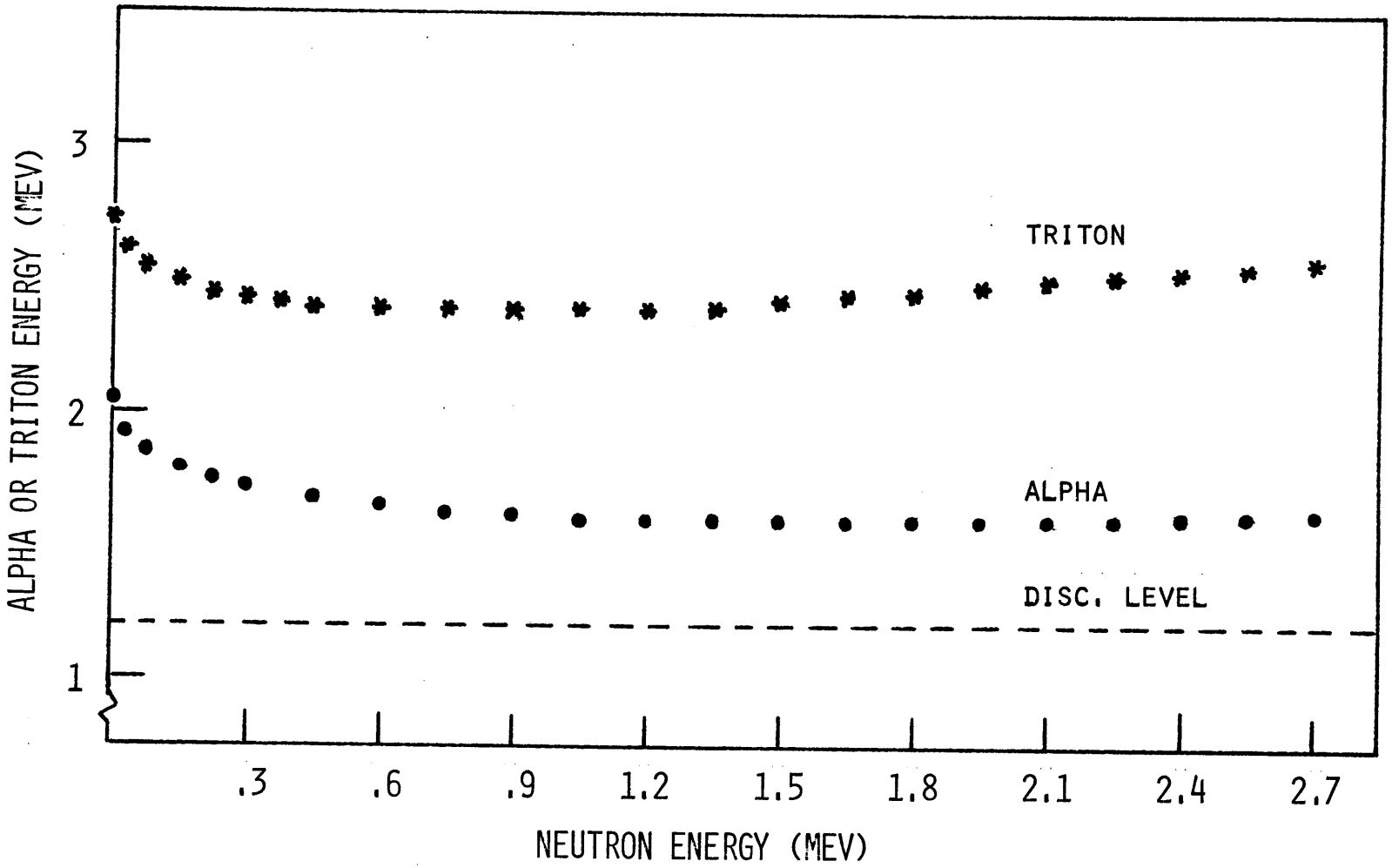

FIG. 3.4 MINIMUM KINETIC ENERGY OF THE TRITON AND ALPHA PARTICLES

TABLE 3.1

The $^{6}Li(n,\alpha)T$-Cross Section (150 keV to 3.8 MeV)

Energy (MeV)	Cross Section (barns)	Energy (MeV)	Cross Section (barns)
.156	0.778 (±.109)	1.351	0.165 (±.012)
.186	1.24 (±.20)	1.456	0.165 (±.012)
.212	1.93 (±.27)	1.562	0.162 (±.011)
.236	2.626 (±.37)	1.700	0.144 (±.012)
.260	2.094 (±.29)	1.772	0.150 (±.012)
.290	1.800 (±.25)	1.800	0.151 (±.012)
.312	1.097 (±.15)	1.877	0.152 (±.012)
.313	1.017 (±.14)	1.900	0.143 (±.012)
.340	0.848 (±.119)	1.918	0.140 (±.011)
.367	0.718 (±.100)	2.000	0.149 (±.012)
.376	0.640 (±.09)	2.094	0.147 (±.012)
.392	0.577 (±.081)	2.100	0.141 (±.011)
.422	0.476 (±.067)	2.188	0.136 (±.011)
.431	0.398 (±.056)	2.200	0.141 (±.011)
.442	0.428 (±.060)	2.289	0.129 (±.010)
.456	0.384 (±.054)	2.300	0.135 (±.011)
.468	0.354 (±.050)	2.393	0.117 (±.009)
.481	0.353 (±.049)	2.400	0.135 (±.011)
.490	0.369 (±.052)	2.500	0.122 (±.010)
.506	0.325 (±.046)	2.600	0.121 (±.010)
.522	0.318 (±.045)	2.700	0.116 (±.009)
.540	0.298 (±.042)	2.800	0.110 (±.009)
.562	0.277 (±.039)	2.900	0.112 (±.009)
.566	0.312 (±.044)	3.000	0.105 (±.008)
.590	0.275 (±.039)	3.100	0.102 (±.008)
.618	0.253 (±.035)	3.200	0.0957 (±.008)
.620	0.262 (±.026)	3.300	0.0962 (±.008)
.640	0.239 (±.024)	3.400	0.0983 (±.008)
.807	0.106 (±.014)	3.500	0.0917 (±.007)
.917	0.201 (±.014)	3.600	0.0831 (±.007)
1.026	0.192 (±.013)	3.700	0.0867 (±.007)
1.134	0.176 (±.012)	3.800	0.0785 (±.006)
1.242	0.174 (±.012)		

TABLE 3.2

The $^{6}Li(n,\alpha)T$-Cross Section (1 keV to 150 keV)

E_n (keV)	Cross Section (barns)	E_n (keV)	Cross Section (barns)
1	4.732	35	0.855
2	3.351	40	0.810
3	2.740	45	0.774
4	2.377	50	0.745
5	2.129	55	0.722
6	1.947	60	0.703
7	1.806	65	0.687
8	1.692	70	0.675
9	1.598	75	0.666
10	1.518	80	0.659
12	1.391	85	0.655
14	1.292	90	0.653
16	1.214	95	0.653
18	1.148	100	0.655
20	1.094	110	0.666
22	1.047	120	0.685
24	1.007	130	0.715
26	0.971	140	0.757
28	0.940	150	0.813
30	0.912		

3.3.4 Measurement of the Cf-252 Spontaneous-Fission Neutron Spectrum

The Cf-252 neutron spectrum has been measured in detail by various authors (T1,M3,G2). Most of them agree that the spectrum shape is Maxwellian,

$$\phi(E) = \sqrt{E} \exp(-E/T), \qquad (3.3)$$

so that it is completely specified by the single parameter T, the Maxwellian "Temperature". A number of measurements of this parameter have been made; Green (G2) summarized some of the values and remeasured the parameter using an experimental technique accurate enough to resolve the discrepancy. He concluded that T = 1.39 ± 0.04 MeV. This value and Eq. (3.3) were used in the present work as the standard neutron spectrum to test the Li-6 system operating in the Sum Method.

The source employed contains 7.2 μgm of Cf-252 and emits about 10^7 neutrons/sec. It is enclosed in a lead cylinder of 3/4 in. diameter and 1 1/2 in. length. The Cf-252 source was suspended from the ceiling of a large concrete vault (12 X 19 X 31 ft.) to minimize the effect of back-scattering from the walls. The detector was also placed in a holder surrounded with boron to absorb scattered neutrons.

The theoretical spectrum and the unfolded spectrum are shown in Fig. 3.5. The charged particle spectrum was unfolded using the computer program SUMMA (Appendix B). It can be seen that the agreement is good over most of the energy range observed. The larger discrepancies occur in the lowest energy

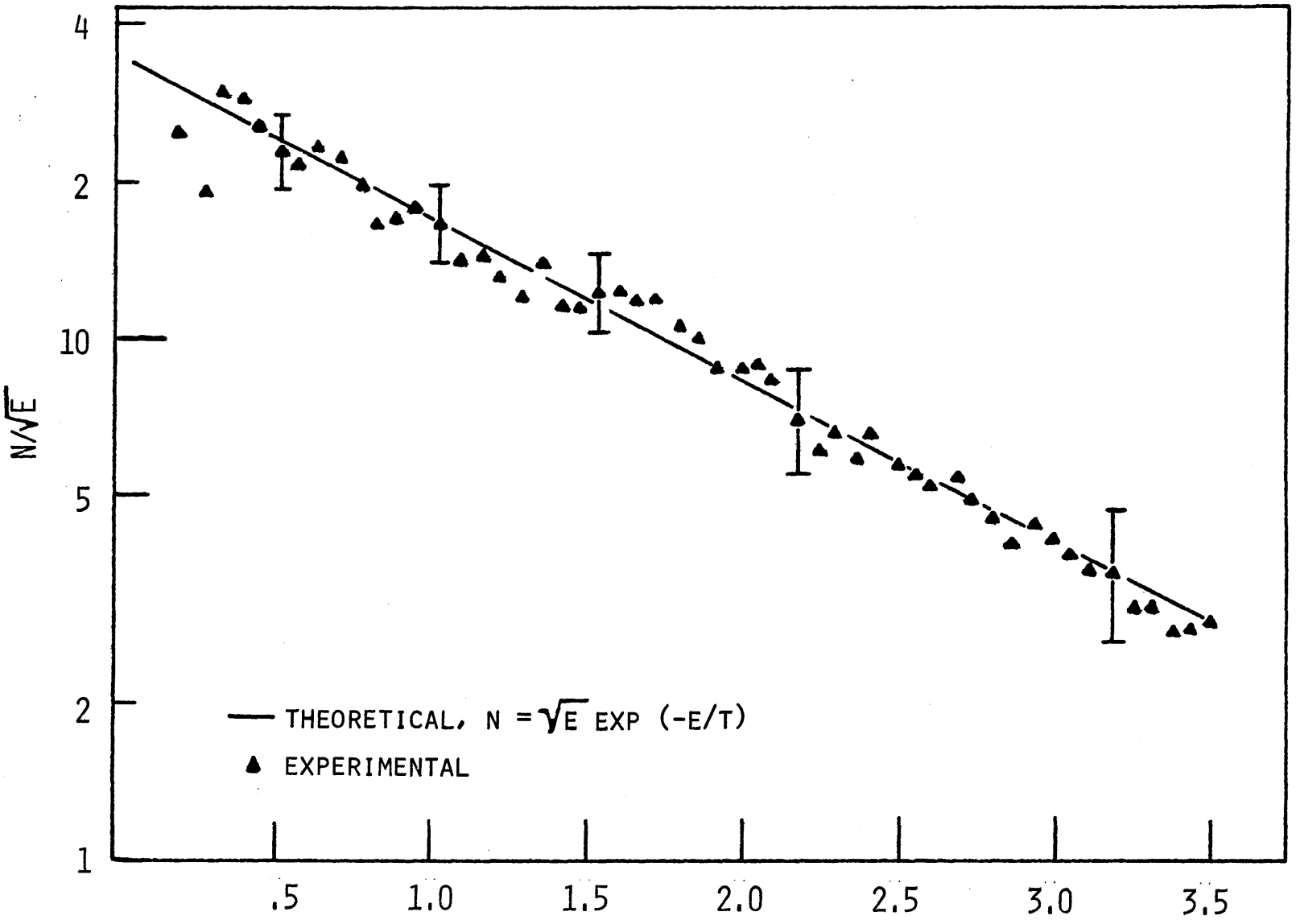

FIG. 3.5 CF-252 SPONTANEOUS NEUTRON SPECTRUM

region, due to the strong variation of the $^{6}Li(n,\alpha)T$-cross section around the broad resonance at 250 keV. The ratio of the theoretical spectrum to the measured spectrum is used to correct the systematic anomaly shown by the detector in the energy region from 10 keV to 400 keV. This correction was applied to the neutron flux measurements in Blanket Mockup No. 2, discussed in the next section.

3.3.5 Neutron Flux in Blanket Mockup No. 2

The Li-6 semiconductor detector was placed in the test subassembly, described in section 1.4, to measure the fast neutron flux. The signal plus background and background measurements are shown in Fig. 3.6. A large signal-to-background ratio is observed over the entire energy region; this ratio is larger for the Li-6 system than for the He-3 system due to the better gamma discrimination of the former. This was expected because of the higher Q value of the $^{6}Li(n,\alpha)T$-reaction.

The experimental data was collected in 160 channels of the multichannel pulse height analyzer and was unfolded with the SUMMA program. The computer program output was corrected by hand, using the response function of the detector (Fig. 3.7). The unfolded neutron spectrum covers an energy range from 160 keV to 3.1 MeV; it shows a broad peak around 350 keV and falls rapidly as the neutron energy increases (Fig. 3.8). Around 1 MeV a small dip is observed caused by the 1 MeV scattering resonance of oxygen. Two small peaks at 1.5 MeV and 2.3 MeV

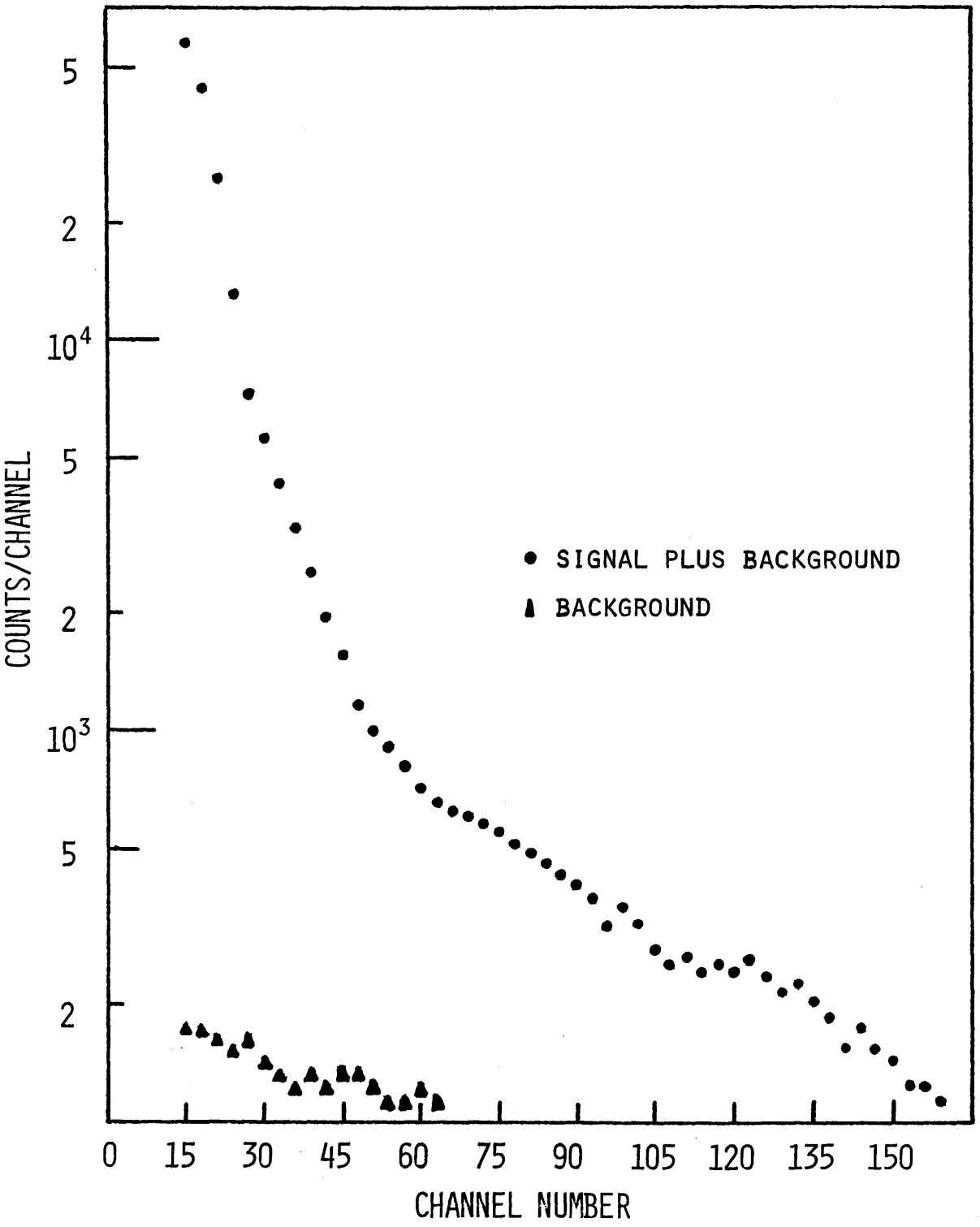

FIG. 3.6 SIGNAL+BACKGROUND AND BACKGROUND MEASUREMENTS USING THE Li-6 DETECTOR OPERATING IN THE SUM MODE

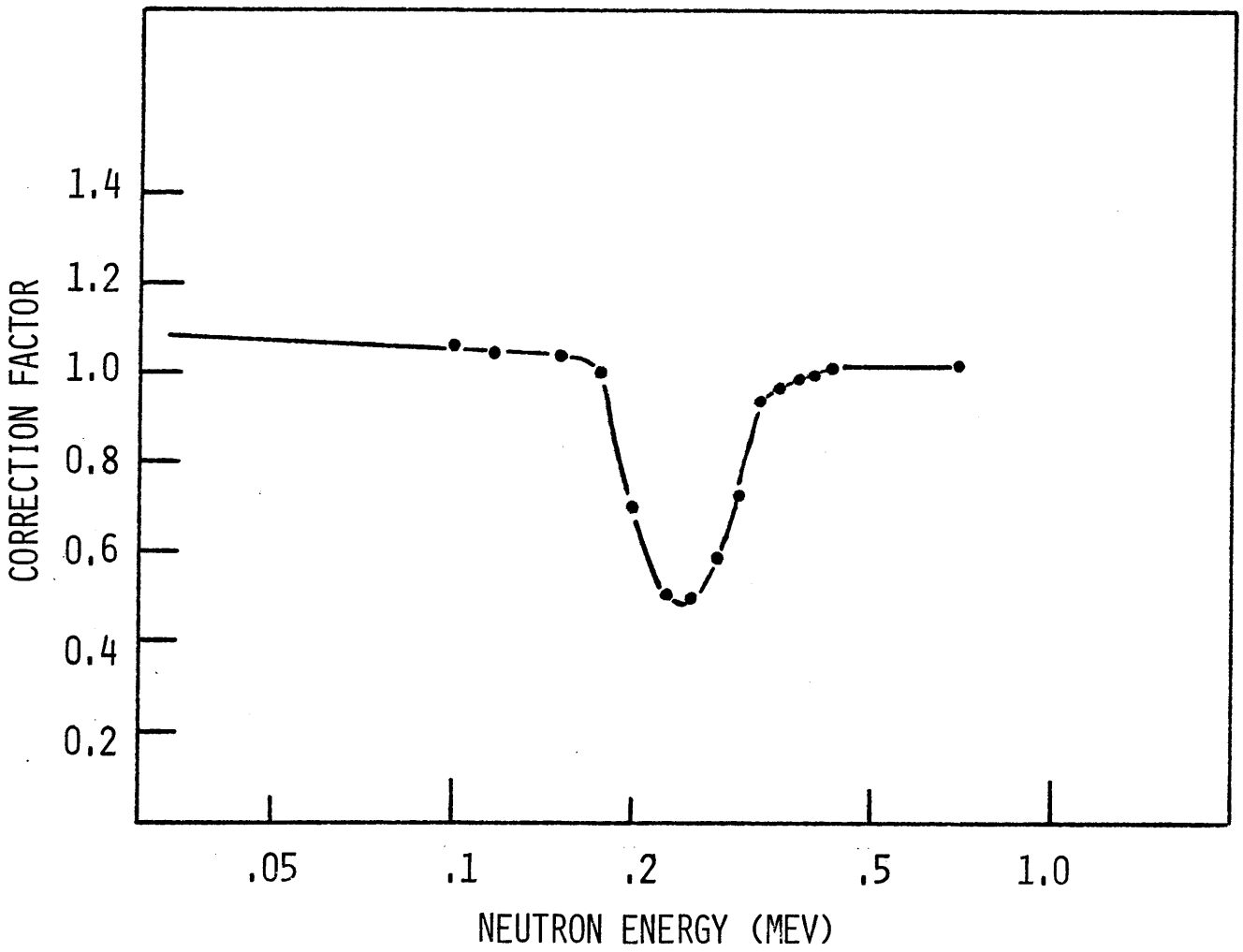

FIG. 3.7 CORRECTION FACTOR FOR THE RESPONSE FUNCTION OF THE Li-6 SYSTEM

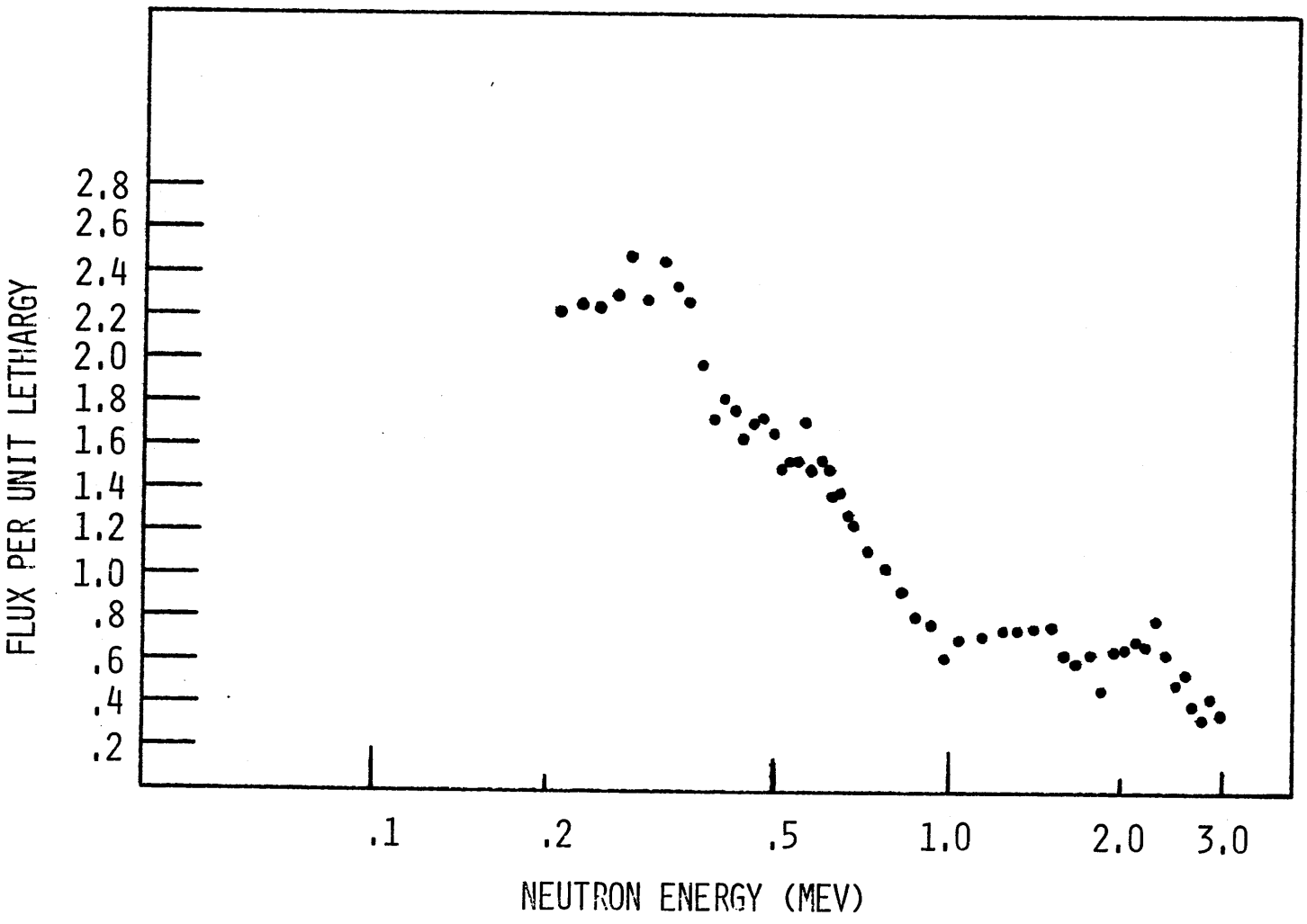

FIG. 3.8 NEUTRON SPECTRUM IN BLANKET NO.2, Li-6 SYSTEM, SUM METHOD

are shown. These have also been observed in several fast neutron spectrum measurements (S3,B8,Y1). They are a consequence of very pronounced minima in the sodium and oxygen cross sections in these energy regions. Measurements done in Blanket Mockup No. 2 using a neutron spectrometer based on gamma spectroscopy (K1) also show peaks near 1.5 MeV and 2.3 MeV.

3.3.6 Error Estimates

The error analysis discussed in section 2.4.5 was also applied to the Li-6 semiconductor detector. The estimated errors range from 14% at 400 keV to 30% at 3.1 MeV. The statistical error is the larger contributor to the total error at the high-energy end, and the cross section uncertainty dominates in the low-energy region.

3.4 DIFFERENCE METHOD

3.4.1 Description of the Technique

The Difference Method (R1,M2) is mainly used to improve the resolution of the system at low neutron energies, since the gamma and noise rejection of the system is very good due to the high Q value of the reaction. The block diagram of the electronic system is the same as described in section 2.5.1 and shown in Fig. (2.9).

The channel-energy calibration is obtained by exposing the detector to a thermal neutron flux. If only one detector output is connected to the difference amplifier two peaks are

observed due to the alpha and triton particles. It is important to adjust the amplifier inputs such that each detector output produces the same response. This will compensate for any small differencesin the detector or in the preamplifiers. When both detectors are connected to the amplifier a peak is observed corresponding to a difference energy of Q/7. The transformation from difference energy to neutron energy is obtained from Eq. (2.59) using the values of Eq. (3.2). Table 3.3 shows that the maximum difference energy (cos Θ = 1) of the charged particles is a more sensitive function of the neutron energy than the sum energy.

3.4.2 Construction of the Response Function

The measured difference spectrum is related to the incident neutron flux by Eq. (2.46). The probability function is given by Eq. (2.48) because the ^{6}Li(n,α)T-reaction is non-isotropic in the center of mass. Following the discussion of reference (M1), the differential cross section is represented by a second order Legendre polynomial expansion.

$$\sigma_\Omega(E, \cos\Psi) = \frac{BOx10^3}{4} + B1 \cos\Psi + B2(3\cos^2\Psi - 1), \quad (3.4)$$

where

BO is the ^{6}Li(n,α)T-cross section in barns; and the coefficients B1 and B2 are functions of energy (M1).

3.4.3 Effect of the Electronics on the Response Function

The difference amplifier is unable to distinguish the case $(E_\alpha - E_T)$ from $(E_T - E_\alpha)$ for positive differences. Therefore for

TABLE 3.3

Li-6 SYSTEM-COMPARISON OF DIFFERENCE METHOD AND SUM METHOD

E_1 (keV)	E_3 (keV)	E_4 (keV)	Δ^*_{max} E_3-E_4 (keV)	SUM E_3+E_4 (keV)
0	2730	2050	680	4780
0.5	2750	2030.5	719.5	4780.5
1.0	2758	2022	736	4781
2.0	2769	2013	756	4782
3.0	2778	2005	773	4783
10.0	2819	1971	848	4790
25.0	2875	1930	945	4805
50.0	2943	1887	1056	4830
100.0	3047	1833	1214	4880
200.0	3214	1766	1448	4980
500.0	3610	1670	1940	5280
750.0	3899	1631	2268	5530
1000.0	4170	1610	2560	5780
1500.0	4636	1594	3092	6280

*Corresponding to $\Theta = 0^o$, $\phi = 180^o$

those neutron energies at which the absolute value of Δ_{min} becomes greater than Q/7, the magnitude of the probability is twice the value given by Eq. (2.48), as shown in Fig. (3.9).

3.4.4 Unfolding Using the Derivative Technique

The unfolding technique discussed in section 2.5.7 also applies to the Li-6 semiconductor detector. The only difference is that the differential absorption cross section is non-isotropic is the center of mass, and therefore a subroutine called THETA2 was included in the DIFFE program to take into account the non-isotropic effect.

Equations (2.69) and (2.70) are used to obtain the unfolded neutron spectrum from the measured difference spectrum. The program output consists of the neutron flux per unit lethargy at constant fractional energy increments.

3.4.5 Unfolding Using the Integral Technique

The unfolding technique of section 2.5.8 can also be applied to the Li-6 semiconductor detector. A subroutine in the computer program MATRIX calculates the neutron flux per unit lethargy at fifty different energies fixed by the program. It also calculates the response function based on the kinematics equation of the $^{6}Li(n,\alpha)T$-reaction. Other subroutines contained in the program take into account the anisotropic nature of the reaction and the effect of the electronics (Appendix A).

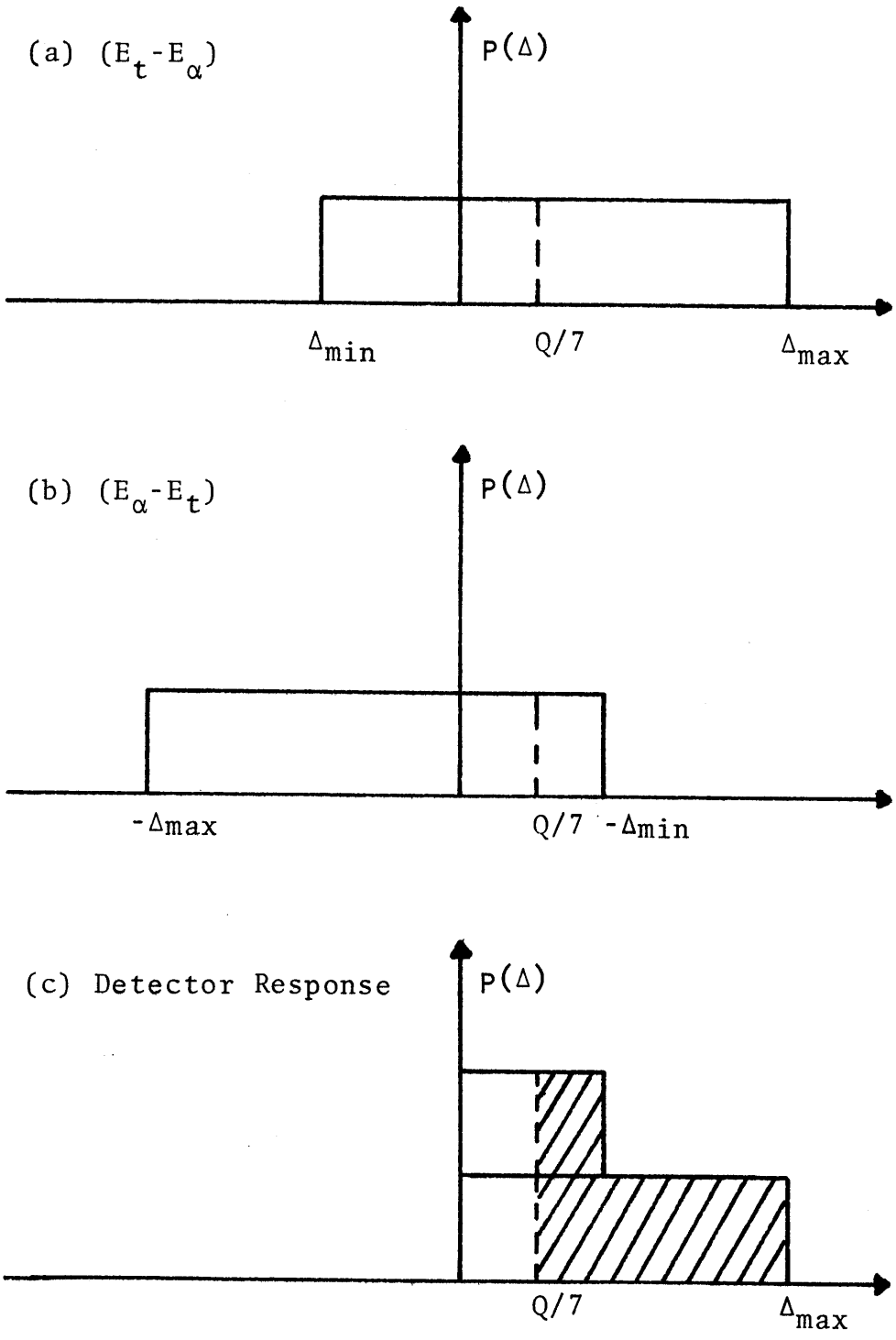

FIG. 3.9 CONSTRUCTION OF THE RESPONSE FUNCTION (Li-6, DIFFERENCE TECHNIQUE)

3.4.6 Experimental Results

The neutron flux in Blanket No. 2 was measured using the Li-6 semiconductor detector, operating in the difference mode. Figure 3.10 shows the flux per unit lethargy as a function of neutron energy from 10 keV to 600 keV. It was unfolded using the integral technique discussed in the previous section. For reasons explained below the differential unfolding technique did not yield acceptable results.

By unfolding theoretical particle spectra (i.e. spectra having realistic shapes, but for which exact relations between charged particle and neutron spectra could be formulated), it was found that the computer program using the derivative technique for unfolding is very sensitive to errors associated with the differential cross section and to statistical errors in the measured particle spectra. This leads to spurious oscillations and anomalies in the unfolded neutron spectra. Hence, at the minimum, a subroutine to smooth the data before calculating derivatives should be added to improve the stability of the program before further application to the Li-6 detector is attempted. From the results reported in Chapter 2, we may conclude that the smoother and more accurately known absorption cross section of He-3, and the isotropic nature of the reaction in the center of mass makes use of the unimproved differential approach at least marginally acceptable for that system.

A factor affecting the neutron flux measurements done

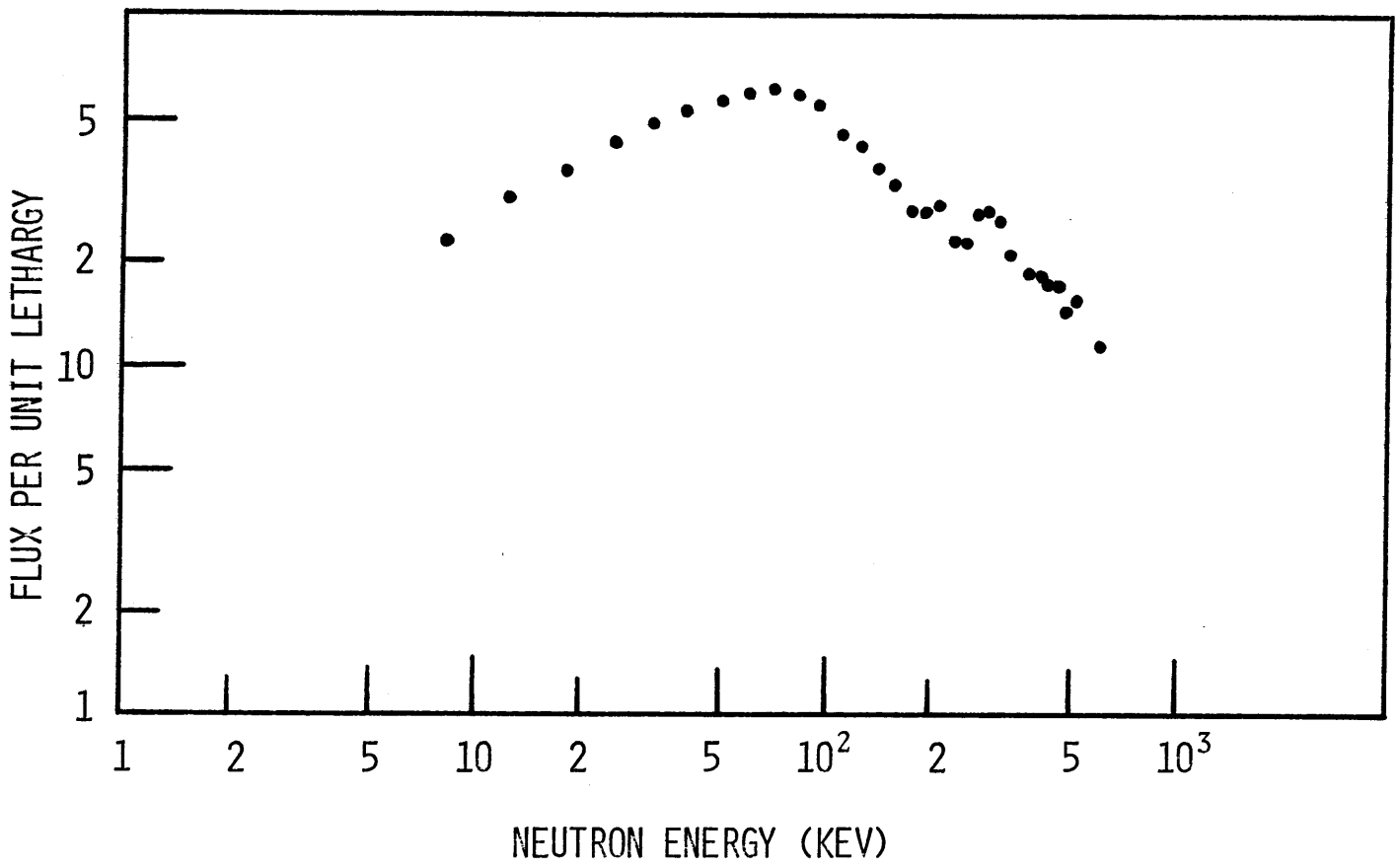

FIG. 3.10 FAST NEUTRON SPECTRUM IN BLANKET MOCKUP NO.2, Li-6 SYSTEM DIFFERENCE METHOD

with the detector operating in the Difference Method, is the broadness of the alpha peak which causes a broad difference peak. The broadness of the alpha peak is mainly due to the energy lost by the alpha particle in the Li-6 foil. This can be improved by using a detector having a thinner Li-6 foil (15 $\mu gm/cm^2$).

3.5 TRITON TECHNIQUE

3.5.1 Description of the Technique

In this technique (R2,M3) only one of the detector outputs is registered in the multichannel analyzer, but the output of both detectors are required to be in coincidence to register a count. The alpha and triton spectrum, obtained from the output of the detector are well separated (See Fig. 3.1), so it is possible to analyze the data above the center of the triton peak without having to correct for the presence of the alpha spectrum.

The full-width at half-maximum (FWHM) of the triton peak, when the detector is exposed to a thermal neutron flux, is about 60 keV, in comparison to 250 keV for the sum peak. This increase in resolution allows improved measurements in the low-energy region of a neutron spectrum. The Triton Method can cover an energy region from 10 keV to 600 keV.

The channel-energy calibration of the Triton Method is the same as the Sum Method (section 3.3.1). Equation 2.5 gives the relation between the maximum energy of the triton

particle (cos Θ = 1) and the incident neutron energy. Table 3.3 shows the maximum triton energy as a function of neutron energy. It is seen that for a given change in neutron energy the change in the maximum difference energy is about twice as large as the change in the maximum triton energy. Therefore the difference method is the most sensitive mode of operation of the Li-6 detector for measuring low-energy neutrons, assuming that the FWHM of the difference peak is approximately the same that the FWHM of the triton peak for thermal neutrons.

3.5.2 Response Function Calculation

By analogy with Eq. 2.48, the response function for the Triton Method can be represented as

$$P(E,E_3)dE_3 = 2\pi d(\cos \Psi)\sigma_\Omega(E, \cos \Psi) \qquad (3.5)$$

The differential cross section, $\sigma_\Omega(E, \cos \Psi)$, is very non-isotropic in the center of mass and is approximated by Eq. (3.4). Figure 3.11 shows three typical distributions obtained for the response function.

3.5.3 Solution of the Matrix Equation

The matrix equation discussed in section 2.5.8 is used to unfold the measured spectrum of the triton particles. Each term of the response matrix is calculated using the response function mentioned in the preceeding section. In this form a diagonal matrix was constructed in terms of the maximum triton energy (E_{3max}). This response matrix and the method described in section 2.5.8 were used to unfold the measured triton spectra.

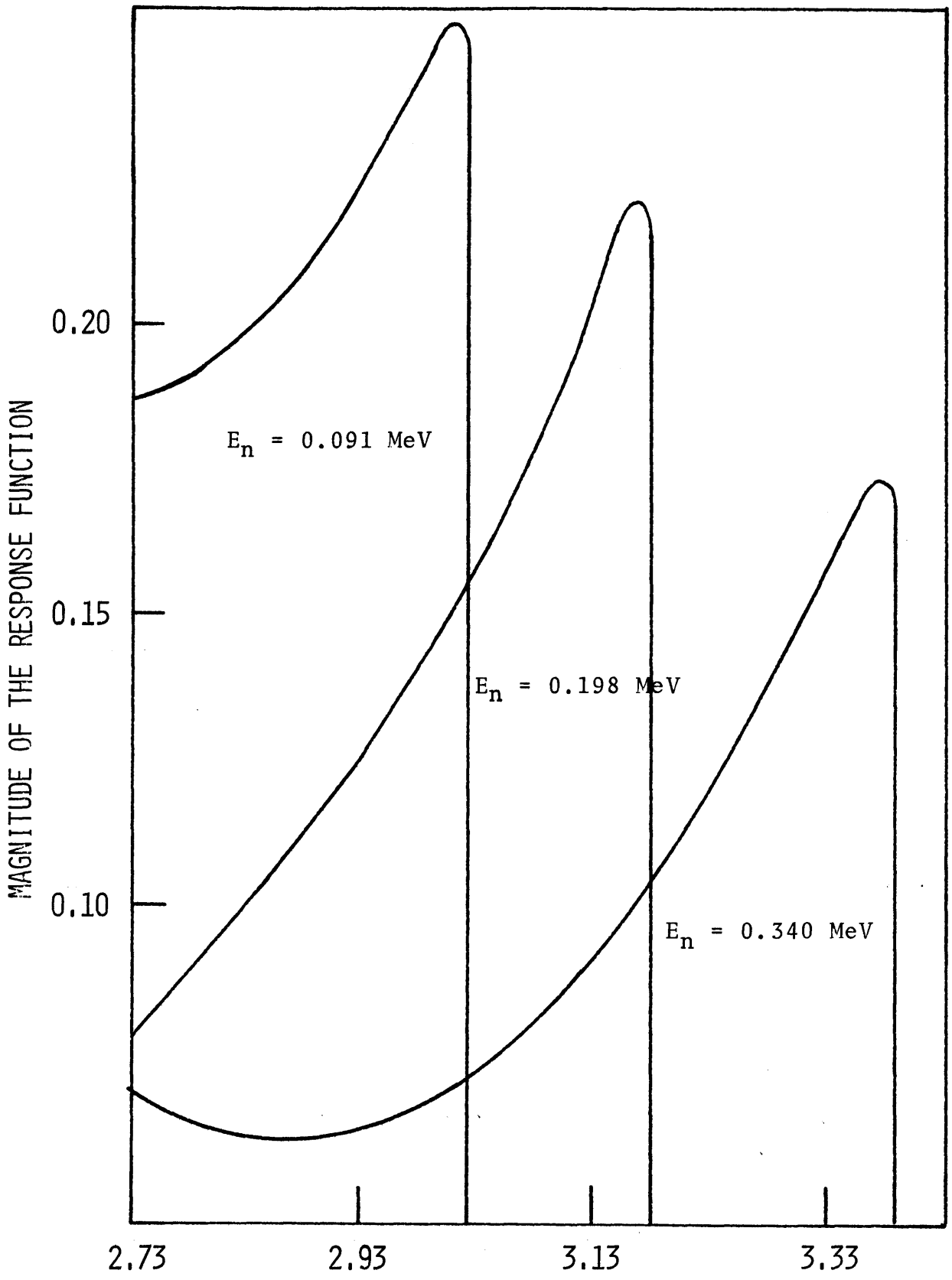

FIG. 3.11 THE SHAPE OF THE TRITON RESPONSE FUNCTION

3.5.4 Neutron Flux Measurements

The Li-6 semiconductor detector, operating in the Triton Method, was placed in Blanket Mockup No. 2 to measure the fast neutron spectrum. The same experimental setup as described in section 1.4, was used. Figure 3.12 shows the unfolded neutron flux per unit lethargy as function of neutron energy from 10 keV to 600 keV. It starts with a small number of low-energy neutrons and then increases steadily until 150 keV. In the energy range from 150 keV to 400 keV the flux per unit lethargy, $\phi(u)$, experiences a large decrease in magnitude. This may be due to the presence of the Li-6 cross section resonance at about 250 keV, even though this spectrum has been corrected with the response function calculated from the Cf-252 neutron spectrum measurements (Fig. 3.8). The presence of large scattering resonances at 250 keV and 400 keV in sodium and oxygen also contribute dips in the neutron flux.

3.5.5 Error Estimates

The errors associated with this method are basically the same as with the Sum Method over the energy range from 200 keV to 600 keV. In the low-energy region the cross section uncertainty is the main contributor to the total error, which is about 14%.

3.6 SUMMARY

The Li-6 semiconductor detector, operating in the Sum, Triton and Difference Modes was used to measure the fast

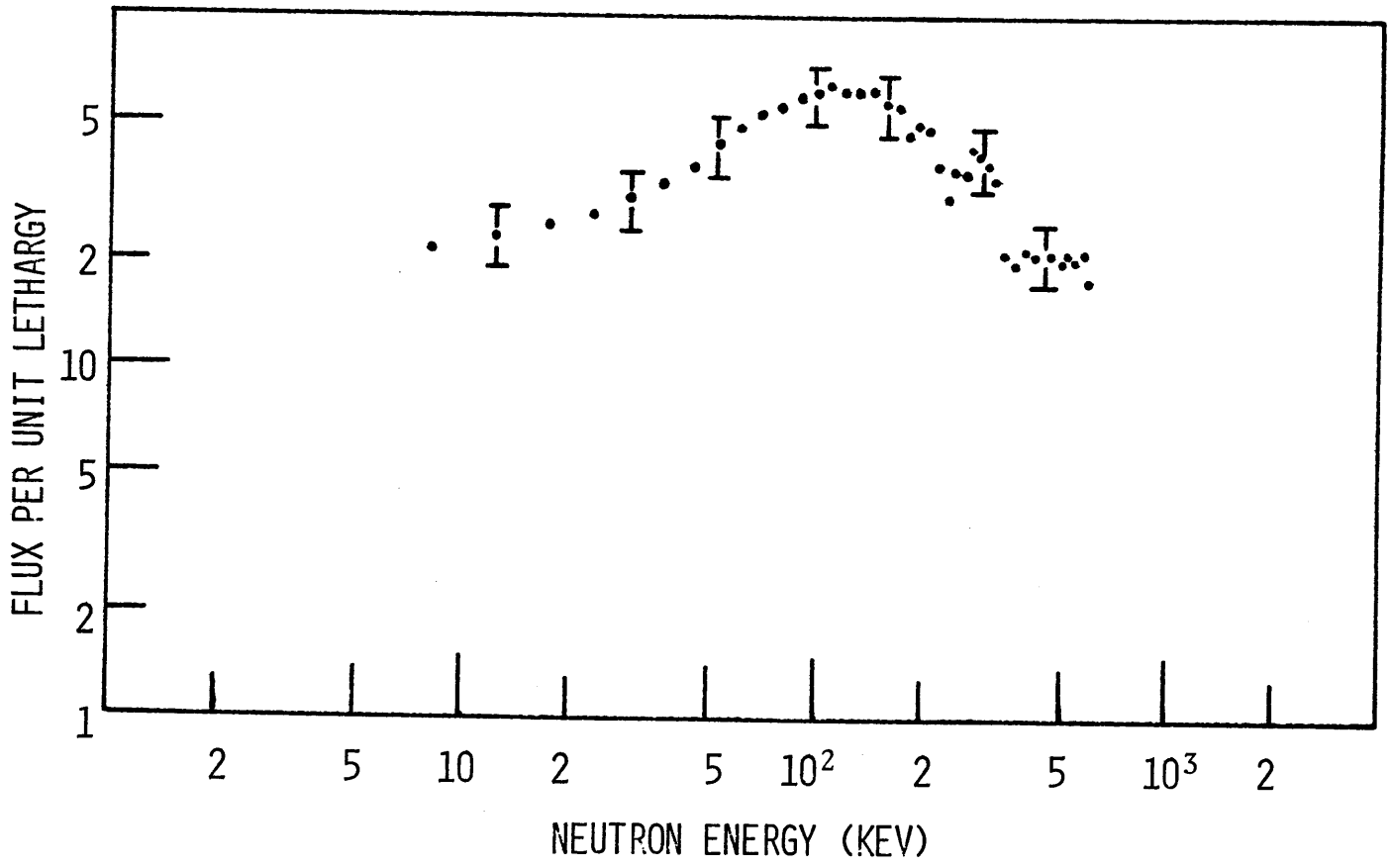

FIG. 3.12 NEUTRON SPECTRUM IN BLANKET MOCKUP NO. 2 Li-6 DETECTOR-TRITON METHOD

neutron spectrum in Blanket Mockup No. 2. The Sum Method covered an energy range from 160 keV to 3.1 MeV. The Triton Method extends the low-energy limit to 10 keV, and the high energy limit is 600 keV. Both measurements were normalized over the energy region of 160 keV to 250 keV. Figure 3.13 shows the neutron flux per unit lethargy as a function of neutron energy, obtained by combining the results of both methods.

The resolution in the neutron flux measurements using the Difference Method is affected by the broad shape of the alpha peak. The computer program MATRIX, based on the Integral Technique, is recommended for unfolding the measured particle spectra.

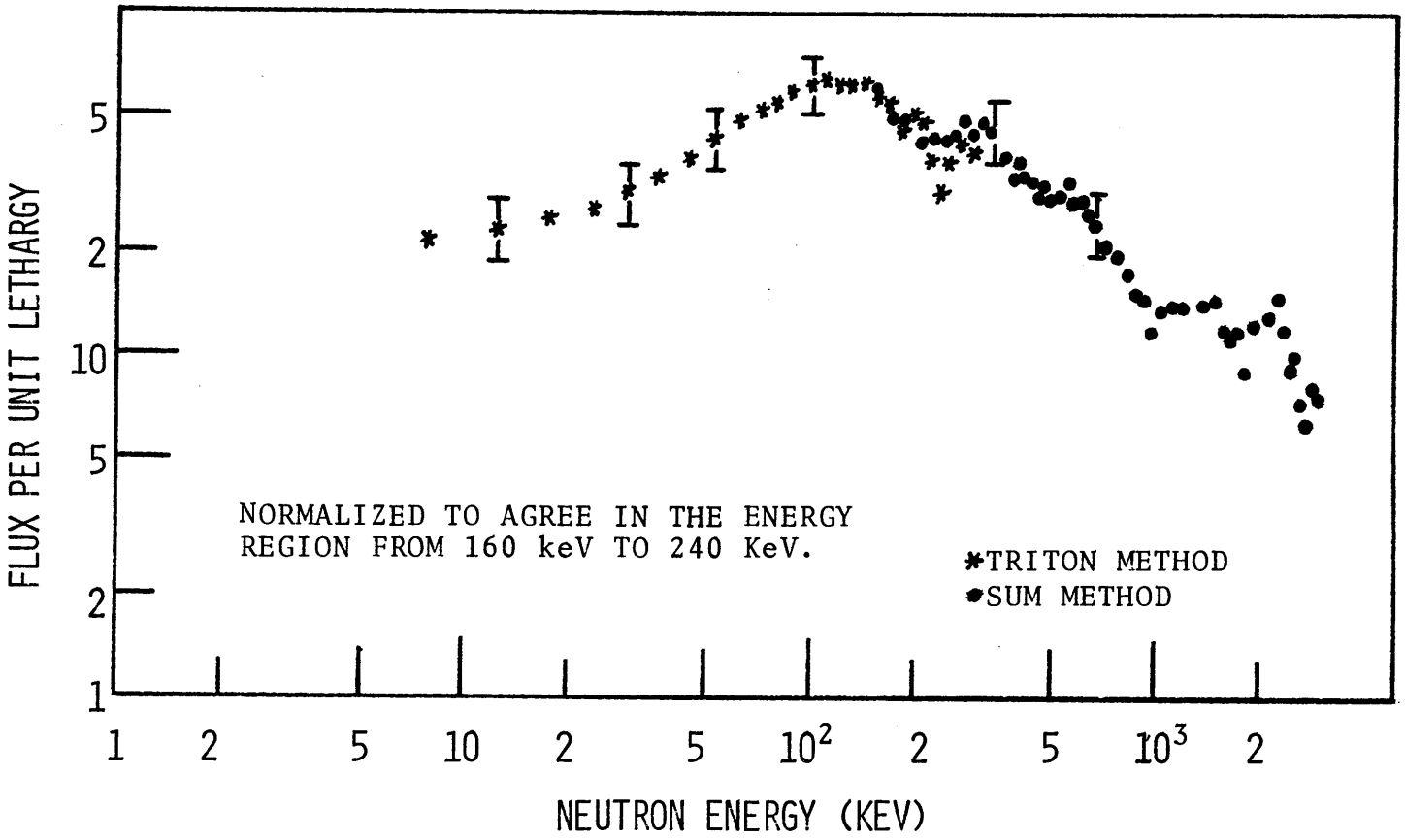

FIG. 3.13 NEUTRON SPECTRUM IN BLANKET MOCKUP NO. 2 Li-6 SEMICONDUCTOR DETECTOR

Chapter 4

PROTON RECOIL DETECTOR

4.1 Basic Considerations

Proton-Recoil proportional counters have been used extensively to measure neutron spectra (B2,B3). A short description of the various corrections applied to the data taken with these detectors is presented here; a more comprehensive discussion of the technique is provided elsewhere (G2,B5).

In a neutron-proton collision all proton energies below that of the incident neutron energy are equally probable. This rectangular response function of the proton spectrum has to be unfolded to arrive at the neutron spectrum. One method of unfolding consists of differentiation of the proton-recoil distribution. The relationship between the corrected proton-recoil distribution M(E) and the neutron flux per unit lethargy $\phi(u)$, is

$$\phi(u) = - \frac{E^2}{NT\sigma_H(E)} \frac{dM(E)}{dE} , \qquad (4.1)$$

where $\sigma_H(E)$ is the neutron-proton scattering cross section represented by the empirical equation (B5)

$$\sigma_H(E) = \frac{11010}{E+4041} \quad \frac{2387}{E+135.5} , \qquad (4.2)$$

with E in kilovots and σ in barns. T is the time of accumulation of M(E) and N is the total number of hydrogen atoms in the counter.

The measured proton-recoil spectra must be corrected for various effects before the unfolding. The main corrections which were applied in the present work are described below.

(1) Correction for the Carbon and Nitrogen Recoil

The carbon and nitrogen atoms present in the methane and hydrogen-filled counters will also experience neutron scattering interactions. The effect is not insignificant in comparison with hydrogen-recoils. A correction for this effect was made. It was assumed that the scattering is isotropic in the center of mass system and that the total cross section may be represented by the empirical equation (B5)

$$\sigma_C(E) = \frac{5520}{E+1150} \quad , \tag{4.3}$$

and

$$\sigma_N(E) = \frac{1250}{E+250} \quad , \tag{4.4}$$

with the energy, E, in keV, and σ in barns. Scattering by these nuclei will affect mainly the results at low-energies, especially in the measurement of a hard spectrum.

(2) Energy per ion pair, W

The measured proton-recoil spectrum per unit ionization must be divided by the energy necessary to create an ion pair,

W, to obtain the proton-recoil spectrum per unit energy. The magnitude of W has been found (W3) to be constant from 10 keV to the MeV region for protons slowing down in hydrogen. In the low-energy region W varies with energy; the prescription for W suggested by Bennett (B4) was used in this work. The W for the methane-filled counter is assumed to be constant.

(3) Correction for Wall-and-End Effects

If the recoiling proton hits the counter wall or enters the dead end-region, the recoil spectrum is distorted. The data was corrected with the response function of the counter (B4). The correction is considered adequate for the energy region below 1 MeV. At higher energies the proton tracks become longer than the effective length of the counter and large errors are introduced.

4.2 DETECTORS AND ELECTRONICS

Two detectors were used in the measurements, as shown in Fig. 4.1. The smaller detector in Fig. 4.1 is filled with about 8 atm of predominately hydrogen gas. It was used to measure proton-recoil spectra below 100 keV. The larger detector is filled with about 3 atm of predominately methane gas. The methane detector was used for energies greater than 100 keV. Each counter contains a small amount of nitrogen for calibration. The detectors were enclosed in a lead sleeve 0.020 in. thick to reduce their sensitivity to soft gamma rays.

A block diagram of the system is shown in Fig. 4.2. The system has two channels, the energy channel and the rise-time-

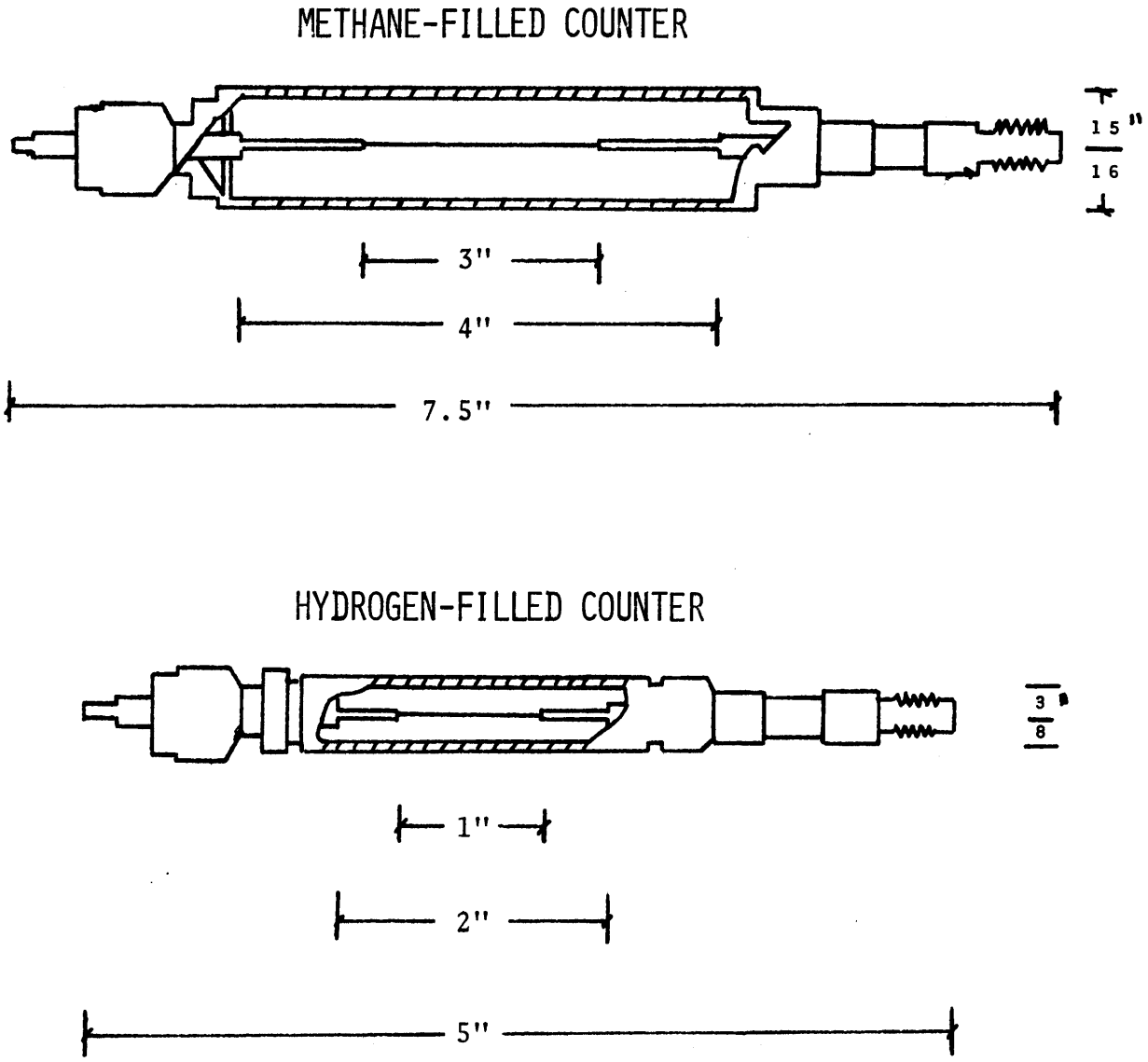

FIG. 4.1 SCHEMATIC OF THE PROTON-RECOIL PROPORTIONAL COUNTERS

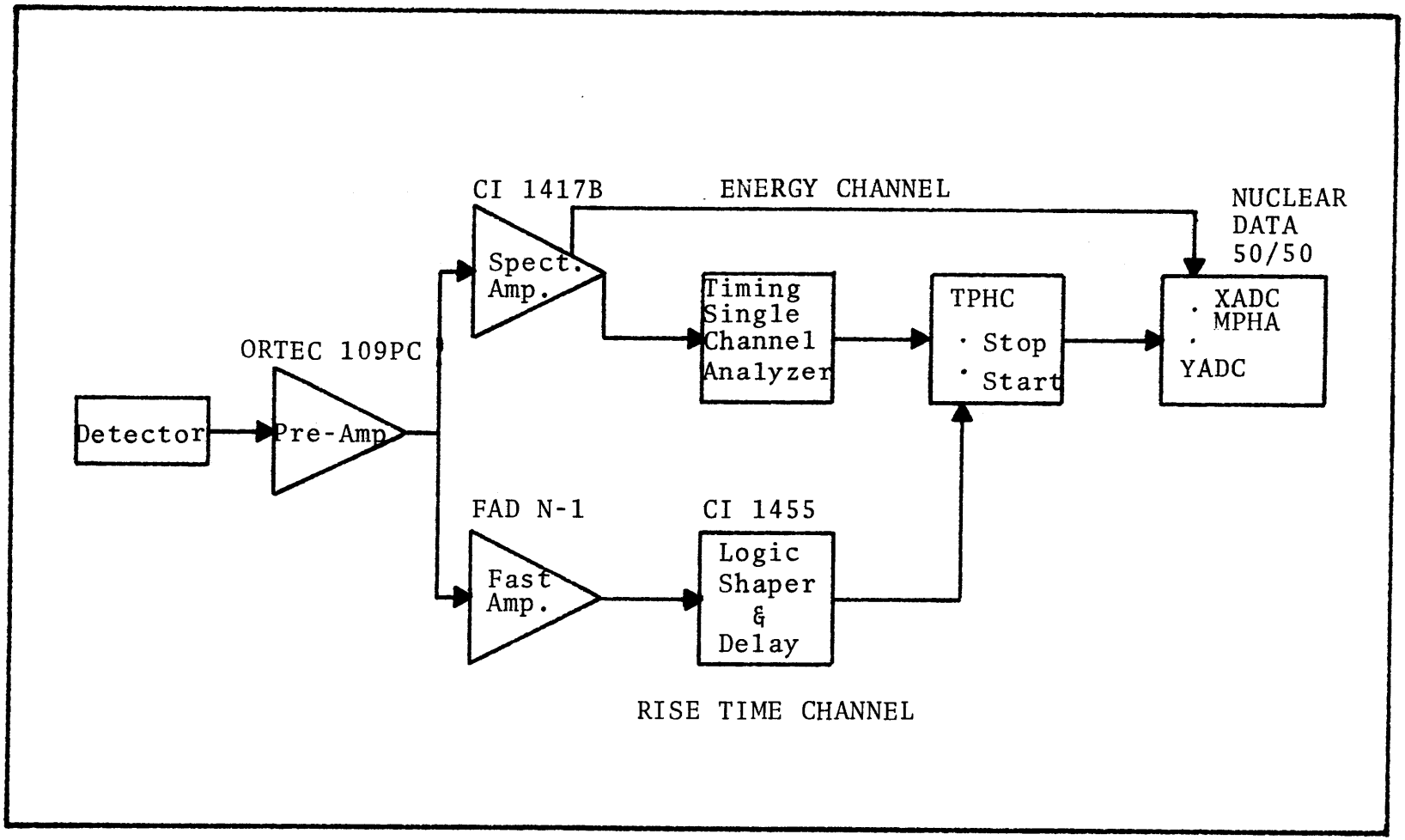

FIG. 4.2 BLOCK DIAGRAM OF THE SYSTEM USED FOR NEUTRON SPECTROSCOPY WITH PROTON-RECOIL PROPORTIONAL COUNTERS

to-amplitude converter channel. The former produces a pulse whose height is proportional to the ionization; it consists of a pole-zero compensated spectroscopy amplifier with baseline restorer. The other channel measures the rise time of the pulses. It consists of a fast amplifier, a delay unit, a timing single channel analyzer (TSCA), a time-to-pulse-height converter (TPHC) and two-parameter multichannel analyzer.

4.3 ENERGY CALIBRATION

The energy scale is calibrated by exposing the detector to a thermal neutron flux; a peak at about 615 keV equivalent proton energy is observed due to the $^{14}N_7(n,p)C^{14}$-reaction. A gain-voltage relationship is obtained by following the peak amplitude of the $^{14}N(n,p)C^{14}$-reaction as a function of voltage. An empirical equation which provides a good fit to the measured values of the multiplication, A, as a function of voltage, is (B4).

$$\frac{\log A}{V^Q} = CV+D \ , \qquad (4.5)$$

where

A = gas gain

V = Bias voltage

Q = power factor

The power factor, Q, the slope, C, and the intercept, D, are derived by a least-square fitting procedure. The peak amplitude of the nitrogen reaction can be registered as a function

of voltage for A values so large that space charge effects begin to distort the distribution. Therefore Equation (4.5) is used to extrapolate to the A values for higher voltages.

The hydrogen-filled detector was operated from 3250 volts to 4500 volts and the methane-filled detector from 3200 volts to 3750 volts. The calculated values for Q,C and D are: 0.7, 0.7450E-05 and 0.9750E-02 respectively.

4.4 GAMMA DISCRIMINATION

The proton-recoil proportional counter will also respond to the background of gamma rays which accompany the neutron flux. Bennett has developed a shape rejection technique for gamma induced events (B3). This technique is based upon the large difference in specific ionization (ion pairs per cm of track) between a recoil proton and a fast electron of the same total ionization. The distribution of the ionization due to electrons is, on the average, extended over a large fraction of the counter radius. A recoiling proton by contrast, has negligible range and its ionization is highly localized; therefore the pulse rise time will be shorter for the proton-recoil than for the fast electron.

The electronic system used in this work to reject gamma induced events is a modification of the one suggested by Bennett (B2). It consists of a fast amplifier with a discriminator level which is adjusted just over the noise level. If a pulse from the preamplifier exceeds the discriminator level a pulse is sent by the fast amplifier to start the TPHC.

When the signal pulse crosses the baseline of the TSCA, a pulse is sent to stop the TPHC unit. In other words, the magnitude of the output of the TPHC will be proportional to the time elapsed between the start of a signal pulse and when it crosses the baseline (Fig. 4.3). A logic shaper and delay unit is used to delay and reshape the fast amplifier output to make it compatible with the TPHC input.

The output of the TPHC is smaller in magnitude for proton events than for electron events causing the same ionization. Therefore when fed in coincidence with the ionization pulse to a two-parameter multichannel analyzer two peaks are observed; the proton and gamma ray peaks (Fig. 4.4). Only the data under the proton-recoil peak is analyzed to unfold the incident neutron spectrum.

4.5 UNFOLDING OF NEUTRON SPECTRA FROM PROTON-RECOIL DISTRIBUTIONS

The computer program PSNS written at ANL (B5) was used to unfold the measured proton-recoil spectrum. The original program was rewritten in Fortran IV language and the energy dependence of W (energy per ion pair) was modified to include the results of recent measurements. Corrections for wall-and-end effects, and the recoil of heavy nuclei are also included in the program. The calculation of the neutron flux per unit lethargy is based on Eq. 4.1 and the results are given at a constant fractional energy increment.

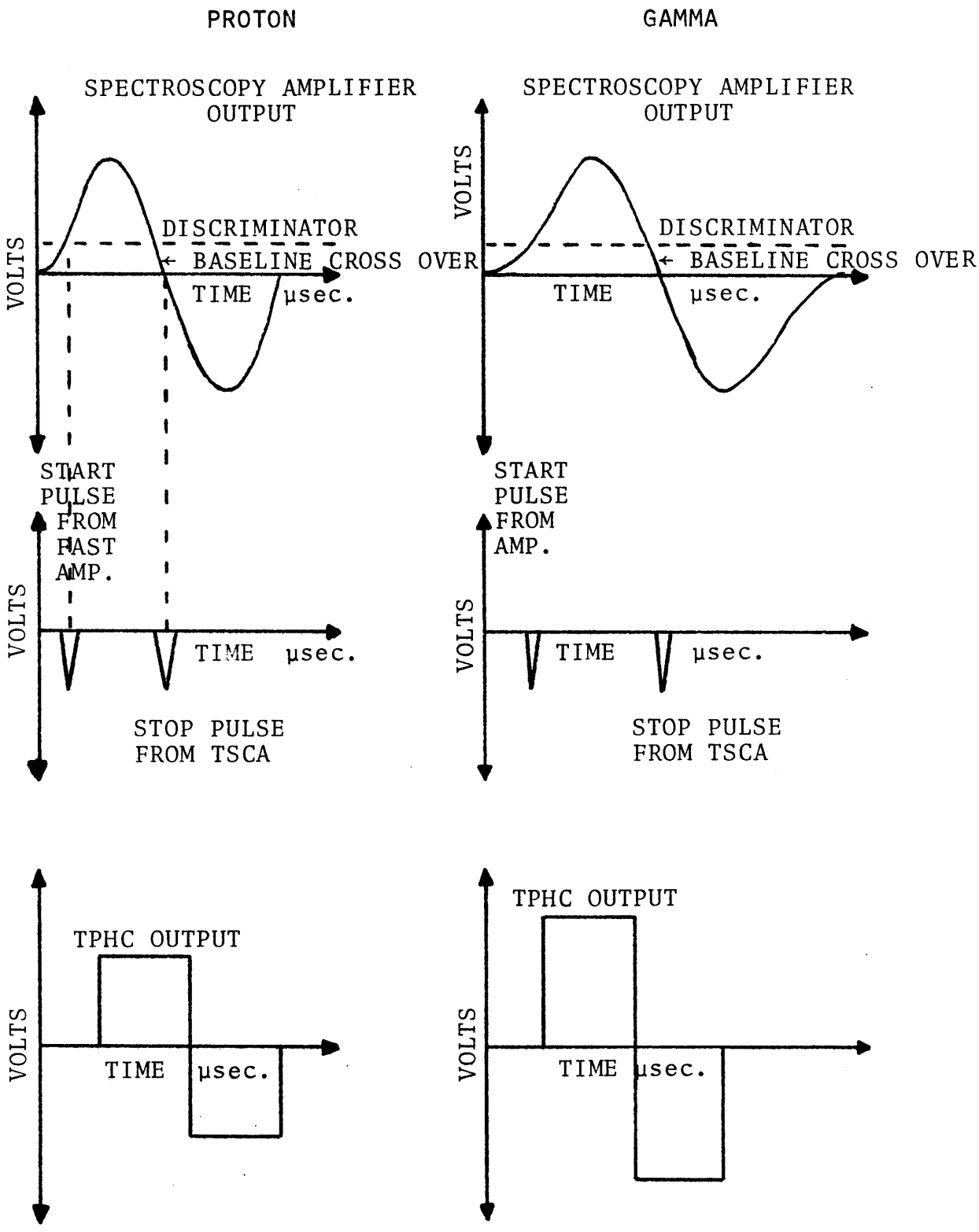

FIG. 4.3 PULSE SHAPE DISCRIMINATION

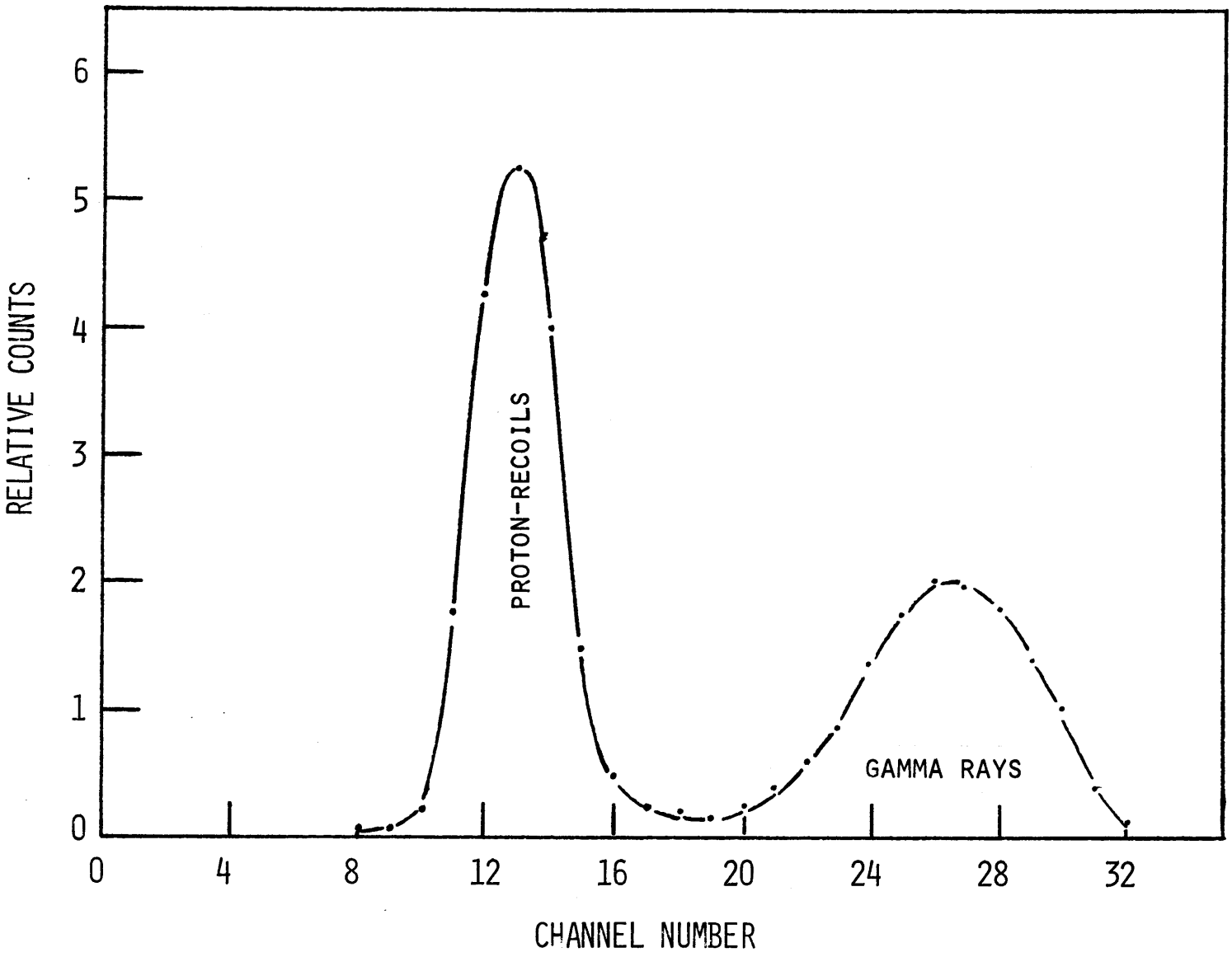

FIG. 4.4 TYPICAL PROTON-RECOIL AND GAMMA RAY PEAKS

4.6 EXPERIMENTAL RESULTS

The fast neutron spectrum was measured over the energy region from 2 keV to 1.5 MeV in Blanket Mockup No. 2 (section 1.4). Data were obtained with the hydrogen-filled counter using eight high voltage settings at 150 volt intervals beginning at 3250 volts. The methane-filled detector was used with high voltage settings of 3200 vots, 3500 volts and 3750 volts. An energy overlap exists between the two counters to assure that the data is properly normalized. Also an energy overlap exists for each of the eight hydrogen data sets and for each of the three methane-filled counter data sets. The detectors were operated at a count rate less than 7000 counts per second to assure that pulse pile-up would not distort the spectrum.

The neutron spectrum is shown in Fig. (4.5). Depressions due to various scattering resonances are seen: Oxygen resonances at 400 keV and 1 MeV, a chromium resonance at 50 keV, an iron resonance at 30 keV and a sodium resonance at 3 keV.

4.7 ERROR ESTIMATES

The estimated error for the neutron-proton scattering cross section (Eq. 4.2) is about 2%. The relative error in W is estimated to be ±3% between 2 keV and 8 keV. The experimental error varies from about 13% over most of the energy range to almost 33% in the region around 3 keV, where statistics in ionization become very poor.

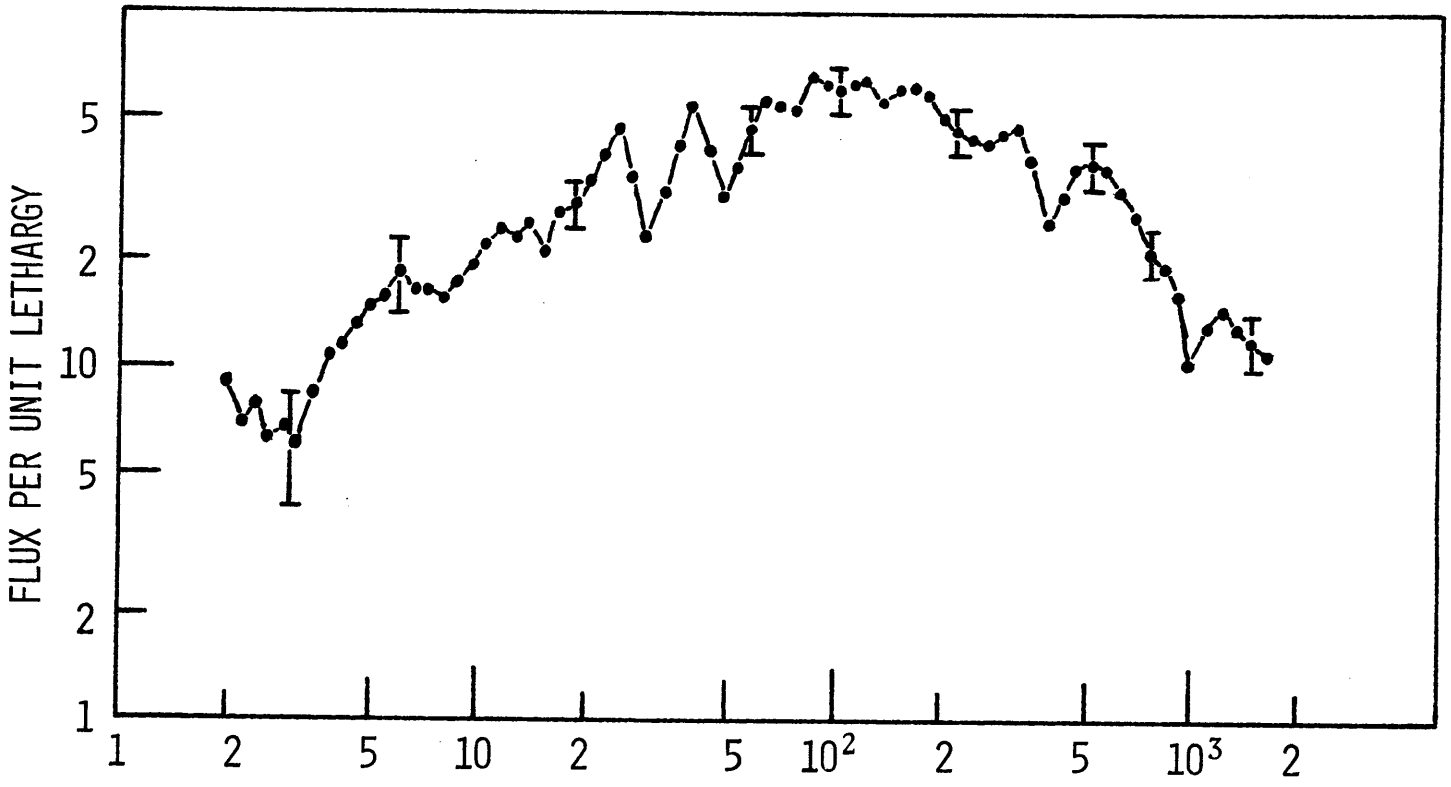

FIG. 4.5 FAST NEUTRON SPECTRUM IN BLANKET MOCKUP NO.2, PROTON RECOIL PROPORTIONAL COUNTER

4.8 SUMMARY

The fast neutron spectrum in Blanket Mockup No. 2 was measured from 2 keV to 1.5 MeV using Proton-Recoil proportional counters. The neutron spectrum shows the effect of various scattering resonances in sodium, iron, chromium and oxygen.

Chapter 5

RESULTS AND CONCLUSIONS

5.1 DISCUSSION OF RESULTS

This work has involved evaluation of different instrumental methods for measuring the fast neutron spectrum in Blanket Mockup No. 2. A brief description of the blanket and the experimental setup is presented in Chapter 1. The three detectors used in this work, the He-3 semiconductor detector, the Li-6 semiconductor detector and the Proton-Recoil proportional counter, are described in Chapters 2, 3, and 4, respectively. The methods applied are shown in Table 5.1. In this final chapter, the experimental results from previous chapters are intercompared. They are also compared with numerical calculations from the ANISN code, and to foil activation measurements.

5.1.1 Intercomparison of Present Results

The same experimental setup was used for the three detectors mentioned above, as described in section 1.4. The neutron spectrum was measured at only one depth, Z = 22.6 cm into the blanket because previous calculations and results (L1) showed that the variation of the shape of the neutron spectrum with position for this particular

TABLE 5.1

Summary of Instrumental and Unfolding Methods used to Measure the Fast Neutron Spectrum in the Blanket Mockup No. 2

Detector	Mode of Operation	Unfolding Method	Remarks
He-3	Sum	direct	See Figs. 2.8 and 5.1 for results.
	Difference	integral	See Figs. 2.13 and 2.16 for results.
		derivative	See Fig. 2.13 for results.
Li-6	Sum	direct	See Figs. 3.8 and 5.1 for results.
	Difference	integral	See Fig. 3.10 for results.
		derivative	It was not successfully employed on the Li-6 data. See section 3.4.6.
	Triton	integral	See Figs. 3.12 and 5.3 for results.
Proton-Recoil		derivative	PSNS code from ANL. See Figs. 4.5 and 5.3 for results.

blanket was less than the experimental error of the instrumental methods being applied in the present work.

The results obtained with the He-3 semiconductor detector operating in the Sum and Difference modes are in reasonable agreement (Fig. 2.16). The He-3 Sum Method results are also in good agreement with the Li-6 semiconductor detector Sum Mode measurements over the energy region from 200 keV to 1.1 MeV (Fig. 5.1). In the low-energy region (10 keV to 100 keV), the He-3 Difference Method results differ from those obtained using the Li-6 detector (Fig. 5.2). This is mainly due to the effect of the discriminator setting on the He-3 Difference Method, which introduces large uncertainties and reduces the sensitivity for measuring low-energy neutrons. The results from the Li-6 semiconductor detector and the Proton-Recoil proportional counter are in very good agreement over the entire energy range of the measurements (Fig. 5.3).

5.1.2 Comparison with ANISN Calculation

The one-dimensional transport code ANISN, with the ABBN cross section set and self-shielded U^{238} cross sections, was used in the S_8 option to calculate the theoretical neutron spectrum in Blanket No. 2, at 24.75 cm. into the blanket (L1). Figure 5.4 shows the 26 group calculation and the experimental results obtained by collapsing the

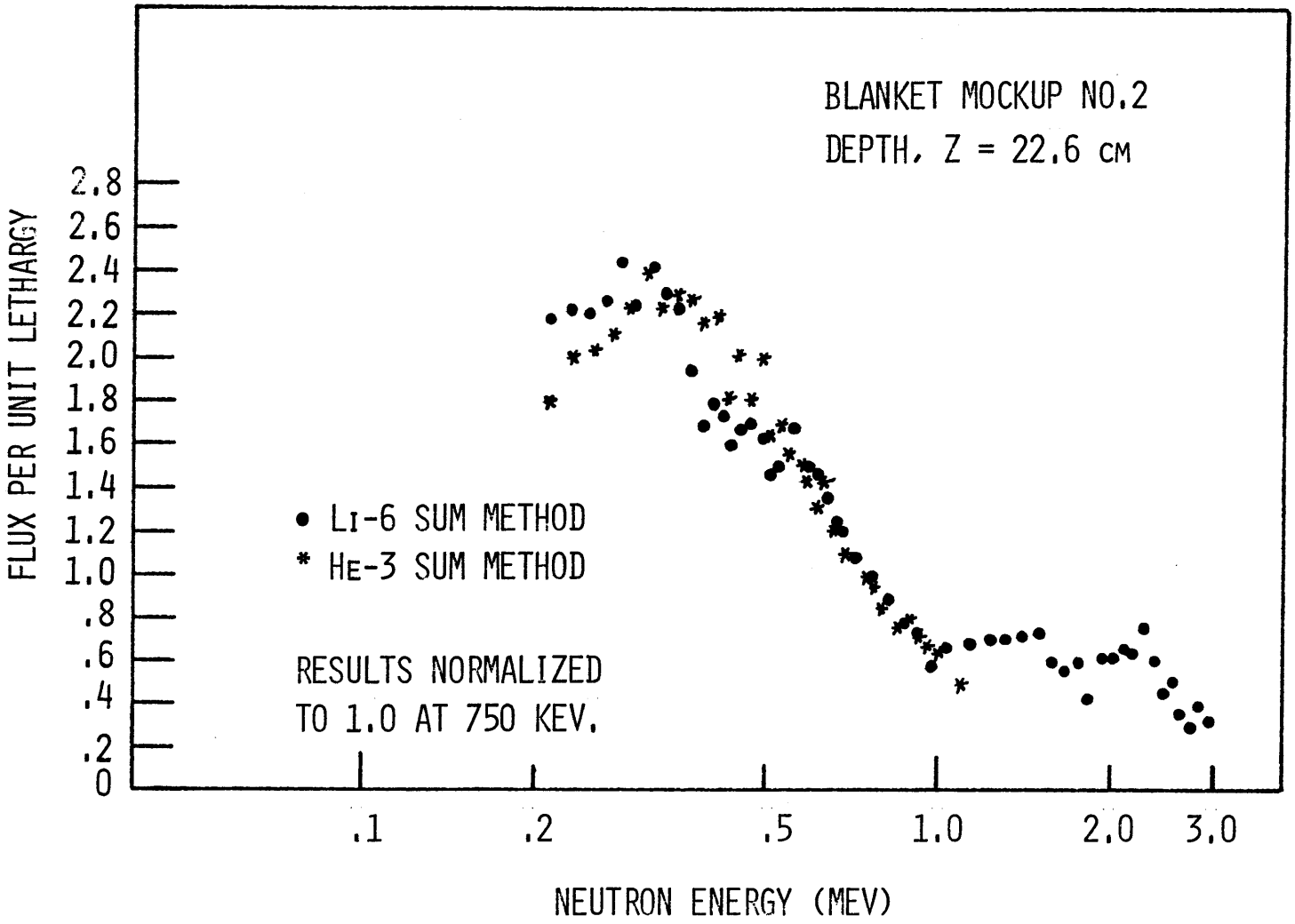

FIG. 5.1 COMPARISON OF NEUTRON SPECTRA FOR THE LI-6 AND HE-3 SUM METHODS

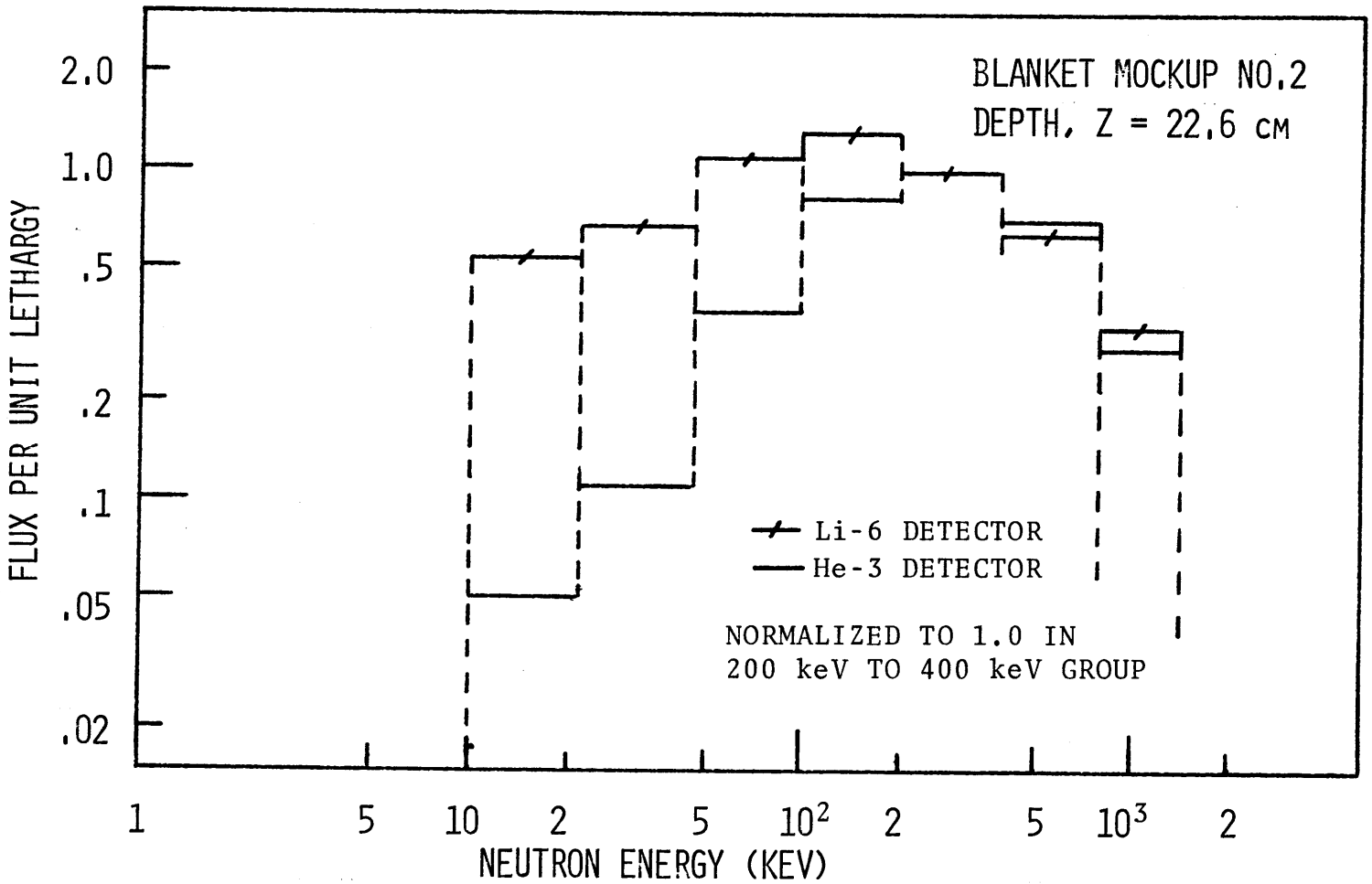

FIG. 5.2 COMPARISON OF NEUTRON SPECTRA FOR Li-6 AND He-3 DETECTORS IN DIFFERENCE MODE

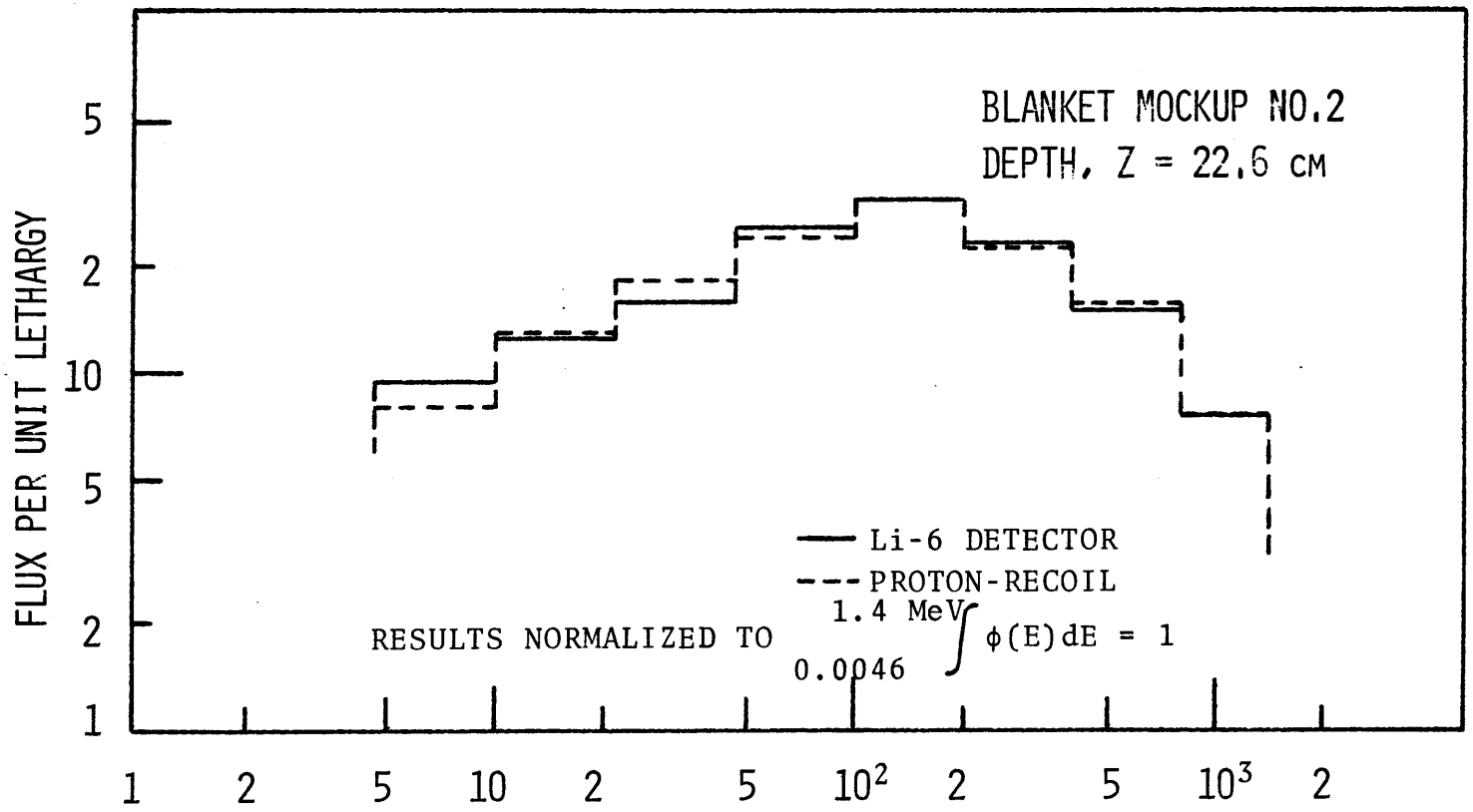

FIG. 5.3 COMPARISON OF NEUTRON SPECTRA FROM PROTON-RECOIL AND Li-6 DETECTORS

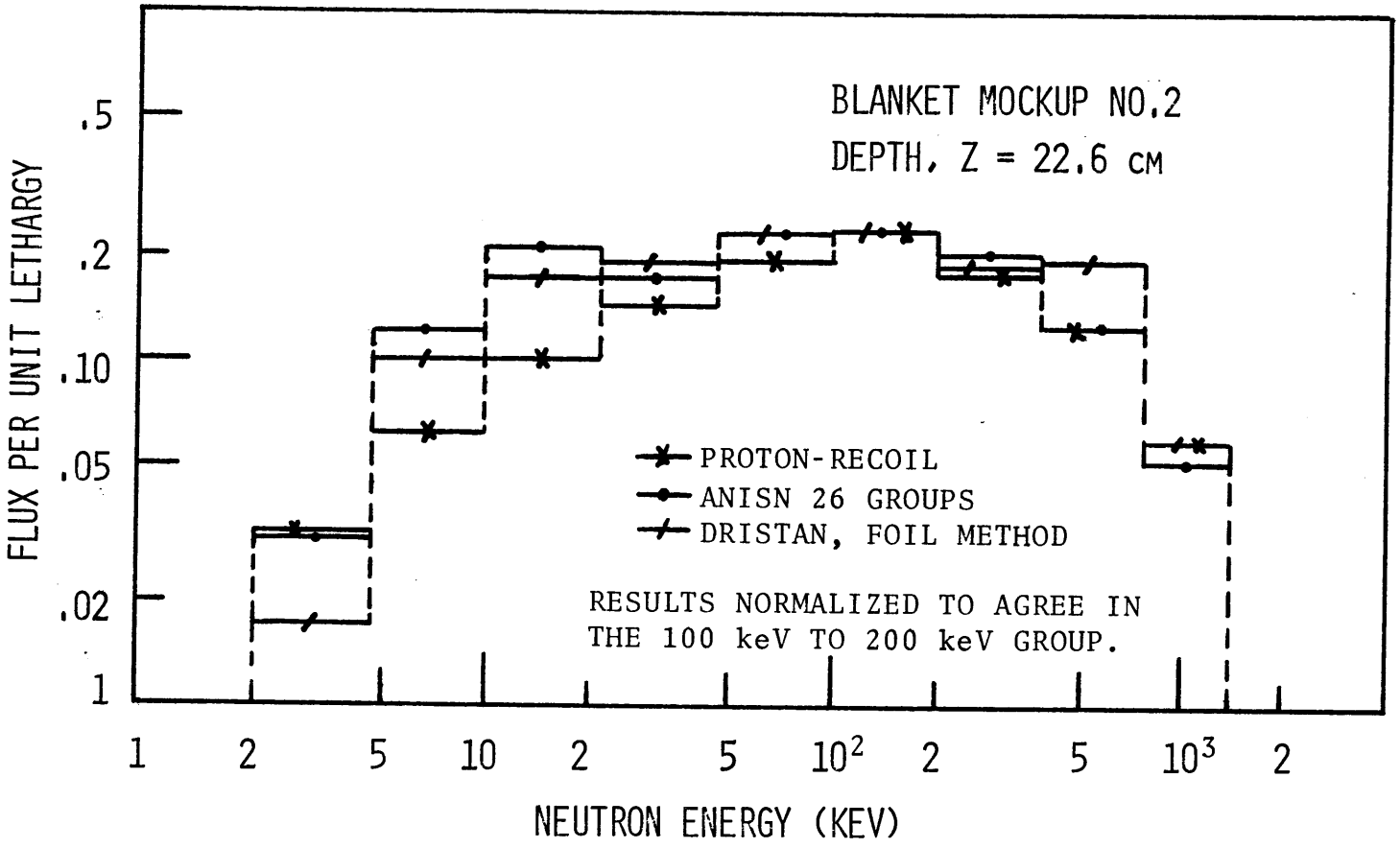

FIG. 5.4 COMPARISON OF 26 GROUP RESULTS

Proton-Recoil data into the same group structure. Relatively poor agreement in the low-energy region is observed between the calculated and measured spectrum; the former shows a flatter distribution in the energy region from 5 keV to 100 keV. A likely explanation is that the averaging-out of the iron and chromium scattering resonances involved in the preparation of the 26 group cross section set has contributed errors which lead to overestimation of the neutron flux in that energy region. The good agreement obtained between the different instrumental measurements, however, engenders considerable confidence in the reliability of the experimental results: different combinations of detectors, operating modes and unfolding techniques all gave comparable results.

5.1.3 Comparison with Foil Results

The three-foil experimental data unfolded by Leung with the DRISTAN code (L1) are shown in Fig. 5.4 together with the Proton-Recoil results. The agreement is again poor in the low-energy region. Leung's results are subject to the same source of systematic error in the iron and chromium scattering cross section as the ANISN calculations since his unfolding method is based upon fitting to a smooth slowing down density and extracting the flux through division by $\xi\Sigma_T$. Leung used the ABBN

cross section set to determine $\xi\Sigma_T$, which may explain the consistency of his results with the ANISN calculations using the same cross section set. Foil experiments which include a larger number of foils sensitive in the energy region from 3 keV to 50 keV should be performed to resolve the discrepancy. Leung's unfolding method should also be applied using $\xi\Sigma_T$ values derived from an independent source.

5.1.4 Comparison with Ge(Li) Data

The neutron spectrum above 0.8 MeV leaking from Blanket Mockup No. 2 was measured by C.S. Kang (K1) using a Ge(Li) crystal and a novel approach based on gamma line broadening. His results and the measurements from the Li-6 Sum Method are compared in Fig. 5.5. There is relatively good agreement between the experimental results.

5.1.5 Comparison with ZPPR-2-Core-Neutron Spectrum

The converter lattice (see section 1.4), that provides the fast neutron spectrum to drive Blanket Mockup No. 2, was designed (F1) to achieve a neutron leakage spectrum similar to that of the ZPPR-2-Core. Figure 5.6 shows the ZPPR-2-Core-Neutron Spectrum (K3) and the Blanket Mockup No. 2 neutron spectrum, both measured with Proton-Recoil proportional counters. The experimental results were collapsed into the same group structure. Both neutron spectra have a similar shape, but the Blanket Mockup No. 2

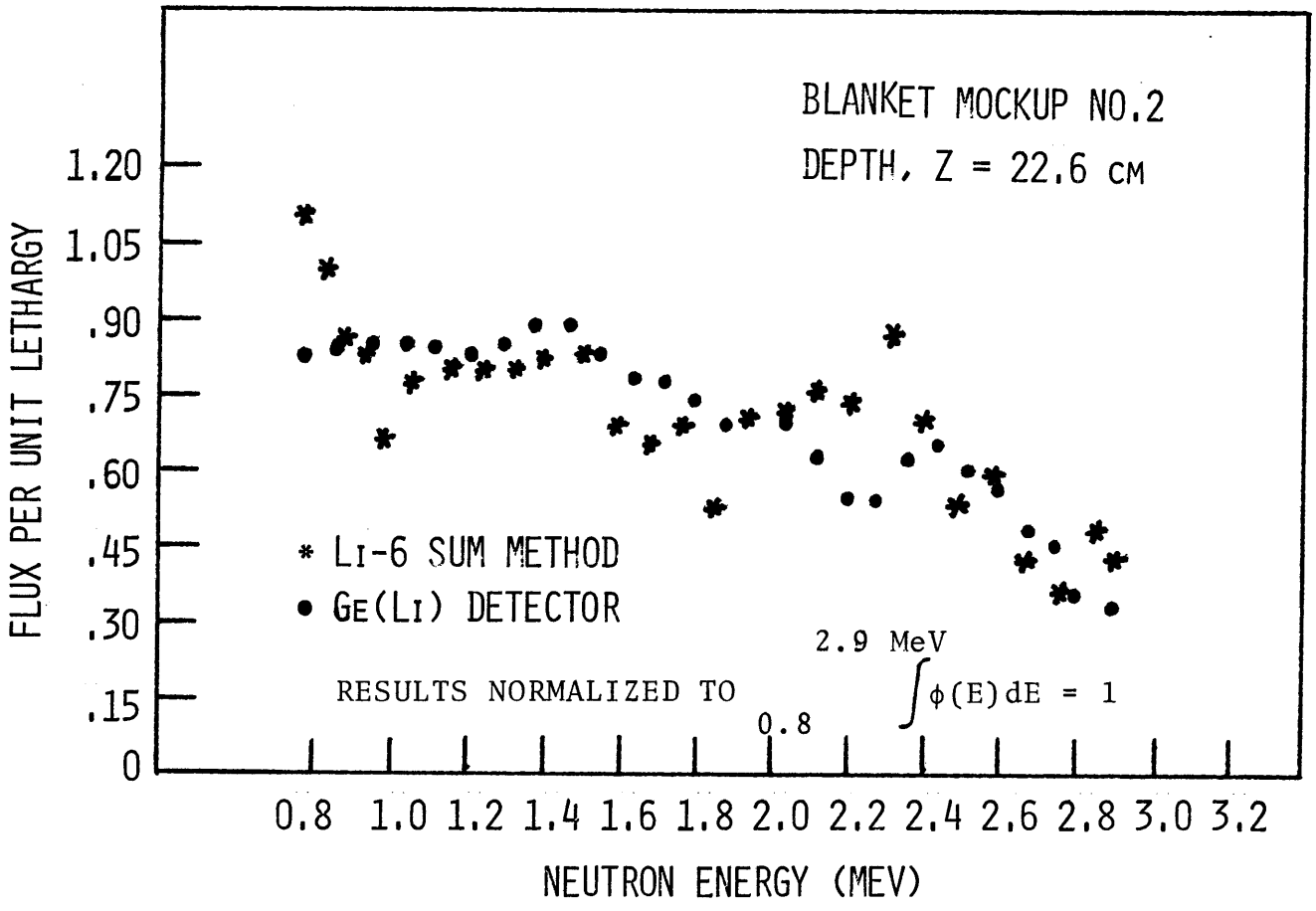

FIG. 5.5 COMPARISON OF NEUTRON SPECTRA FOR Li-6 SUM METHOD AND GE(Li) DETECTOR

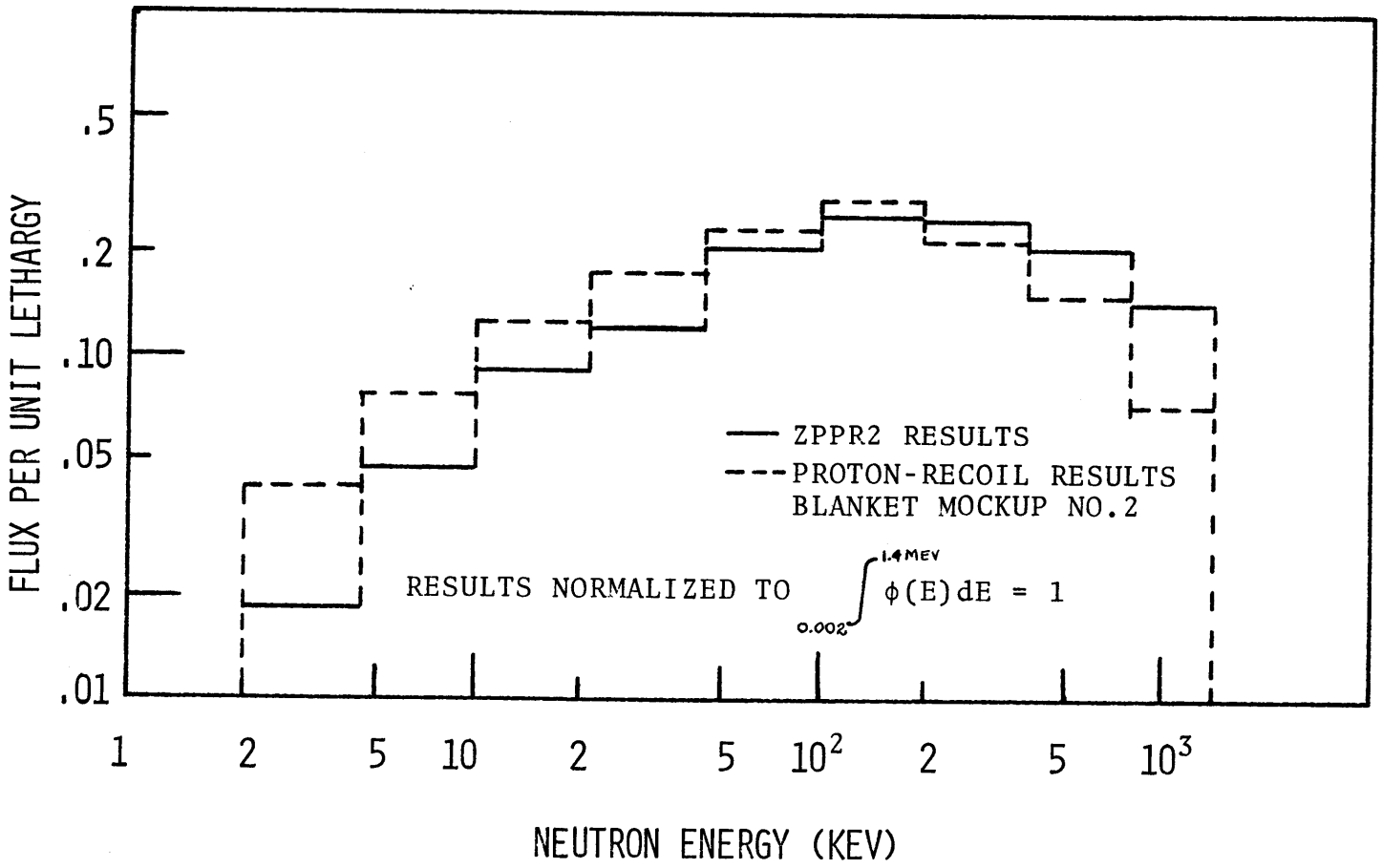

FIG. 5.6 COMPARISON OF ZPPR-2 AND BLANKET MOCKUP NO. 2 SPECTRA

spectrum is systematically softer, as expected. As shown in Fig. 5.7, the fine-group spectra show the same characteristic signature of the scattering resonances in sodium, iron, chromium and oxygen.

5.2 CONCLUSIONS

In this research several instrumental methods were used to measure fast neutron spectra in a Blanket Mockup simulating a LMFBR blanket. As result of this study the following conclusions were reached:

1. He-3 Semiconductor Detector

This detector can be used to obtain differential neutron spectrum measurements in the energy region from 100 keV to about 1 MeV. Boththe Sum and Difference Methods provided similar results over this energy range. The effect of the energy discriminator setting in the Difference Method adversely affected its sensitivity for measuring the low-energy region. Nevertheless, the Difference Method provided a better signal-to-noise ratio than the Sum Method. This is useful when measuring neutron spectra in the presence of high gamma and noise background.

2. Li-6 Semiconductor Detector

The Li-6 semiconductor detector was used to measure fast neutron spectra in the 10 keV to 3.1 MeV energy region.

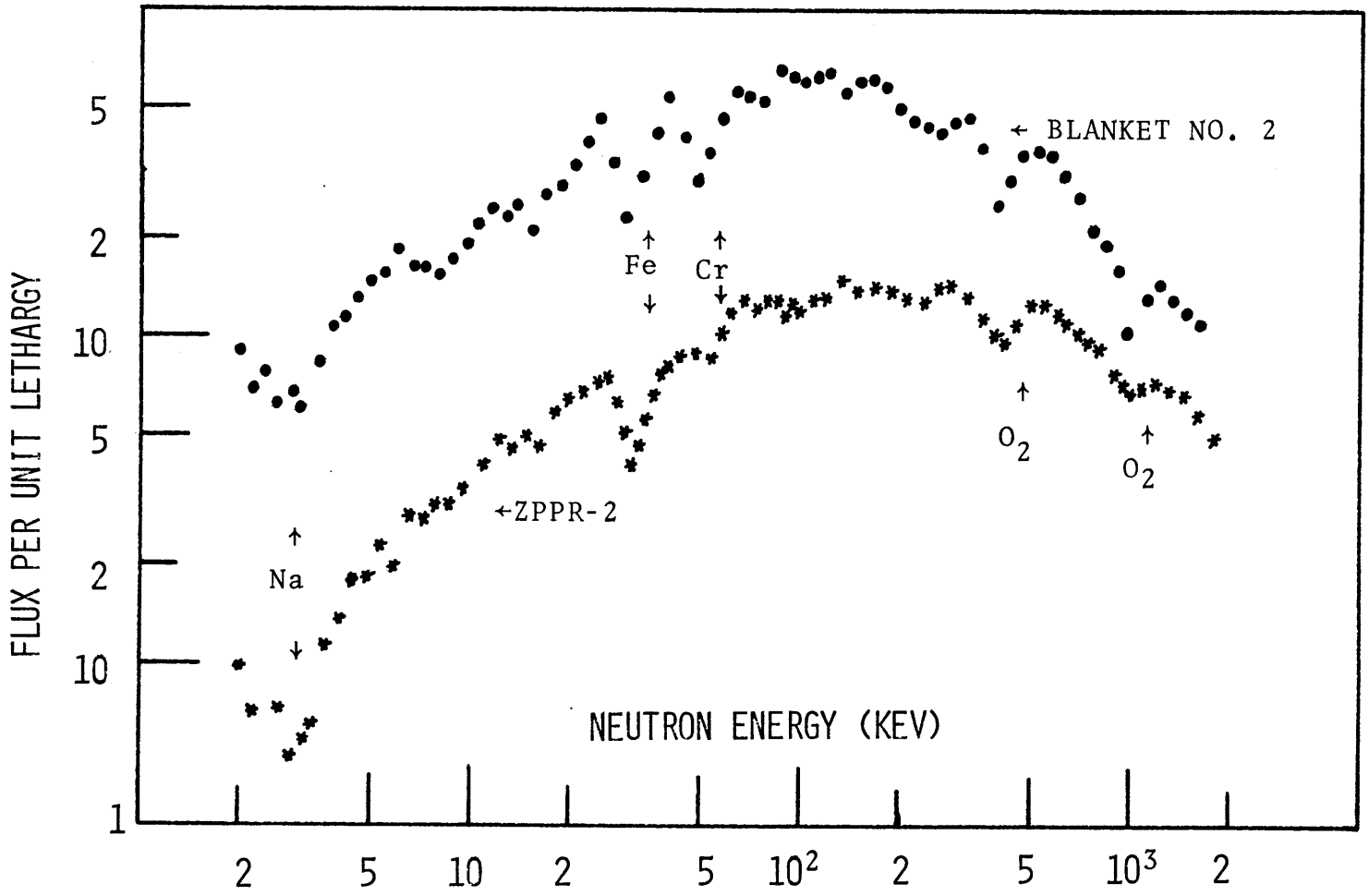

FIG. 5.7 COMPARISON OF ZPPR-2 AND BLANKET MOCKUP NO. 2 FINE-GROUP SPECTRA

Unfolding of the Li-6 detector data consistently showed an anomaly around 250 keV, attributed to the $^{6}Li(n,\alpha)T$-reaction resonance at 250 keV. Because of this a Cf-252 source was used to measure the response function of the detector and then to correct the unfolded neutron spectra. The integral unfolding technique as embodied in the computer code MATRIX is recommended for unfolding the particle spectrum measured with the Li-6 Difference Method. The Li-6 semiconductor showed a better signal-to-background ratio than the He-3 semiconductor detector in all modes of operation, which is attributable to the larger Q value of the governing nuclear reaction.

3. Proton Recoil Proportional Counter

It was possible to measure the neutron spectrum in Blanket Mockup No. 2 from 2 keV to 1.5 MeV using Proton-Recoil proportional counters. These results were in good agreement with the data from the Li-6 system. They are also in good agreement with the He-3 system data in the energy range from 200 keV to 1.1 MeV.

4. Comparison of Results

These is a large (factor of 2) systematic discrepancy between the present results, and the ANISN code numerical calculations or the three-foil experimental data unfolded by the DRISTAN code, in the energy region below 100 keV.

All the instrumental methods showed a neutron spectrum with steeper slope in the energy region from 10 keV to 100 keV than the numerical or foil results. Relatively good agreement was obtained between the present results and the Ge(Li) experimental data in the high-energy region. The measured neutron spectrum is similar in shape to the ZPPR-2-core-neutron spectrum but systematically softer, as expected.

5.3 RECOMMENDATIONS FOR FUTURE WORK

Several recomendations for future work are suggested, based on the experience obtained during this research:

1. A Li-6 semiconductor detector with a thinner ^{6}LiF layer should be obtained to measure the low energy region of the neutron spectrum, operating in the Difference Mode. The use of a thinner ^{6}LiF layer will reduce the energy lost by the alpha particle in the layer, thereby improving the resolution. For example, with a thin (350 Å) ^{6}LiF layer the resolution for the difference energy peak for thermal neutrons will be about 40 keV. This will extend the low energy limit of the measurements to about 1 keV and will allow operation of the detector in three different modes (Sum, Difference, Triton) using essentially the same electronic system. The simplicity of the system makes it atractive and it can compete favorably in many respects

with the more complicated Proton-Recoil system. This detector is recommended for future fast neutron spectrum measurements in the Blanket Test Facility. A difference amplifier that provides a positive output for both positive and negative input signals should be obtained for the Difference Mode of operation.

2. A subroutine to smooth the experimental data from the Li-6 semiconductor detector operating in the Difference Method should be added to the computer code DIFFE. Otherwise the integral unfolding technique should be employed since the present differential method is unreliable.

3. It would be very useful to have a known neutron spectrum to measure the response function of the detectors in the intermediate-energy region. For example, an intense Cf-252 source in a graphite moderator assembly could be employed.

4. A neutron filter will be useful for calibration of Proton-Recoil proportional counters. A strong Cf-252 source in conjuction with appropiate moderators and filters such as iron and scandium (R3) may be a feasible approach.

5. Additional experiments, including use of a larger number of foils and application of improved spectrum-

unfolding codes should be carried out to resolve the discrepancy between the present study and Leung's foil activation results.

6. Calculations of the neutron spectrum should be carried out using newer multigroup cross section sets, and preferably with more groups in the 10 to 100 keV region to resolve the discrepancy between the present results and ANISN 26-group calculations using the ABBN cross section set.

In conclusion, the results from the instrumental methods used in this work are in relatively good agreement and no unexplained behavior was observed in the neutron spectrum measured from 2 keV to 3.1 MeV. This gives confidence in the BTF concept as a valid technique to study mockups of LMFBR blankets.

Appendix A

MATRIX - A PROGRAM TO CALCULATE NEUTRON SPECTRA BY THE DIFFERENCE AND TRITON ANALYSIS TECHNIQUES

A.1 Introduction

In this appendix, the listings are given for the computer program MATRIX. It also contains a description of the format of the input data and output of the program.

MATRIX is a program written in FORTRAN IV language. It will calculate fast neutron spectra from He-3 and Li-6 semiconductor detectors operating in the difference and triton analysis modes. The response matrices are calculated for each technique in separate subroutines. The measured neutron spectrum is unfolded from the experimental results by means of the calculated 50 X 50 response matrix.

A.2 The Difference Technique - He-3 System

The unfolding of the measured spectrum using the difference technique is based on the matrix equation (Eq. 2.71) which relates the measured charged particle spectrum to the incident neutron flux. The program calculates the detector response matrix using Eq. 2.58. It also calculates the transpose of the response function, which is required to solve the problem following the approach presented in section 2.5.8.

The input data for the He-3 case and other variables used in the program are defined in Tables A.1 and A.2. Typical values of the control card data are shown in parenthesis.

A.3 The Difference Technique - Li-6 System

The unfolding of the charged particle spectrum from the $^{6}Li(n,\alpha)T$-reaction is similar to the procedure for the $He^{3}(n,p)T$-reaction described above. Equation 2.48 is used to calculate the response matrix because the reaction is non-isotropic in the center of mass. The differential cross section is based on Eq. 3.4 and is calculated in subroutine THETA2.

The subroutine TRIDIF contains the kinematics equations related to the Li-6 difference technique. It is used to form the difference energy scale and the response matrix.

Table A.3 shows the input card format for the Li-6 case, together with typical values of some key variables.

A.4 The Triton Technique - Li-6 System

The subroutine TRITON is used to unfold the triton spectrum produced by a fast neutron flux incident on a Li-6 semiconductor detector. The subroutine makes use of Eq. 2.5 to calculate the incident neutron energy from the maximum triton energy. It also calculates the differential cross section from Eq. 3.4 and the response matrix based on

TABLE A.1

He-3 Difference Technique

Card	Variable	Format	Description
1	IND	I2	Technique identification: enter 0 for the Li-6 Technique: 1 for the Triton Technique, and -1 for the He-3 difference case.
2	EDISC	E13.4	The discriminator level setting in MeV (eg. 0.150 MeV).
3	RINC	E13.4	This quantity defines the matrix energy scale and is equal to 37 keV.
4	RES	F5.1	The FWHM of the thermal peak in multiples of RINC (eg. 4.0).
5	N	I6	Number of data points (assumed to be identical for both foreground and background). (Typical value 250).
	LSTART	I6	Channel corresponding to difference energy of 382 keV (typical value 2).
6	ENERG.	E12.4	Calibration (eg. 0.00767 MeV/ch).
	EMAX	E12.4	Maximum difference energy (2.00 MeV).
	E0	E12.4	Energy corresponding to first data channel minus 382 keV (-0.00767 MeV for LSTART = 2).

TABLE A.1 (CONT'D)

He-3 Difference Technique

Card	Variable	Format	Description
7	T1	F6.4	Time for which foreground counts were accumulated (80,000 secs.).
	T2	F6.4	Time for which background was accumulated (80,000 secs.).
8	CARDID	18A4	Problem identification.
9[a]...	P(K)	(10X,5F10.0)	(P(K), K = 1, N) Experimental data points (in card form).
	PB(K)	(10X,5F10.0)	(PB(K), K = 1, N) Experimental background data.
10	N	I6	Number of points in the matrix (=50).
11	NIT	I6	Number of maximum iterations (=200).

[a] The number of experimental data points may be as high as 500.

TABLE A.2

Other Variables used in MATRIX

Variable	Description
A(I,J)	Response matrix.
WNU(I)	The transpose of the response matrix times the measured spectrum.
S(I,J)	Measured Spectrum.
SS(I,J)	The transpose of the response matrix times the response matrix.
PN(I)	Difference energy (MeV) of each data point.
RE(I,J)	Resolution matrix.
ERROR(I)	Statistical error associated with the output neutron spectrum.
SIG(I)	Cross Section.
SPECT(I)	Unfolded neutron spectrum.
X(I)	Guess at a solution.
DELMAX(I)	Maximum difference energy.
DELMIN(I)	Minimum difference energy.
DIFF(I)	Difference energy corresponding to each channel.

TABLE A.3

MATRIX Input for Li-6 Difference Technique

Card	Variable	Format	Description
1	IND	I2	Technique identification: 0 for the Li-6 technique.
2	RINC	E13.4	This quantity defines the energy scale increment (.037 MeV). If it is changed, the Li-6 cross section data must also be changed.
6 to 7	BO(I)	10F7.3	BO(I), I = 1, N. BO is the $^{6}Li(n,\alpha)T$-cross section value.
8 to 12	BI(I)	10F7.3	BI(I), I = 1, N.
13 to 17	B2(I)	10F7.3	B2(I), I = 1, N. B1 and B2 are the values of the coefficients in the second order Legendre polynomial expansion of the differential cross section. (see Eq. 3.4 of Chapter 3).
18	RES	F5.1	RES is the FWHM of the thermal peak in multiple of RINC (typical value 6.7).
19	N	I6	Number of data points (eg. 125).
	LSTART	I6	Channel corresponding to difference energy of 687 keV (3).

TABLE A.3 (CONT'D)

MATRIX Input for Li-6 Difference Technique

Card	Variable	Format	Description
20	ENERG	3E12.4	Energy per channel (0.0174 MeV/ch).
	EMAX		Maximum difference energy (2.00 MeV).
	EO		Energy corresponding to first data channel -0.682 MeV (-0.0348 MeV/ch).
21	T1,T2	2F6.4	Time for which foreground counts were accumulated. (86,000 secs.). Time for which background was accumulated (86,000 secs.).
22	CARDID	18A4	Data Identification.
23	P(I)	10X,5F10.0	Experimental data points (in card form).
24	CARDID	18A4	Data Identification.
25	PB(I)	10X,5F10.0	Experimental background data.
26	N	I6	Number of points in the matrix (50).
27	NIT	I6	Maximum number of iterations (200).

Eq. 2.48. The thermal neutron peak (2.732 MeV) is used as the base energy for the formation of the detector response matrix. It is possible to form the matrix in terms of maximum triton energy to produce a diagonal matrix.

The input data requirements are shown in Table A.4. Other subroutines of the MATRIX program are described briefly in Table A.5.

The output of the program consists of 50 neutron flux points and associated statistical error.

TABLE A.4

MATRİX Input for Triton Technique

Card	Variable	Format	Description
1	IND	I2	Technique identification: enter 1 for the triton technique.
2 to 6	BO(I)	10F7.3	BO is the $^{6}Li(n,\alpha)T$-cross section value.
	B1(I)	10F7.3	B1 and B2 are the values of the coefficients in second order Legendre
	B2(I)	10F7.3	polynomial expansion.
17	RES	F5.1	The FWHM of the triton peak obtained with thermal neutrons (4).
18	N,LSTART	2I6	N = Number of data points. (110.) LSTART = Channel corresponding to triton energy of 2.732 MeV (1).
19	ENERG,	3E12.4	Energy per channel (0.0214 MeV/ch).
	EMAX,		Maximum triton energy.
	EO		Energy corresponding to first data channel -2.732 MeV (0.0).
20	T1,T2	2F6.4	T1 = Time for which foreground was accumulated (86,000 secs.). T2 = Time for which background was accumulated (86,000 secs.)

TABLE A.4 (CONT'D)

MATRIX Input for Triton Technique

Card	Variable	Format	Description
21	CARDID	18A4	Data Identification.
22	P(I)	10X,5F10.0	Experimental data points.
23	CARDID	18A4	Data Identification.
24	PB(I)	10X,5F10.0	Experimental background data.
25	N	I6	Number of points (NXN) in the matrix (50).
26	NIT	I6	Maximum number of iterations (200).

TABLE A.5

Other Subroutines in the MATRIX Program

Subroutine Name	Description
MATSYM	Forms the transpose of the response function. It also calculates the product of the transpose of the response function times the measured spectrum, and the product of the transpose of the response function times the response function.
DATAIN	Reads the input data. It also subtracts the background from the foreground and calculates the energies of the rows in the response matrix.
FOLD	Forms the normalized matrix using a gaussian resolution function. It also folds the detector response matrix with the resolution matrix.
THETA 2	Calculates the differential cross section for the $^{6}L_{i}(n,\alpha)T$-reaction.

```
C--------PROGRAM TO  ANALYZE EXPERIMENTAL DATA ---------
C--------FROM HE-3 AND LI-6 DETECTOR ---------
C--------OPERATING IN THE DIFFERENCE AND TRITON METHOD ---------
      DIMENSION PHI(50),SIG(50),DIST(50),SS(50,50),X(50),X1(50),WNU(50)
      DIMENSION FF(50)
      DIMENSION ERROR(50)
      DIMENSION W(50),R(50),SUMN(50),SPECT(50)
      DIMENSION EN(50),DELMAX(50),DELMIN(50),DIFF(50),A(50,50)
      DIMENSION DELT(50),A1(50),A2(50)
      COMMON A,SS,WNU,DIST,EN,DELT,SIG
      DOUBLE PRECISION SUM,SUM1,R,X
      DOUBLE PRECISION SIG
    1 FORMAT (1H1,1X,'RESPONSE FUNCTION OF THE DETECTOR')
    3 FORMAT (3(/),1X,'K=',I3)
   21 FORMAT (6E12.5)
      READ(5,1001)IND
 1001 FORMAT(I2)
      IF(IND)1002,1003,1000
 1002 CONTINUE
      FACT=1.00
      DO 90 L=1,50
      DO 91 K=1,50
      A(K,L)=0.0
   91 CONTINUE
   90 CONTINUE
      READ(5,81)EDISC
      READ(5,81)RINC
   81 FORMAT(E13.4)
      DO 77 K=1,50
      S=K
   77 DELMAX(K)=0.382+S*RINC
      DO 78 K=1,50
      EN(K)=DELMAX(K)-0.764+2.*EDISC
      ENGE=-(DELMAX(K)+0.764)/2.+0.5*SQRT(9.*DELMAX(K)**2+3.*0.764**2-6.
     X*DELMAX(K)*0.764)
      IF(EN(K).LT.0.0)GO TO 80
```

```
      FF(K)=1.0
      GO TO 1500
   80 FF(K)=(DELMAX(K)+0.764+2.*EN(K))/(4.*DELMAX(K)-2.*0.764-EN(K))
      EN(K)=ENGE
 1500 CONTINUE
   78 CONTINUE
      DO 79 K=1,50
      RI=0.75*SQRT(EN(K)*(EN(K)+1.3333*0.764))
      DELMIN(K)=0.382+EN(K)/4.-RI
      DMIN=2.*EDISC-EN(K)-0.764
      IF(DELMIN(K).LT.DMIN)DELMIN(K)=DMIN
      IF(DELMIN(K)+0.382)85,84,84
   84 CONTINUE
      DO 79 L=1,K
      T=1.0
      CALL THETA(EN(K),L,FACT,T,RINC)
   79 A(K,L)=(1./(2.*RI))*FACT
      GO TO 97
   85 DO 86 M=K,50
      RI=0.75*SQRT(EN(M)*(EN(M)+1.3333*0.764))
      DELMIN(M)=0.382+EN(M)/4.-RI
      DMIN=2.*EDISC-EN(M)-0.764
      IF(DELMIN(M).LT.DMIN)DELMIN(M)=DMIN
      J=(-0.382-DELMIN(M))/RINC
      DO 87 L=1,M
      T=1.0
      CALL THETA(EN(M),L,FACT,T,RINC)
   87 A(M,L)=(1./(2.*RI))*FACT
      IF(J)88,88,89
   88 J=1
   89 DO 71 L=1,J
      T=-1.0
      CALL THETA(EN(M),L,FACT,T,RINC)
   71 A(M,L)=A(M,L)+(1./(2.*RI))*FACT
   86 CONTINUE
   97 CONTINUE
```

```
      DO 82 K=1,50
   82 DELT(K)=DELMAX(K)-0.382
      CALL FOLD
      DO 121 K=1,50
      SIG(K)=0.199538E01-0.359164E01*EN(K)+0.370455E01*EN(K)**2
     X-0.167006E01*EN(K)**3+0.356273E00*EN(K)**4-0.353941E-01*EN(K)**5
     Y+0.131039E-02*EN(K)**6
  121 CONTINUE
      GO TO 250
 1003 CALL TRIDIF(A,EN,FF,DELT,SIG)
      CALL FOLD
      DO 1005 K=1,50
 1005 FF(K)=0.070+0.495*(0.978*EN(K)+2.732)/SQRT(0.489*EN(K)**2+
     X2.732*EN(K))
      GO TO 250
 1000 CALL TRITON(A,EN,FF,DELT,SIG)
      CALL FOLD
  250 WRITE (6,1)
      DO 20 K=1,50
      WRITE (6,3) K
      WRITE(6,21)(A(K,J),J=1,50)
   20 CONTINUE
      DO 120 K=1,50
      PHI(K)=(EN(K)**0.5)*(EXP(-EN(K)/1.39))
  120 CONTINUE
      SUM=0.0
      DO 117 K=1,50
      SUM=SUM+PHI(K)
  117 CONTINUE
      DO 118 K=1,50
  118 PHI(K)=(PHI(K)/SUM)*1.0E05/FF(K)
C-------TO  CALCULATE  DISTRIBUTION------
   51 FORMAT(2E13.4)
      DO 101 K=1,50
      DIST(K)=0.0
      DO 102 L=1,50
```

```
      DIST(K)=DIST(K)+A(L,K)*PHI(L)*SIG(L)
  102 CONTINUE
  101 CONTINUE
  500 CALL DATAIN
      DO 600 K=1,50
      DO 600 L=1,50
  600 SS(K,L)=A(L,K)
      DO 601 K=1,50
      DO 601 L=1,50
  601 A(L,K)=SS(L,K)
      WRITE(6,322)
  322 FORMAT (3(/),1X,'FOLDED DISTRIBUTION')
      WRITE(6,105)(DIST(K),K=1,50)
  105 FORMAT (6E12.5)
      DO 83 K=1,50
      WNU(K)=DIST(K)
      DO 83 L=1,50
   83 SS(L,K)=A(L,K)
      CALL MATSYM
C-------FORM  BOUND  FOR  ARRESTING  CRITREION----------
      BND=0.0
      DO 100 I=1,50
      ERR=1./SQRT(WNU(I))
  100 BND=BND+(ERR*WNU(I))**2
      IT=1
      READ(5,122)NIT
  122 FORMAT(I6)
      DO 106 K=1,50
      S=K
  106 X1(K)=DIST(K)
       L=0
  705 L=L+1
      IF(L.GT.50)GO TO 706
      IF(WNU(L).LT.1.0E-06)GO TO 707
      GO TO 705
  706 L=50
```

```
      GO TO 708
  707 L=L-1
  708 CONTINUE
C
  190 CONTINUE
C
  220 SUM1=0.0
      DO 240 I=1,L
      SUM=0.0
      DO 230 J=1,50
  230 SUM=SUM+SS(I,J)*X1(J)
      X(I)=X1(I)*WNU(I)/SUM
      W(I)=SUM
      R(I)=WNU(I)-W(I)
      SUM1=SUM1+R(I)*R(I)
  240 SUMN(I)=SUM1
      WRITE(6,321)IT
      IF(SUMN(L)-BND)270,270,280
  280 CONTINUE
  321 FORMAT(2X,13HITERATION NO.,I3)
  320 FORMAT(I6,4E15.4)
  340 IT=IT+1
      IF(IT-NIT)350,350,370
  350 DO 360 I=1,L
  360 X1(I)=X(I)
      GO TO 190
  270 WRITE(6,281)
  281 FORMAT(1X,29HARRESTING CONDITION SATISFIED)
      WRITE(6,282)IT,BND
  282 FORMAT(1X,13HITERATION NO.,I3,6HBOUND=,E13.5)
  370 CONTINUE
      DO 371 I=1,L
      SPECT(I)=X(I)/SIG(I)
      ERROR(I)=(R(I)/DIST(I))*100.
      SPECT(I)=EN(I)*SPECT(I)
      SPECT(I)=SPECT(I)*FF(I)
```

```
      PHI(I)=EN(I)*PHI(I)
      PHI(I)=PHI(I)*FF(I)
  371 CONTINUE
      WRITE (6,374)
      DO 372 I=1,L
  372 WRITE (6,373) EN(I),PHI(I),SPECT(I)
  373 FORMAT(3E15.4)
  374 FORMAT (1H1,2X'NEUTRON ENERGY',2X,'FISSION SPECT',2X,'NEUTRON FLUX
     X')
      CALL EXIT
      END
      SUBROUTINE MATSYM
      DIMENSION ST(50,50)
      COMMON A(50,50),SS(50,50),WNU(50),DIST(50),EN(50),DELT(50),SIG(50)
      READ(5,8)N
    8 FORMAT(I6)
      DO 1 J=1,50
      DO 1 I=1,50
    1 ST(J,I)=A(I,J)
C
C-----FORM  WNU=ST*DIST----------
C
      DO 2 I=1,N
      SUM=0.0
      DO 2 J=1,N
      SUM=SUM+ST(I,J)*DIST(J)
    2 WNU(I)=SUM
C
C-------FORM  SS=ST+SME---------
C
      DO 3 I=1,N
      DO 3 J=1,N
      SUM=0.0
      DO 3 L=1,N
      SUM=SUM+ST(I,L)*A(L,J)
    3 SS(I,J)=SUM
```

```
      RETURN
      END
      SUBROUTINE DATAIN
      DIMENSION PB(500),CARDID(2,18)
      DIMENSION PN(500),P(500)
      COMMON A(50,50),SS(50,50),WNU(50),DIST(50),EN(50),DELT(50),SIG(50)
      READ(5,3)N,LSTART
      READ(5,2)ENERG,EMAX,EO
      READ(5,20)T1,T2
      READ (5,22)(CARDID(1,I),I=1,18)
      READ(5,1)(P(K),K=1,N)
      READ (5,22) (CARDID(2,I),I=1,18)
      READ (5,15) (PB(K),K=1,N)
      WRITE (6,23) N,LSTART,ENERG,EO,T1,T2
      WRITE (6,24) (CARDID(1,I),I=1,18)
      WRITE (6,1) (P(K),K=1,N)
      WRITE (6,24) (CARDID(2,I),I=1,18)
      WRITE (6,1) (PB(K),K=1,N)
      DO 21 K=1,N
   21 P(K)=P(K)-PB(K)*T1/T2
      PMAX=0.75*SQRT(EMAX*(EMAX+1.333*0.764))
      PMAX=PMAX+0.382+EMAX/4.
      DO 4 K=1,N
      S=K-1
    4 PN(K)=S*ENERG+EO
      IF(DELT(50)-PN(N))5,5,250
    5 DO ° K=1,50
      L=0
    6 L=L+1
      M=L+LSTART
      IF(PN(L)-DELT(K))6,7,8
    7 DIST(K)=P(M)
      GO TO 9
    8 IF(M)10,10,11
   10 DIST(K)=P(M)
      GO TO 9
```

```
 11 J=M-1
    DIST(K)=P(J)+(P(M)-P(J))*(ENERG-PN(L)+DELT(K))/ENERG
  9 CONTINUE
    GO TO 13
250 WRITE(6,14)
 14 FORMAT (1X,'SCALE OUT OF RANGE')
 13 CONTINUE
  1 FORMAT (10X,5F10.0)
 22 FORMAT (18A4)
 23 FORMAT  (1H1,3X,'N=',I3,2X,'LSTART=',I3,2X,'ENERG(MEV)=',F7.4,2X,
   X'EO(MEV)=',F7.4,2X,'T1=',F7.4,2X,'T2=',F7.4)
 24 FORMAT (3(/),18A4)
  2 FORMAT(3E12.4)
  3 FORMAT(2I6)
 15 FORMAT (10X,5F10.0)
 20 FORMAT(2F6.4)
    RETURN
    END
    SUBROUTINE THETA(EN,L,FACT,T,SCALE)
    DOUBLE PRECISION C1,C2
    IF(EN-1.0)100,100,1
  1 CONTINUE
    C1=0.176137D 02-0.400911D 02*EN+0.306477D 02*EN**2
   X-0.102074D 02*EN**3+0.154656D 01*EN**4-0.864758D-01*EN**5
    C2=0.566733D 01-0.129979D 02*EN+0.111452D 02*EN**2
   X-0.364029D 01*EN**3+0.502874D 00*EN**4-0.232549D-01*EN**5
    IF(T)3,3,2
  2 RIMIT=L*SCALE+0.382
    ANGLE=0.6667*(2.*RIMIT-0.764-EN/2.)/SQRT(EN*(EN+1.333*0.764))
    IF(ANGLE.LT.-1.0.OR.ANGLE.GT.1.0)ANGLE=1.0
    FACTOR=1+C1*ANGLE+C2*ANGLE**2
    FNORM=4.*3.1412*(1.+C2/3.)
    FACTOR=FACTOR/FNORM
    GO TO 101
  3 RIMIT=-L*SCALE-0.382
    ANGLE=0.6667*(2.*RIMIT-0.764-EN/2.)/SQRT(EN*(EN+1.333*0.764))
```

```
      IF(ANGLE.LT.-1.0.OR.ANGLE.GT.1.0)ANGLE=-1.0
      FACTOR=1+C1*ANGLE+C2*ANGLE**2
      FNORM=4.*3.1412*(1.+C2/3.)
      FACTOR=FACTOR/FNORM
      GO TO 101
  100 CONTINUE
      FACTOR=1./(4.*3.1412)
  101 CONTINUE
      FACT=FACTOR
      RETURN
      END
      SUBROUTINE FOLD
      DIMENSION RE(50,50)
      COMMON A(50,50),SS(50,50),WNU(50),DIST(50),EN(50),DELT(50),SIG(50)
      READ(5,6)RES
      WRITE(6,8)RES
    6 FORMAT(F5.1)
    8 FORMAT (3(/),1X,'RESOLUTION=',F5.1)
      DO 1 K=1,50
      S=K
      DO 1 L=1,50
      T=L
      RR=((S-T)/RES)**2
      CONST=2.773
      P=CONST*RR
      IF(P.GT.20.0)GO TO 7
      RE(K,L)=1./EXP(P)
      GO TO 1
    7 RE(K,L)=0.0
    1 CONTINUE
      DO 2 K=1,50
      SUM=0.0
      DO 3 L=1,50
    3 SUM=SUM+RE(K,L)
      DO 4 L=1,50
    4 RE(K,L)=RE(K,L)/SUM
```

```
 2 CONTINUE
   DO 5 I=1,50
   DO 5 J=1,50
   SUM=0.0
   DO 5 L=1,50
   SUM=SUM+A(I,L)*RE(J,L)
 5 SS(I,J)=SUM
   DO 10 I=1,50
   DO 10 J=1,50
10 A(I,J)=SS(I,J)
   RETURN
   END
   SUBROUTINE TRITON(A,EN,FF,ET,SIG)
   DIMENSION FF(50)
   DIMENSION RINT(50)
   DIMENSION BO(50),B1(50),B2(50),SIG(50),EL(200),FACTOR(200)
   DIMENSION FUNC(200),INT(50),PJ(50),A(50,50)
   DIMENSION ET(50),EN(50),ETMIN(50),AEN(50),BEN(50),ANGLE(200)
   DOUBLE PRECISION SIG
   DO 1 K=1,50
   P=K
   ET(K)=2.730+0.020*P
   EN(K)=82.688*ET(K)-175.665-SQRT(2701.125*ET(K)**2-6455.69*ET(K))
 1 EN(K)=EN(K)/27.5625
   SL=SQRT(0.75)
   SM=7.0
   P=SM*1.75
   DO 3 K=1,50
   XO=SQRT(1.0/((1.+4.780/EN(K))*SM-1.0))
   ETMIN(K)=EN(K)*((1.-SL*XO)**2)/(P*XO**2)
   AEN(K)=P*XO/(2.*EN(K)*SL)
   BEN(K)=(1.+(SL**2)*XO**2)/(2.*SL*XC)
 3 CONTINUE
   READ(5,10)(BO(K),K=1,50)
   READ(5,10)(B1(K),K=1,50)
   READ(5,10)(B2(K),K=1,50)
```

```
10 FORMAT(10F7.3)
   WRITE (6,5)
 5 FORMAT (3(/),1X,'LI-6 NEUTRON CROSS SECTION BO COMPONENT')
   WRITE (6,10) (BO(K),K=1,50)
   WRITE (6,6)
 6 FORMAT (3(/),1X,'LI-6 DIFFERENCE CROSS SECTION B1 COMPONENT')
   WRITE (6,23) (B1(K),K=1,50)
   WRITE (6,7)
 7 FORMAT (3(/),1X,'LI-6 DIFFERENCE CROSS SECTION B2 COMPONENT')
   WRITE (6,23) (B2(K),K=1,50)
23 FORMAT (10F7.2)
   DO 11 K=1,50
   SIG(K)=BO(K)*1.0E03
11 BO(K)=(BO(K)/(4.*3.1412))*1.0E03
   DO 25 K=1,50
   DO 25 L=1,50
25 A(K,L)=0.0
   DO 12 K=1,50
   M=2*K+1
   DO 13 L=1,M
   S=L
   EL(L)=S*0.01+2.730
   IF(L-M)15,14,14
14 ANGLE(L)=1.0
   GO TO 16
15 ANGLE(L)=AEN(K)*EL(L)-BEN(K)
16 CONTINUE
   FACTOR(L)=BO(K)+B1(K)*ANGLE(L)+0.5*B2(K)*(3.0*ANGLE(L)**2-1.)
13 FUNC(L)=FACTOR(L)*AEN(K)/2.
   J=1
   MM=M-2
   DO 17 L=1,MM
   N=L+1
   NN=L+2
   RINT(J)=(0.01/3.)*(FUNC(L)+4.*FUNC(N)+FUNC(NN))
   L=NN-1
```

```
17 J=J+1
18 FORMAT(10E12.4)
   DO 19 J=1,K
19 PJ(J)=(RINT(J)/SIG(K))*6.282
20 FORMAT(28HNORMALISED DISTRIBUTION ROW=,I3)
21 FORMAT(10E12.4)
   DO 22 L=1,K
22 A(K,L)=PJ(L)
12 CONTINUE
   DO 50 K=1,50
50 FF(K)=0.535+0.495*(0.489*EN(K)+1.366)/SQRT(0.489*EN(K)**2+
  X2.732*EN(K))
   RETURN
   END
   SUBROUTINE TRIDIF(A,EN,FF,DELT,SIG)
   DIMENSION SIG(50)
   DIMENSION BO(50),B1(50),B2(50)
   DIMENSION DELMAX(50),EN(50),DELMIN(50),A(50,50),DELT(50),FF(50)
   DOUBLE PRECISION SIG
   FACT=1.0
   DO 1 L=1,50
   DO 1 K=1,50
 1 A(K,L)=0.0
   READ(5,2)RINC
 2 FORMAT(E13.4)
   WRITE (6,18) RINC
18 FORMAT (3X,'RINC=',F7.3)
   READ(5,95)(BO(K),K=1,50)
   READ(5,95)(B1(K),K=1,50)
   READ(5,95)(B2(K),K=1,50)
95 FORMAT(10F7.3)
   WRITE (6,19)
19 FORMAT (3(/),3X,'LI-6-NEUTRON CROSS SECTION BO COMPONENT')
   WRITE (6,95) (BO(K),K=1,50)
   WRITE (6,20)
20 FORMAT (3(/),3X,'LI-6-NEUTRON DIFFERENTIAL CROSS SECTION B1 COMP')
```

```
      WRITE (6,98) (B1(K),K=1,50)
      WRITE (6,21)
   21 FORMAT (3(/),3X,'LI-6-NEUTRON DIFF. CROSS SECTION B2 COMP.')
      WRITE (6,98) (B2(K),K=1,50)
   98 FORMAT (10F7.2)
      DO 96 K=1,50
      BO(K)=BO(K)*1.0E03
      SIG(K)=BO(K)
   96 BO(K)=BO(K)/(4.*3.1412)
      DO 3 K=1,50
      S=K
    3 DELMAX(K)=0.684+S*RINC
      DO 4 K=1,50
      EN(K)=-5.4427-0.2951*DELMAX(K)+2.1081*SQRT(7.55380-1.87283*
     XDELMAX(K)+1.917*DELMAX(K)**2)
    4 EN(K)=EN(K)/2.
      P=7.0*1.75
      SL=SQRT(0.75)
      DO 7 K=1,50
      XO=SQRT(1.0/((1.+4.780/EN(K))*7.0-1.0))
      RI=(8.0*EN(K)*SL)/(P*XO)
      SI=(1.-SL*XO)/XO
      DELMIN(K)=(2.*SI**2)*EN(K)/P-EN(K)-4.780
      IF(DELMIN(K)+0.684)8,9,9
    9 CONTINUE
      DO 7 L=1,K
      T=1.0
      CALL THETA2(EN(K),L,FACT,T,RINC,XO,BO(K),B1(K),B2(K))
    7 A(K,L)=(1./(2.*RI))*FACT
      GO TO 97
    8 DO 10 M=K,50
      XO=SQRT(1.0/((1.+4.780/EN(M))*7.0-1.0))
      RI=(8.0*EN(M)*SL)/(P*XO)
      SI=(1.-SL*XO)/XO
      DELMIN(M)=(2.*SI**2)*EN(M)/P-EN(M)-4.780
      I=(-0.684-DELMIN(M))/RINC
```

```
      DO 11 L=1,M
      T=1.0
      CALL THETA2(EN(M),L,FACT,T,RINC,XO,BO(M),B1(M),B2(M))
   11 A(M,L)=(1./(2.*RI))*FACT
      IF(J)12,12,13
   12 J=1
   13 DO 14 L=1,J
      T=-1.0
      CALL THETA2(EN(M),L,FACT,T,RINC,XO,BO(M),B1(M),B2(M))
   14 A(M,L)=A(M,L)+(1./(2.*RI))*FACT
   10 CONTINUE
   97 CONTINUE
      DO 15 K=1,50
   15 DELT(K)=DELMAX(K)-0.684
      RETURN
      END
      SUBROUTINE THETA2(EN,L,FACT,T,SCALE,XO,BO,B1,B2)
      SL=SQRT(0.75)
      SM=7.0
      P=SM*(1.+SL**2)
      A=(P/EN)*XO/(2.*SL)
      B=(1.+(SL*XO)**2)/(2.*SL*XO)
      IF(T)3,3,2
    2 RIMIT=L*SCALE+0.684
      RIMIT=0.5*(RIMIT+EN+4.780)
      ANGLE=A*RIMIT-B
      IF(ANGLE.LT.-1.0.OR.ANGLE.GT.1.0)ANGLE=1.0
      FACTOR=BO+B1*ANGLE+0.5*B2*(3.*ANGLE**2-1.)
      FACTOR=FACTOR/(4.*BO*3.1412)
      GO TO 101
    3 RIMIT=-L*SCALE-0.684
      RIMIT=0.5*(RIMIT+EN+4.780)
      ANGLE=A*RIMIT-B
      IF(ANGLE.LT.-1.0.OR.ANGLE.GT.1.0)ANGLE=-1.0
      FACTOR=BO+B1*ANGLE+0.5*B2*(3.*ANGLE**2-1.)
      FACTOR=FACTOR/(4.*BO*3.1412)
```

```
101 CONTINUE
    FACT=FACTOR
    RETURN
    END
```

Appendix B

SUMMA - A COMPUTER PROGRAM TO CALCULATE NEUTRON SPECTRA USING THE SUM METHOD

This appendix includes a description of the input data and the listing of the computer program SUMMA. The program unfolds the charged particle spectrum obtained from exposing the He-3 or Li-6 semiconductor detector to a fast neutron flux.

SUMMA uses Eq. 2.34 to compute the collision density from the experimental data. The neutron flux is then related to the collision density by Eq. 2.15. The statistical error is calculated using Eq. 2.42.

Table B.1 lists the input data required for the Li-6 case. The input data for the He-3 system is similar to the Li-6 input data and is shown in Table B.2. Since the He-3 cross section is a smooth function of the neutron energy, only two polynomials of fifth order are used to fit the cross section data over the energy region 100 keV to 1.4 MeV, and 1.4 MeV to 3.5 MeV, respectively. Four polynomials of fifth order are used to fit the $^{6}Li(n,\alpha)T$-reaction cross section from 100 keV to 4 MeV.

The output of the program provides the neutron flux

per unit energy and the neutron flux per unit lethargy. A flux point and the statistical error associated with each point, is printed or punched for each input data channel. The output data is also collapsed into the number of groups indicated in the input instruction to facilitate comparisons with multigroup calculations.

TABLE B.1

SUMMA Input for Li-6 Sum Technique

Card	Variable	Format	Description
1	METH	I5	Detector identification: enter 0 for the He-3, 1 for the Li-6.
2	GO,G1,G2 G3,G4,G5	6E12.6	Coefficients of the fifth order polynomial used to fit the cross section data in the energy region from 100 keV to 200 keV.
3	G6,G7,G8 G9,GN,GM	6E12.6	Ibid. 200 keV to 400 keV.
4	CO,C1,C2 C3,C4,C5	6E12.6	Ibid. 400 keV to 1500 keV.
5	PO,P1,P2 P3,P4,P5	6E12.6	Ibid. 1500 keV to 4 MeV.
6	NG	I4	Number of groups into which to collapse the neutron results (e.g. 5).
	EMAX	F6.1	Maximum neutron energy (e.g.4000)
7	GROUP(N)	10F7.1	Group energy limits (e.g. 2500, 1400, 800, 400, 200 keV).
8	CARDID	18A4	Problem identification.
9	INCHAN	I6	Energy corresponding to the lowest channel of the thermal neutron peak used to calculate the response function of the detector (e.g. 342 keV see section 2.4.3).

TABLE B.1 (CONT'D)

SUMMA Input for Li-6 Sum Technique

Card	Variable	Format	Description
	LTCHAN	I4	Energy corresponding to the highest channel of the thermal neutron peak (e.g. 190 keV).
	IN1	I4	Initial data channel of the fast neutron spectrum (e.g. 220)
	LAST	I4	Last data channel of the fast neutron spectrum (e.g. 389).
	SLOPE	E14.7	keV/channel (e.g. 17.66).
	YINT	E14.7	Intercept of the energy axis (e.g. 752 keV).
	IPNCH	I2	>0, Punch-out results on cards <0, No results are to be punched.
	ACTR	F5.2,IX	Ratio of the average reactor power during the foreground and background measurements.
	FWHM	F6.1	Full width half maximum of the thermal neutron peak (e.g. 238 keV).
	DELTA	F6.1	Energy interval for response function calculation (e.g. 20 keV).
	AVOG	3X,E10.4	Number of Li-6 atoms in detector (units of 10^{24} e.g. 0.0001).
10	TIME 1	6X,E11.5	Foreground counting time.
	TIME 2	7X,E11.5	Background counting time.
11	CARDID	18A4	Data Identification.

TABLE B.1 (CONT'D)

SUMMA Input for Li-6 Sum Technique

Card	Variable	Format	Description
12	SPECT(I)	10X,5F10.0	Experimental data (maximum 550).
13	CARDID	18A4	Data Identification.
14	BACKG(I)	10X,5F10.0	Background data.

TABLE B.2

SUMMA Input He-3 Sum Technique

Card	Variable	Format	Description
1	METH	I5	Enter 0 for He-3 detector.
2	GO,G1,G2	6E12.6	Coefficients of the fifth order polynomial used to fit the cross section data in the energy region from 100 keV to 1.4 MeV.
3	G6,G7,G8 G9,GN,GM	6E12.6	Ibid 1.4 MeV to 3.5 MeV.
4 to 12			Same information as on cards 6 to 14 in table D.1.
			Typical values are:
			NG = 5
			EMAX = 1600 keV
			GROUP(N) = 800, 400, 200, 100 keV
			INCHAN = 169 keV
			LTCHAN = 91 keV
			IN1 = 230
			LAST = 549
			SLOPE = 4 keV/ch
			YINT = 91.5 keV
			FWHM = 80 keV
			DELTA = 20 keV
			AVOG = 0.0001

```
C    INCHAN = FIRST CHANNEL OF THE THERMAL NEUTRON SPECTRUM
C    LTCHAN = LAST CHANNEL OF THE THERMAL NEUTRON SPECTRUM
C    IN 1 = INITIAL CHANNNEL OF THE FAST NEUTRON SPECTRUM
C    LAST = LAST CHANNEL OF THE FAST NEUTRON SPECTRUM
C    SLOPE = KEV/CHANNEL     E = SLOPE * CHANNEL + YINT
C    YINT = INTERCEPT IN THE ENERGY AXIS
C    PNCH<0 RESULTS ARE NOT PUNCHED
C    ACTR = ACTIVITY RATIO
C    DELTA= ENERGY INTERVAL (KEV) RESPONSE FUNCTION CALC.
C    SIGMA=STANDARD ERROR OF THE COLLISION DENSITY
C
C     HELIUM 3 AND LITHIUM 6 DETECTOR FOR FAST NEUTRON SPECTROSCOPY
C    RESPONSE FUNCTION AND COLLISION DENSITY CALCULATIONS
C    USING TAYLOR  SERIES EXPANSION
C
      DIMENSION CARDID(4,18),SPECT(550),BACKG(550),ETOT(550),E(550),
     1SIGMA(550),COEF(550),F(550),FLUX(550),GROUP(25)
    1 FORMAT (I5)
    2 FORMAT (10X,5F10.0)
    3 FORMAT (6E12.6)
    4 FORMAT (4X,10F7.0)
    5 FORMAT (18A4)
    6 FORMAT (///18A4)
    7 FORMAT (2X,I4,I4,I4,I4,2E14.7,I2,F5.2,1X,2F6.1)
    8 FORMAT (4X,10F6.0)
    9 FORMAT(3(/),3X,'PROGRAM TO PROCESS DATA FROM HELIUM-3 DETECTOR'
     1  /  3X,'A THERMAL NEUTRON SPECTRUM IS USED FOR RESOLUTIONS CORR.'
     2  /  3X,'A TAYLOR SERIES EXPANSION TO CALCULATE DERIVATIVES')
   10 FORMAT (3(/),3X,'THIS PROGRAM IS FOR:')
   11 FORMAT (3(/),3X,'ENERGY CALIBRATION:    ',6HSLOPE=E14.7,3X,
     1    12HY INTERCEPT=E14.7,3X,'FWHM=',F6.1)
   12 FORMAT (3(/),3X,16HINITIAL CHANNEL=I4,3X,13HLAST CHANNEL=I4,3X,
     1  12HACTV. RATIO=F5.2)
   13 FORMAT (3(/),3X,'INPUT DATA')
   14 FORMAT (I4,F6.1)
   15 FORMAT (10F7.1)
```

```
   16 FORMAT (3(/),3X,16HINITIAL CHANNEL=I4,3X,13HLAST CHANNEL=I4)
   17 FORMAT (3(/),3X,11HENERGY(KEV),5X,18HCORRECTED SPECTRUM,
     1    5X,11HTOTAL ERROR,6X,'NEUTRON FLUX',8X,'FLUX LETHARGY')
   18 FORMAT (3X,E10.4,8X,E11.5,10X,E10.4,8X,E11.5,9X,E11.5)
   19 FORMAT (1X,5(E12.6,2X))
   20 FORMAT (1H1,'RESOLUTION USING THERMAL NEUTRON FLUX',/,20X,'A=',
     4E12.5,2X,'B=',E12.5,2X,'C=',E12.5,2X,'D=',E12.5)
   21 FORMAT (1H ,'D1= ',E12.5,2X,'D2=',E12.5,2X,'D3=',E12.5,2X,'D4=',
     5E12.5)
   22 FORMAT (2(/),3X,'GROUP NUM.=',I2,3X,'LOW.LIM.ENERGY',F8.2,3X,
     1'SUM GROUP=',E11.5)
   23 FORMAT (3X,E10.4,6X,E11.5,7X,E11.5)
   24 FORMAT (1H1,3X,'EMAX=',F6.1)
   25 FORMAT (3(/),3X,'ENERGY(KEV)',5X,'NEUTRON FLUX',5X,'FLUX LETHARG')
   26 FORMAT  (3(/),3X,'AVOG.=',E10.4,3X,'TIME1=',E11.5,3X,'TIME2=',
     1E11.5)
   30 FORMAT(3(/),3X,'PROGRAM TO PROCESS DATA FROM LITHIUM-6 DETECTOR'
     1  /  3X,'A THERMAL NEUTRON SPECTRUM IS USED FOR RESOLUTIONS CORR.'
     2  /  3X,'A TAYLOR SERIES EXPANSION TO CALCULATE DERIVATIVES')
C
C    INPUT DATA
C
      READ (5,1) METH
      IF (METH .EQ. 1) GO TO 27
      READ (5,3) G0,G1,G2,G3,G4,G5
      READ (5,3) G6,G7,G8,G9,GN,GM
      WRITE(6,9)
      GO TO 28
   27 READ (5,3) G0,G1,G2,G3,G4,G5
      READ (5,3) G6,G7,G8,G9,GN,GM
      READ (5,3) C0,C1,C2,C3,C4,C5
      READ (5,3) P0,P1,P2,P3,P4,P5
      WRITE (6,30)
   28 READ (5,14) NG,EMAX
      READ (5,15) (GROUP(N),N=1,NG)
      READ (5,5) (CARDID(1,I),I=1,18)
```

```
      READ (5,7) INCHAN,LTCHAN,IN1,LAST,SLOPE,YINT,IPNCH,ACTR,FWHM,DELTA
      READ (5,23) AVOG,TIME1,TIME2
      READ (5,5) (CARDID(3,I),I=1,18)
      READ (5,2) (SPECT(I),I=IN1,LAST)
      READ (5,5) (CARDID(4,I),I=1,18)
      READ (5,2) (BACKG(I),I=IN1,LAST)
C
C   PRINT INPUT DATA
C
      WRITE (6,10)
      WRITE (6,6) (CARDID(1,I),I=1,18)
      WRITE (6,11) SLOPE,YINT,FWHM
      WRITE (6,12) INCHAN,LTCHAN,ACTR
      WRITE (6,26)  AVOG,TIME1,TIME2
      WRITE (6,13)
      WRITE (6,6) (CARDID(3,I),I=1,18)
      WRITE (6,16) IN1,LAST
      WRITE (6,4) (SPECT(I),I=IN1,LAST)
      WRITE (6,6) (CARDID(4,I),I=1,18)
      WRITE (6,16) IN1,LAST
      WRITE (6,4) (BACKG(I),I=IN1,LAST)
C
C     BACKGROUND SUBTRACTION FROM FAST NEUTRON FLUX
C
      DO 101  I=IN1,LAST
      SPECT(I)=((SPECT(I)*ACTR/TIME1)-(BACKG(I)/TIME2))/AVOG
      IF (SPECT(I)) 102,103,103
  102 SPECT(I)=0.0
  103 ETOT(I)=SLOPE*FLOAT(I)+YINT
      E(I)=ETOT(I)-4780. +125.
      IF (METH .EQ. 0) E(I)=ETOT(I)-764.
  101 CONTINUE
C
C   COEF. OF THE RESPONSE FUNC. THERMAL NEUTRON EXP. THEO. GAUSSIAN DIS.
C
      SIGMM=FWHM/2.35
```

```
      EEA=FLOAT(INCHAN)
      EEB=FLOAT(LTCHAN)
      EA=EEA/(1.414*SIGMM)
      EB=EEB/(1.414*SIGMM)
      EA2=EA**2
      EB2=EB**2
      AB=0.2821
      CF1=EXP(-EA2)
      CF2=EXP(-EB2)
      A=AB*(CF2-CF1)
      B2=0.5*((EB+EA)*A+0.5)-A**2
      B=B2**0.5
      C=((EB2-EA2)*A+AB*(CF1-CF2))/3.
      D=((EB**3+EA**3)*A+3.*AB*(0.886-0.5*(EB*CF2+EA*CF1)))/4.
      D1=A/(2.*DELTA)
      D2=(A**2-B**2)/(2.*DELTA**2)
      D3=(C-6.*A*B**2)/(12.*DELTA**3)
      D4=(-D+8.*A*(C-3.*A*B**2)+6.*(B**4-A**4))/(96.*(DELTA**4))
C
C   RESP. FUNC. CORREC. FOR THE COLLISION DENSITY F(E)
C
      II=IN1+3
      LL=LAST-3
      DO 105 I=II,LL
      F(I)=SPECT(I) +D1*(SPECT(I+1) -SPECT(I-1)) +D2*(SPECT(I+1) -
     12.*SPECT(I) +SPECT(I-1)) +D3*(SPECT(I+2) -2.*SPECT(I+1) +
     22.*SPECT(I-1) -SPECT(I-2)) +D4*(SPECT(I+3) -2.*SPECT(I+2)
     3-SPECT(I+1) +4.*SPECT(I) -SPECT(I-1) -2.*SPECT(I-2) +SPECT(I-3))
      COEF(I-3)=D4
      COEF(I-2)=-D3-2.*D4
      COEF(I-1)=-D1+D2+2.*D3-D4
      COEF(I)=1.-2*D2+4.*D4
      COEF(I+1)=D1+D2-2.*D3-D4
      COEF(I+2)=D3-2.*D4
      COEF(I+3)=D4
      SIGMA(I)=(COEF(I-3)**2*SPECT(I-3) +COEF(I-2)**2*SPECT(I-2)
```

```
     1+COEF(I-1)**2*SPECT(I-1) +COEF(I)**2*SPECT(I) +COEF(I+1)**2
     2*SPECT(I+1) +COEF(I+2)**2*SPECT(I+2) +COEF(I+3)**2*SPECT(I+3))**.5
      IF (METH .EQ. 0) GO TO 206
      IF (E(I) .GT. 200.) GO TO 200
      CRSEC=G0+G1*E(I)+G2*E(I)**2+G3*E(I)**3+G4*E(I)**4+G5*F(I)**5
      GO TO 201
  200 IF (E(I) .GT. 400.) GO TO 204
      CRSEC=G6+G7*E(I)+G8*E(I)**2+G9*E(I)**3+GN*E(I)**4+GM*E(I)**5
      GO TO 201
  204 IF (E(I) .GT. 1500.) GO TO 205
      CRSEC=C0+C1*E(I)+C2*E(I)**2+C3*E(I)**3+C4*E(I)**4+C5*E(I)**5
      GO TO 201
  205 CRSEC=P0+P1*E(I)+P2*E(I)**2+P3*E(I)**3+P4*E(I)**4+P5*E(I)**5
      GO TO 201
  206 IF (E(I) .GT. 1400.) GO TO 207
      CRSEC=G0+G1*E(I)+G2*E(I)**2+G3*E(I)**3+G4*E(I)**4+G5*E(I)**5
      GO TO 201
  207 CRSEC=G6+G7*E(I)+G8*E(I)**2+G9*E(I)**3+GN*E(I)**4+GM*E(I)**5
  201 FLUX(I)=F(I)/CRSEC
      BACKG(I)=FLUX(I)*E(I)
      SIGMA(I)=SIGMA(I)*0.645/FLUX(I)
  105 CONTINUE
C
C   PRINT OR PUNCH RESULTS
C
      WRITE (6,17)
      WRITE (6,18) (E(I),F(I),SIGMA(I),FLUX(I),BACKG(I),I=II,LL)
      IF (IPNCH  .LT. 1) GO TO 106
      WRITE (7,19) (F(I),I=IN1,LAST)
C
C   NORMALIZE DATA TO F(500 KEV) =1.0
C
  106 I=II
  110 IF (E(I)-500.0) 107,108,108
  107 I=I+1
      GO TO 110
```

```
  108 FNORM=FLUX(I)
      FLTNOR=BACKG(I)
      DO 111 I=II,LL
      F(I)=FLUX(I)/FNORM
      BACKG(I)=BACKG(I)/FLTNOR
  111 CONTINUE
      WRITE (6,25)
      WRITE (6,23) (E(I),F(I),BACKG(I),I=II,LL)
C
C   REDUCE DATA TO NG GROUPS
C
      WRITE (6,24) EMAX
      I=LL
      N=1
  120 IF (E(I) .LT. EMAX) GO TO 109
      I=I-1
      GO TO 120
  109 SUMGR=0.0
  112 IF (E(I) .LT. GROUP(N)) GO TO 113
      SUMGR=SUMGR+F(I)
      I=I-1
      IF (I .LT. II) GO TO 115
      GO TO 112
  113 WRITE (6,22) N,GROUP(N),SUMGR
      N=N+1
      IF (N .GT. NG) GO TO 115
      GO TO 109
  115 STOP
      END

C     INPUT DATA LI-6 DETECTOR

    1
 .139432E 01-.230140E-01 .277542E-03-.171219E-05 .547057E-08-.480769E-11
 .203541E 03 .294389E 01-.161714E-01 .426164E-04-.539416E-07 .261197E-10
 .291462E 01-.125093E-01 .232056E-04-.214032E-07 .971599E-11-.173162E-14
```

```
 .122120E 01-.221204E-02 .183114E-05-.748882E-09 .148845E-12-.115125E-16
   5 4000.
  1600.   800.   400.   200.   100.
 EXP. #327  FBF   SPECTRUM LI-6 DET. SUM METHOD
   342 190 220 389 17.661          752.        -1 1.0  238.  20.
    .0001          86000.             86000.
 EXP. #327 FBF SEC. ROW NEUTRON SPEC. LI-6 DET. SUM METHOD
000000022000000455880000046411000004548700000430180000038017
000000022500000335280000027842000002220100000162590000011576
000000023000000085180000007332000C0065400000006029000000 5751
000000023500000052480000004685000000440500000036050000003357
000000024000000026210000002107000000166100000013280000001073
000000024500000008910000000729000000C699000000057000000000560
000000025000000004720000000434000000040700000004170000000343
000000025500000003310000000306000000026200000002550000000226
000000026000000002070000000195000000017500000001570000000176
000000026500000001400000000121000000014500000001120000000106
000000027000000009900000000940000000098000000006500000000091
000000027500000000800000000590000000070000000062000000 0070
000000028000000005300000000680000000069000000006800000000 62
000000028500000000610000000690000000045000000005700000000060
000000029000000000500000000590000000056000000004700000000055
000000029500000000520000000470000000450000000044000000 0051
000000030000000000420000000380000000041000000049000000 0042
000000030500000000450000000500000000042000000035000000 0039
000000031000000000320000000390000000340000000025000000 0027
000000031500000000260000000400000000025000000039000000 0034
000000032000000000320000000210000000031000000032000000 0024
000000032500000000210000000230000000C019000000024000000 0024
000000033000000000280000000290000000030000000001900000 00022
000000033500000000230000000280000000020000000035000000 0023
000000034000000000250000000260000000032000000022000000 0026
000000034500000000250000000210000000021000000021000000 0025
000000035000000000260000000190000000022000000026000000 0020
000000035500000000180000000170000000017000000001900000 0013
000000036000000000120000000110000000010000000024000000 0015
```

```
0000000365000000001800000000110000000010000000001600000000140000000037000000000100000000016000000000500000000100000000050000000375000000001000000000013000000007000000000800000000090000000380000000001100000000110000000011000000008000000000500000000385000000001000000000080000000070000000012000000000500000000
 EXP. #330 FBF SEC. ROW BACKGROUND    LI-6 DET. SUM METHOD
0000000220000000002200000000050000000190000000025000000001200000000225000000002100000000019000000002800000000220000000015000000002300000000021000000000130000000016000000001500000000140000000023500000000170000000013000000001700000000150000000016000000024000000000170000000016000000015000000009000000001200000000245000000002100000000080000000110000000014000000000800000000250000000001400000000090000000014000000008000000000900000000255000000001000000000010000000007000000001100000000100000000260000000000900000000070000000013000000001700000000080000000265000000001000000000010000000001200000000100000000110000000027000000001300000000060000000008000000008000000001000000002750000000008000000000700000000070000000010000000001200000000280000000000400000000070000000090000000040000000012000000002850000000007000000000500000000070000000011000000001100000000290000000000700000000080000000020000000003000000000400000000295000000000400000000050000000007000000004000000000200000003000000001100000000100000000300000000060000000002000000003050000000003000000000600000000030000000020000000004000000031000000000070000000020000000030000000005000000000700000003150000000007000000000800000000050000000020000000080000000320000000000500000000020000000050000000030000000011000000032500000000040000000020000000030000000020000000020000000033000000000040000000020000000040000000020000000020000000033500000000040000000030000000030000000050000000004000000034000000000100000000070000000020000000030000000010000000345000000000500000000020000000010000000050000000001000000003500000000020000000000000000004000000000100000000030000000035500000000010000000030000000010000000020000000003000000003600000000010000000040000000020000000020000000020000000365000000000100000000010000000020000000010000000006
```

```
00000003700000000050000000020000000000000000010000000001
00000003750000000010000000003000000000200000000020000000004
00000003800000000002000000002000000000000000000010000000002
00000003850000000020000000020000000020000000030000000001
```

Appendix C

DIFFE - A COMPUTER PROGRAM TO OBTAIN NEUTRON SPECTRA USING THE DIFFERENCE METHOD (DERIVATIVE TECHNIQUE)

C.1 Introduction

In chapter 2, it was mentioned that the equation that relates the measured spectrum to the incident neutron flux (Eq. 2.67) can be solved by two methods. The first method called the integral method is used in the computer program, MATRIX (Appendix A). The second, called the derivative method, is described in section 2.5.7 and is the basis of the computer program described in this appendix.

The computer program DIFFE is written in Fortran IV language. It will calculate fast neutron spectra from the experimental data obtained from the He-3 or Li-6 semiconductor detectors operating in the difference mode. The output neutron flux per unit lethargy is given for constant energy increments.

C.2 The Difference Method for the He-3 System

First, the program corrects the experimental data using the thermal neutron resolution function of the detector. Then it calculates the neutron energy corresponding to each data channel by means of Eq. 2.59. Finally, it calculates

the neutron flux from the derivative of the measured spectrum using Eqs. 2.69 and 2.70. The slope-taking subroutine is similar to the one used by Bennett in the PSNS program (B5). Corrections for the effect of the discriminator setting and the electronic system on the response function are also included in the program. Table C.1 describes the input data.

C.3 The Difference Method for the Li-6 System

The unfolding for the Li-6 case is similar to the He-3 case discussed above. The main difference involves the anisotropy in the center of mass of the $^{6}Li(n,\alpha)T$-differential cross section. This effect is taken into account with the subroutine THETA1.

As mentioned in Chapter 3 the derivative tehcnique was not successfully employed on the Li-6 data due to its oversensitivity to random errors in both the input data and the Li-6 cross section data.

TABLE C.1

DIFFE Input Data on He-3 System

Card	Variable	Format	Description
1	METH	I6	0: He-3 System 1: Li-6 System
2	GO,G1,G2 G3,G4,G5	6E12.6	Coefficients of the fifth order polynomial used to fit the cross section data in the energy region from 1 keV to 10 keV.
3	G6,G7,G8 G9,GN,GM	6E12.6	Ibid 10 keV to 200 keV.
4	CO,C1,C2 C3,C4,C5	6E12.6	Ibid 200 keV to 1 MeV.
5	PO,P1,P2 P3,P4,P5	6E12.6	Ibid 1 MeV to 4 MeV
6	CARDID	18A4	Problem identification.
7	INCHAN	I6	Energy corresponding to the lowest channel of the thermal neutron peak used to calculate the resolution function of the detector (e.g. 342 keV see sect. 2.43).
	LTCHAN	I4	Energy corresponding to the highest channel of the thermal neutron peak (e.g. 190 keV).
	IN1	I4	Last data channel of the fast neutron spectrum (e.g. 220).

TABLE C.1 (CONT'D)

DIFFE Input Data on He-3 System

Card	Variable	Format	Description
	LAST	I4	Last data channel of the fast neutron spectrum (e.g. 389).
	SLOPE	E14.7	keV/channel (e.g. 17.66).
	YINT	E14.7	Intercept of the energy axis (keV) (e.g. 752 keV).
	IPNCH	E14.7	$\geq$0, Punch-out results into cards. $<$0, No results are to be punched.
	ACTR	F5.2	Ratio of the average reactor power during the foreground and background measurements.
	FWHM	1X,F6.1	Full-width-half-maximum of the thermal neutron peak (e.g. 238 keV).
	DELTA	F6.1	Energy interval for the resolution calculation (e.g. 20 keV).
	EDISC	1X,F5.1	Energy discriminator level (keV) (e.g. 150 keV).
8	AVOG	E12.5	Number of He-3 atoms in the detector (units of 10^{24}) (e.g. 0.0001).
	TIME 1	E12.5	Foreground conting time (e.g. 86400 secs.).
	TIME 2	E12.5	Background counting time (e.g. 86400 secs.).

TABLE C.1 (CONT'D)

DIFFE Input Data on He-3 System

Card	Variable	Format	Description
	DINC	E12.5	Energy increment used to form an energy sequence with fixed fractional spacing (e.g. .01).
	RA	E12.5	Energy-independent slope-taking half-interval factor. Half Interval = RA + RB/$\sqrt{\text{energy}}$ (e.g. 0.05 Ref. B5).
	RB	E12.5	Energy-dependent slope-taking half-interval factor (e.g. .05).
9	CARDID	18A4	Data identification.
10	SPECT(I)	10X,5F10.0	Experimental data points (card form).
11	CARDID	18A4	Background identification.
12	BACKG(I)	10X,5F10.0	Experimental background data.

```
C    HELIUM-3 FAST NEUTRON SPECTROMETER
C    NEUTRON FLUX CALC. USING THE DERIV. OF THE DIFFERENCE SPECTRUM
C
C    INCHAN = FIRST CHANNEL OF THE THERMAL NEUTRON SPECTRUM
C    LTCHAN = LAST CHANNEL OF THE THERMAL NEUTRON SPECTRUM
C    IN 1 = INITIAL CHANNNEL OF THE FAST NEUTRON SPECTRUM
C    LAST = LAST CHANNEL OF THE FAST NEUTRON SPECTRUM
C    SLOPE = KEV/CHANNEL     E = SLOPE * CHANNEL + YINT
C    YINT = INTERCEPT IN THE ENERGY AXIS
C    PNCH<0 RESULTS ARE NOT PUNCHED
C    ACTR = ACTIVITY RATIO
C    DELTA= ENERGY INTERVAL (KEV) RESPONSE FUNCTION CALC.
C    SIGMA=STANDARD ERROR OF THE COLLISION DENSITY
C
      DIMENSION CARDID(4,18),SPECT(350),BACKG(350),EN(350),SIGMA(350),
     1COEF(350),F(350),FLXL1(350),FLXL2(350),ERFL(350),EDEN(350),E(200),
     2FLXMN(350),FLXMC(350)
    1 FORMAT (3(/),3X,'K',2X,'NEUTRON FLUX ',2X,'EDIT ENERGY',2X,'ENERGY
     X GR')
    2 FORMAT (10X,5F10.0)
    3 FORMAT (6E12.6)
    4 FORMAT (4X,10F7.0)
    5 FORMAT (18A4)
    6 FORMAT (///18A4)
    7 FORMAT (2X,I4,I4,I4,I4,2E14.7,I2,F5.2,1X,2F6.1,1X,F5.1)
    8 FORMAT (10X,5F10.0)
    9 FORMAT(3(/),3X,'PROGRAM TO PROCESS DATA FROM HELIUM-3 DETECTOR'
     1   /  3X,'A THERMAL NEUTRON SPECTRUM IS USED FOR RESOLUTIONS CORR.'
     2   /  3X,'THE DERIV. OF THE DIFF. IS USED TO CALC. NEUTRON SPEC.')
   10 FORMAT (3(/),3X,'THIS PROGRAM IS FOR:')
   11 FORMAT (3(/),3X,'ENERGY CALIBRATION:  ',6HSLOPE=E14.7,3X,
     1    12HY INTERCEPT=E14.7,3X,'FWHM=',F6.1,2X,'DISCR. LEVEL=',F5.1)
   12 FORMAT (3(/),3X,16HINITIAL CHANNEL=I4,3X,13HLAST CHANNEL=I4,3X,
     1  12HACTV. RATIO=F5.2)
   13 FORMAT (3(/),3X,'INPUT DATA')
   14 FORMAT (3(/),3X,'N ',2X,'RAW FLUX*PDIF',2X,'EDIT ENERGY',2X,
```

```
     1'FLUX/LTY')
   16 FORMAT (3(/),3X,16HINITIAL CHANNEL=I4,3X,13HLAST CHANNEL=I4)
   17 FORMAT (3(/),3X,'ENERGY(KEV)',5X,'MEASURED SPECTRUM',5X,'CORRECTED
     1SPECTRUM',5X,'TOTAL ERROR')
   18 FORMAT (3X,E10.4,8X,E11.5,11X,E11.5,9X,E10.4)
   23 FORMAT (6E12.5)
   25 FORMAT (3(/),4X,'N',2X,'RAW FLUX/LTY',2X,'EDIT ENERGY',3X,
     1 'FLUX/LTY',3X,'FLUX ERROR')
   26 FORMAT  (3(/),3X,'AVOG.=',E10.4,3X,'TIME1=',E11.5,3X,'TIME2=',
     1E11.5, 'DINC=',E10.4,'RA=',F8.3,'RB=',F8.3)
  400 FORMAT (1X,I3,5E13.4)
  401 FORMAT (1X,I3,3E13.4)
  402 FORMAT (1X,'I=',I3,2X,'RAW FLUX=',E12.4,2X,'E=',E12.4,2X,'FLUX=',
     XE12.4)
C
C    INPUT DATA
C
      READ (5,3) G0,G1,G2,G3,G4,G5
      READ (5,3) G6,G7,G8,G9,GN,GM
      READ (5,3) C0,C1,C2,C3,C4,C5
      READ (5,3) P0,P1,P2,P3,P4,P5
      READ (5,5) (CARDID(1,I),I=1,18)
      READ (5,7) INCHAN,LTCHAN,IN1,LAST,SLOPE,YINT,IPNCH,ACTR,FWHM,DELTA
     1,EDISC
      READ (5,23) AVOG,TIME1,TIME2,DINC,RA,RB
      READ (5,5) (CARDID(3,I),I=1,18)
      LASTMD=LAST - IN1 + 1
      READ (5,8) (SPECT(I),I=1,LASTMD)
      READ (5,5) (CARDID(4,I),I=1,18)
      READ (5,2) (BACKG(I),I=1,LASTMD)
C
C    PRINT INPUT DATA
C
      WRITE(6,9)
      WRITE (6,10)
      WRITE (6,6) (CARDID(1,I),I=1,18)
```

```
      WRITE (6,11) SLOPE,YINT,FWHM,EDISC
      WRITE (6,12) INCHAN,LTCHAN,ACTR
      WRITE (6,26)  AVOG,TIME1,TIME2,DINC,RA,RB
      WRITE (6,13)
      WRITE (6,6) (CARDID(3,I),I=1,18)
      WRITE (6,16) IN1,LAST
      WRITE (6,4) (SPECT(I),I=1,LASTMD)
      WRITE (6,6) (CARDID(4,I),I=1,18)
      WRITE (6,16) IN1,LAST
      WRITE (6,4) (BACKG(I),I=1,LASTMD)
      WRITE (6,1)
C
C   BACKGROUND SUBSTRACTION FROM FAST NEUTRON SPECTRUM
C
      DO 101 I=1,LASTMD
      SPECT(I)=((SPECT(I)*ACTR/TIME1)-(BACKG(I)/TIME2))/(AVOG*SLOPE*0.5)
      IF (SPECT(I)) 102,101,101
  102 SPECT(I)=0.0
  101 CONTINUE
C
C   COEF. OF THE RESPONSE FUNC. THERMAL NEUTRON EXP. THEO. GAUSSIAN DIS.
C
      SIGMM=FWHM/2.35
      EEA=FLOAT(INCHAN)
      EEB=FLOAT(LTCHAN)
      EA=EEA/(1.414*SIGMM)
      EB=EEB/(1.414*SIGMM)
      EA2=EA**2
      EB2=EB**2
      AB=0.2821
      CF1=EXP(-EA2)
      CF2=EXP(-EB2)
      A=AB*(CF2-CF1)
      B2=0.5*((EB+EA)*A+0.5)-A**2
      B=B2**0.5
      C=((EB2-EA2)*A+AB*(CF1-CF2))/3.
```

```
      D=((EB**3+EA**3)*A+3.*AB*(0.886-0.5*(EB*CF2+EA*CF1)))/4.
      D1=A/(2.*DELTA)
      D2=(A**2-B**2)/(2.*DELTA**2)
      D3=(C-6.*A*B**2)/(12.*DELTA**3)
      D4=(-D+8.*A*(C-3.*A*B**2)+6.*(B**4-A**4))/(96.*(DELTA**4))
C
C   RESP. FUNC. CORREC. FOR THE COLLISION DENSITY F(E)
C
      II=4
      LL=LASTMD-3
      DO 105 I=II,LL
      F(I)=SPECT(I) +D1*(SPECT(I+1) -SPECT(I-1)) +D2*(SPECT(I+1) -
     12.*SPECT(I) +SPECT(I-1)) +D3*(SPECT(I+2) -2.*SPECT(I+1) +
     22.*SPECT(I-1) -SPECT(I-2)) +D4*(SPECT(I+3) -2.*SPECT(I+2)
     3-SPECT(I+1) +4.*SPECT(I) -SPECT(I-1) -2.*SPECT(I-2) +SPECT(I-3))
      COEF(I-3)=D4
      COEF(I-2)=-D3-2.*D4
      COEF(I-1)=-D1+D2+2.*D3-D4
      COEF(I)=1.-2*D2+4.*D4
      COEF(I+1)=D1+D2-2.*D3-D4
      COEF(I+2)=D3-2.*D4
      COEF(I+3)=D4
      SIGMA(I)=(COEF(I-3)**2*SPECT(I-3) +COEF(I-2)**2*SPECT(I-2)
     1+COEF(I-1)**2*SPECT(I-1) +COEF(I)**2*SPECT(I) +COEF(I+1)**2
     2*SPECT(I+1) +COEF(I+2)**2*SPECT(I+2) +COEF(I+3)**2*SPECT(I+3))**.5
  105 CONTINUE
      DO 106 I=1,3
      F(I)=SPECT(I)
  106 CONTINUE
      KK=LASTMD-2
      DO 107 I=KK,LASTMD
      F(I)=SPECT(I)
  107 CONTINUE
C
C   FORM CHANNEL ENERGY AND NEUTRON ENERGY DISTRIBUTION
C
```

```
      IF(EN(LASTMD) - TEST1)604,604,605
  605 IF (EN(1)-TEST2)606,28,28
  606 ITEST=LASTMD
  623 IF (EN(ITEST)-TEST1)670,669,669
  669 ITEST=ITEST-1
      GO TO 623
  670 N2=ITEST+1
      ITEST=1
  614 IF (EN(ITEST)-TEST2)615,615,616
  615 ITEST=ITEST+1
      GO TO 614
  616 N1=ITEST-1
C
C  DETERMINE SLOPES AND ERRORS
C
      L=N1
      T1=0.0
      T2=0.0
      T3=0.0
      T4=0.0
      TP1=0.0
      TP3=0.0
      TP5=0.0
  687 T1=T1+EN(L)*F(L)
      T2=T2+EN(L)
      T3=T3+F(L)
      T4=T4+EN(L)**2
      TP1=TP1+EN(L)*SPECT(L)
      TP3=TP3+SPECT(L)
      TP5=TP5+SPECT(L)*EN(L)**2
      L=L+1
      IF(N2-L)688,687,687
  688 T2SQ=T2**2
      V=N2-N1+1
      SLOP1=(T1*V-T2*T3)/(T4*V-T2SQ,
      SLOP2=(TP1*V-T2*TP3)/(T4*V-T2SQ)
```

```
      ERSL=SQRT ((TP5*V*V+TP3*T2SQ-2.*TP1*T2*V)/(SLOPE*TIME1))/(T4*V-
     1T2SQ)*F(N1)/SPECT(N1)
      IF (EDIT .GT. 10.) GO TO 200
      CRSEC=G0+G1*EDIT+G2*EDIT**2+G3*EDIT**3+G4*EDIT**4+G5*EDIT**5
      GO TO 201
  200 IF (EDIT .GT. 200.) GO TO 204
      CRSEC=G6+G7*EDIT+G8*EDIT**2+G9*EDIT**3+GN*EDIT**4+GM*EDIT**5
      GO TO 201
  204 IF (EDIT .GT. 1000.) GO TO 205
      CRSEC=C0+C1*EDIT+C2*EDIT**2+C3*EDIT**3+C4*EDIT**4+C5*EDIT**5
      GO TO 201
  205 CRSEC=P0+P1*EDIT+P2*EDIT**2+P3*EDIT**3+P4*EDIT**4+P5*EDIT**5
  201 COFAC=SQRT(EDIT*(EDIT+1018.67))
      IF (EDIT .GT. ENC) GO TO 202
      PDIF=2./(3.*COFAC)
      GO TO 203
  202 ETDIS=191.+3.*(EDIT+COFAC)/8.-EDISC
      PDIF=2./(3.*ETDIS)
  203 TEMP=1./(PDIF*CRSEC)
C
C  CALCULATE NEUTRON FLUX AND ERRORS
C
      FLXL1(K)=-TEMP*SLOP1
      FLXL2(K)=-TEMP*SLOP2
      ERFL(K)=TEMP*ERSL*EDIT
      FLXMN(K)=PDIF*CRSEC*FLXL1(K)
      FLXMC(K)=PDIF*CRSEC*FLXL2(K)
      EDELTA=382.+0.25*EDIT+0.75*COFAC
      EMIND=0.5*(SQRT(3.*(3.*(EDELTA)**2+1528.*EDELTA+583696.))+EDELTA-
     X 764.)
      WRITE (6,401) K,FLXL2(K),EDIT,EMIND
C
C  CONTRIBUTION FROM HIGH ENERGY NEUTRONS
C
      DO 211 I=1,K
      DUME=EDEN(I)*(RA+RB/SQRT(EDEN(I)))
```

```
      ENC=(764.-4.*EDISC)**2/(12.*EDISC)
      DELM=382.+ENC/4.+0.75*SQRT(ENC*(ENC+1018.67))
      DO 110 I=1,LASTMD
      EDIF=SLOPE*FLOAT(I+INI-1)+YINT
      IF (EDIF .GE. DELM) GO TO 108
      EN(I)=0.5*(SQRT(3.*(3.*EDIF**2-1528.*EDIF+583696.))-EDIF-764.)
      GO TO 110
  108 EN(I)=EDIF+2.*EDISC-764.
  110 CONTINUE
C
C  FORM EDIT ENERGIES HAVING FIXED LOGARITHMIC SPACING
C
      EDEN(1)=EN(LASTMD)/(1.+(RA+RB/SQRT(EN(LASTMD)))*1.01)
      TEST=EN(1)
      DO 50 I=2,LASTMD
      EDEN(I)=EDEN(I-1)/(1.+DINC)
      ED=EDEN(I)
      IF(ED-ED*(RA+RB/SQRT (ED))*1.01-TEST)15,15,50
   50 CONTINUE
   15 NED=I-1
      DO  61 I=1,NED
      ERFL(I)=0.0
      FLXL1(I)=0.0
      FLXL2(I)=0.0
   61 CONTINUE
C
C  DEFINE RANGE OF DATA FOR SLOPE-TAKING
C
  699 K=1
  601 IF(EN(LASTMD) - EDEN(K))602,602,603
  602 K=K+1
      GO TO 601
  604 K=K+1
  603 EDIT=EDEN(K)
      TEST1=EDIT+EDIT*(RA+RB/SQRT (EDIT))
      TEST2=EDIT-EDIT*(RA+RB/SQRT (EDIT))
```

```
      ELIMA=EDEN(I)+DUME
      ELIMI=EDEN(I)-DUME
      IF (EMIND .GT. ELIMA) GO TO 211
      IF (EMIND .LT. ELIMI) GO TO 211
      FLXL1(K)=FLXL1(K)-FLXMN(I)/(PDIF*CRSEC)
      FLXL2(K)=FLXL2(K)-FLXMC(I)/(PDIF*CRSEC)
      WRITE (6,402) I,FLXL2(K),EDEN(I),FLXL1(K)
  211 CONTINUE
      FLXL1(K)=EDIT*FLXL1(K)
      FLXL2(K)=EDIT*FLXL2(K)
      IF (LASTMD-K) 28,28,604
C
C   NORMALIZE DATA TO AREA EQUAL TO ONE
C
   28 SUM=0.0
      DO 300 I=1,NED
      SUM=SUM+FLXL2(I)
  300 CONTINUE
      DO 301 I=1,NED
      BACKG(I)=FLXL2(I)/SUM
  301 CONTINUE
C
C   PRINT RESULTS
C
      WRITE (6,17)
      WRITE (6,18) (EN(I),SPECT(I),F(I),SIGMA(I),I=1,LASTMD)
      WRITE (6,14)
      WRITE (6,401) (I,FLXMN(I),EDEN(I),FLXMC(I),I=1,NED)
      WRITE (6,25)
      WRITE (6,400) (I,FLXL2(I),EDEN(I),FLXL1(I),ERFL(I),BACKG(I),
     1I=1,NED)
      STOP
      END
```

```
C    INCHAN = FIRST CHANNEL OF THE THERMAL NEUTRON SPECTRUM
C    LTCHAN = LAST CHANNEL OF THE THERMAL NEUTRON SPECTRUM
C    IN 1 = INITIAL CHANNNEL OF THE FAST NEUTRON SPECTRUM
C    LAST = LAST CHANNEL OF THE FAST NEUTRON SPECTRUM
C    SLOPE = KEV/CHANNEL     E = SLOPE * CHANNEL + YINT
C    YINT = INTERCEPT IN THE ENERGY AXIS
C    PNCH<0 RESULTS ARE NOT PUNCHED
C    ACTR = ACTIVITY RATIO
C    DELTA= ENERGY INTERVAL (KEV) RESPONSE FUNCTION CALC.
C    SIGMA=STANDARD ERROR OF THE COLLISION DENSITY
C
C   LITHIUM-6 FAST NEUTRON SPECTROMETER
C    NEUTRON FLUX CALC. USING THE DERIV. OF THE DIFFERENCE SPECTRUM
C
      DIMENSION CARDID(4,18),SPECT(350),BACKG(350),EN(350),SIGMA(350),
     1COEF(350),F(350),FLXL1(350),FLXL2(350),ERFL(350),EDEN(350),E(200),
     2FLXMN(350),FLXMC(350)
     1 FORMAT (3(/),3X,'K',2X,'NEUTRON FLUX ',2X,'EDIT ENERGY',2X,'ENERGY
      X GR')
     2 FORMAT (10X,5F10.0)
     3 FORMAT (6E12.6)
     4 FORMAT (4X,10F7.0)
     5 FORMAT (18A4)
     6 FORMAT (///18A4)
     7 FORMAT (2X,I4,I4,I4,I4,2E14.7,I2,F5.2,1X,2F6.1,1X,F5.1)
     8 FORMAT (10X,5F10.0)
     9 FORMAT(3(/),3X,'PROGRAM TO PROCESS DATA FROM HELIUM-3 DETECTOR'
      1  /  3X,'A THERMAL NEUTRON SPECTRUM IS USED FOR RESOLUTIONS CORR.'
      2  /  3X,'THE DERIV. OF THE DIFF. IS USED TO CALC. NEUTRON SPEC.')
    10 FORMAT (3(/),3X,'THIS PROGRAM IS FOR:')
    11 FORMAT (3(/),3X,'ENERGY CALIBRATION:  ',6HSLOPE=E14.7,3X,
     1    12HY INTERCEPT=E14.7,3X,'FWHM=',F6.1,2X,'DISCR. LEVEL=',F5.1)
    12 FORMAT (3(/),3X,16HINITIAL CHANNEL=I4,3X,13HLAST CHANNEL=I4,3X,
     1  12HACTV. RATIO=F5.2)
    13 FORMAT (3(/),3X,'INPUT DATA')
    14 FORMAT (3(/),3X,'N ',2X,'RAW FLUX*PDIF',2X,'EDIT ENERGY',2X,
```

```
     1'FLUX/LTY')
   16 FORMAT (3(/),3X,16HINITIAL CHANNEL=I4,3X,13HLAST CHANNEL=I4)
   17 FORMAT (3(/),3X,'ENERGY(KEV)',5X,'MEASURED SPECTRUM',5X,'CORRECTED
     1SPECTRUM',5X,'TOTAL ERROR')
   18 FORMAT (3X,E10.4,8X,E11.5,11X,E11.5,9X,E10.4)
   23 FORMAT (6E12.5)
   25 FORMAT (3(/),4X,'N',2X,'RAW FLUX/LTY',2X,'EDIT ENERGY',3X,
     1 'FLUX/LTY',3X,'FLUX ERROR')
   26 FORMAT  (3(/),3X,'AVOG.=',E10.4,3X,'TIME1=',E11.5,3X,'TIME2=',
     1E11.5, 'DINC=',E10.4,'RA=',F8.3,'RB=',F8.3)
  400 FORMAT (1X,I3,5E13.4)
  401 FORMAT (1X,I3,3E13.4)
  402 FORMAT (1X,'I=',I3,2X,'RAW FLUX=',E12.4,2X,'E=',E12.4,2X,'FLUX=',
     XE12.4)
C
C    INPUT DATA
C
      READ (5,3) C0,C1,C2,C3,C4,C5
      READ (5,3) G0,G1,G2,G3,G4,G5
      READ (5,3) G6,G7,G8,G9,GN,GM
      READ (5,3) P0,P1,P2,P3,P4,P5
      READ (5,3) Q0,Q1,Q2,Q3,Q4,Q5
      READ (5,3) R0,R1,R2,R3,R4,R5
      READ (5,5) (CARDID(1,I),I=1,18)
      READ (5,7) INCHAN,LTCHAN,IN1,LAST,SLOPE,YINT,IPNCH,ACTR,FWHM,DELTA
     1,EDISC
      READ (5,23) AVOG,TIME1,TIME2,DINC,RA,RB
      READ (5,5) (CARDID(3,I),I=1,18)
      LASTMD=LAST - IN1 + 1
      READ (5,8) (SPECT(I),I=1,LASTMD)
      READ (5,5) (CARDID(4,I),I=1,18)
      READ (5,2) (BACKG(I),I=1,LASTMD)
C
C    PRINT INPUT DATA
C
      WRITE(6,9)
```

```
      WRITE (6,10)
      WRITE (6,6) (CARDID(1,I),I=1,18)
      WRITE (6,11) SLOPE,YINT,FWHM,EDISC
      WRITE (6,12) INCHAN,LTCHAN,ACTR
      WRITE (6,26)  AVOG,TIME1,TIME2,DINC,RA,RB
      WRITE (6,13)
      WRITE (6,6) (CARDID(3,I),I=1,18)
      WRITE (6,16) IN1,LAST
      WRITE (6,4) (SPECT(I),I=1,LASTMD)
      WRITE (6,6) (CARDID(4,I),I=1,18)
      WRITE (6,16) IN1,LAST
      WRITE (6,4) (BACKG(I),I=1,LASTMD)
      WRITE (6,1)
C
C    BACKGROUND SUBSTRACTION FROM FAST NEUTRON SPECTRUM
C
      DO 101 I=1,LASTMD
      SPECT(I)=((SPECT(I)*ACTR/TIME1)-(BACKG(I)/TIME2))/(AVOG*SLOPE*0.5)
      IF (SPECT(I)) 102,101,101
  102 SPECT(I)=0.0
  101 CONTINUE
C
C    COEF. OF THE RESPONSE FUNC. THERMAL NEUTRON EXP. THEO. GAUSSIAN DIS.
C
      SIGMM=FWHM/2.35
      EEA=FLOAT(INCHAN)
      EEB=FLOAT(LTCHAN)
      EA=EEA/(1.414*SIGMM)
      EB=EEB/(1.414*SIGMM)
      EA2=EA**2
      EB2=EB**2
      AB=0.2821
      CF1=EXP(-EA2)
      CF2=EXP(-EB2)
      A=AB*(CF2-CF1)
      B2=0.5*((EB+EA)*A+0.5)-A**2
```

```
      B=B2**0.5
      C=((EB2-EA2)*A+AB*(CF1-CF2))/3.
      D=((EB**3+EA**3)*A+3.*AB*(0.886-0.5*(EB*CF2+EA*CF1)))/4.
      D1=A/(2.*DELTA)
      D2=(A**2-B**2)/(2.*DELTA**2)
      D3=(C-6.*A*B**2)/(12.*DELTA**3)
      D4=(-D+8.*A*(C-3.*A*B**2)+6.*(B**4-A**4))/(96.*(DELTA**4))
C
C   RESP. FUNC. CORREC. FOR THE COLLISION DENSITY F(E)
C
      II=4
      LL=LASTMD-3
      DO 105 I=II,LL
      F(I)=SPECT(I) +D1*(SPECT(I+1) -SPECT(I-1)) +D2*(SPECT(I+1) -
     12.*SPECT(I) +SPECT(I-1)) +D3*(SPECT(I+2) -2.*SPECT(I+1) +
     22.*SPECT(I-1) -SPECT(I-2)) +D4*(SPECT(I+3) -2.*SPECT(I+2)
     3-SPECT(I+1) +4.*SPECT(I) -SPECT(I-1) -2.*SPECT(I-2) +SPECT(I-3))
      COEF(I-3)=D4
      COEF(I-2)=-D3-2.*D4
      COEF(I-1)=-D1+D2+2.*D3-D4
      COEF(I)=1.-2*D2+4.*D4
      COEF(I+1)=D1+D2-2.*D3-D4
      COEF(I+2)=D3-2.*D4
      COEF(I+3)=D4
      SIGMA(I)=(COEF(I-3)**2*SPECT(I-3) +COEF(I-2)**2*SPECT(I-2)
     1+COEF(I-1)**2*SPECT(I-1) +COEF(I)**2*SPECT(I) +COEF(I+1)**2
     2*SPECT(I+1) +COEF(I+2)**2*SPECT(I+2) +COEF(I+3)**2*SPECT(I+3))**.5
  105 CONTINUE
      DO 106 I=1,3
      F(I)=SPECT(I)
  106 CONTINUE
      KK=LASTMD-2
      DO 107 I=KK,LASTMD
      F(I)=SPECT(I)
  107 CONTINUE
C
```

```
C    FORM CHANNEL ENERGY AND NEUTRON ENERGY DISTRIBUTION
C
       Q=4780.
       ALI=SQRT(3.)/7.
       BLI=4./7.
       CLI=3./7.
       A1LI=(4.*ALI**2+2.0*CLI-1.)**2-16.*(ALI**2+CLI)*ALI**2
       DO 110 I=1,LASTMD
       EDIF=SLOPE*FLOAT(I+IN1-1)+YINT
       B1LI=-2.*(EDIF-2.*BLI*Q+Q)*(4.*ALI**2+2.*CLI-1.)-16.*BLI*Q*ALI**2
       C1LI=(EDIF-2.*BLI*Q+Q)**2
       EN(I)=(-B1LI-SQRT(B1LI**2-4.*A1LI*C1LI))/(2.*A1LI)
  110  CONTINUE
C
C   FORM EDIT ENERGIES HAVING FIXED LOGARITHMIC SPACING
C
       EDEN(1)=EN(LASTMD)/(1.+(RA+RB/SQRT(EN(LASTMD)))*1.01)
       TEST=EN(1)
       DO 50 I=2,LASTMD
       EDEN(I)=EDEN(I-1)/(1.+DINC)
       ED=EDEN(I)
       IF(ED-ED*(RA+RB/SQRT (ED))*1.01-TEST)15,15,50
    50 CONTINUE
    15 NED=I-1
       DO  61 I=1,NED
       ERFL(I)=0.0
       FLXL1(I)=0.0
       FLXL2(I)=0.0
    61 CONTINUE
C
C   DEFINE RANGE OF DATA FOR SLOPE-TAKING
C
   699 K=1
   601 IF(EN(LASTMD) - EDEN(K))602,602,603
   602 K=K+1
       GO TO 601
```

```
  604 K=K+1
  603 EDIT=EDEN(K)
      TEST1=EDIT+EDIT*(RA+RB/SQRT (EDIT))
      TEST2=EDIT-EDIT*(RA+RB/SQRT (EDIT))
      IF(EN(LASTMD) - TEST1)604,604,605
  605 IF (EN(1)-TEST2)606,28,28
  606 ITEST=LASTMD
  623 IF (EN(ITEST)-TEST1)670,669,669
  669 ITEST=ITEST-1
      GO TO 623
  670 N2=ITEST+1
      ITEST=1
  614 IF (EN(ITEST)-TEST2)615,615,616
  615 ITEST=ITEST+1
      GO TO 614
  616 N1=ITEST-1
C
C  DETERMINE SLOPES AND ERRORS
C
      L=N1
      T1=0.0
      T2=0.0
      T3=0.0
      T4=0.0
      TP1=0.0
      TP3=0.0
      TP5=0.0
  687 T1=T1+EN(L)*F(L)
      T2=T2+EN(L)
      T3=T3+F(L)
      T4=T4+EN(L)**2
      TP1=TP1+EN(L)*SPECT(L)
      TP3=TP3+SPECT(L)
      TP5=TP5+SPECT(L)*EN(L)**2
      L=L+1
      IF(N2-L)688,687,687
```

```
  688 T2SQ=T2**2
      V=N2-N1+1
      SLOP1=(T1*V-T2*T3)/(T4*V-T2SQ)
      SLOP2=(TP1*V-T2*TP3)/(T4*V-T2SQ)
      ERSL=SQRT ((TP5*V*V+TP3*T2SQ-2.*TP1*T2*V)/(SLOPE*TIME1))/(T4*V-
     1T2SQ)*F(N1)/SPECT(N1)
      IF (EDIT .GT. 10.) GO TO 30
      CRSEC=C0+C1*EDIT+C2*EDIT**2+C3*EDIT**3+C4*EDIT**4+C5*EDIT**5
      GO TO 201
   30 IF (EDIT .GT. 100.) GO TO 200
      CRSEC=G0+G1*EDIT+G2*EDIT**2+G3*EDIT**3+G4*EDIT**4+G5*EDIT**5
      GO TO 201
  200 IF (EDIT .GT. 200.) GO TO 204
      CRSEC=G6+G7*EDIT+G8*EDIT**2+G9*EDIT**3+GN*EDIT**4+GM*EDIT**5
      GO TO 201
  204 IF (EDIT .GT. 400.) GO TO 206
      CRSEC=P0+P1*EDIT+P2*EDIT**2+P3*EDIT**3+P4*EDIT**4+P5*EDIT**5
      GO TO 201
  206 IF (EDIT .GT. 1500.) GO TO 205
      CRSEC=Q0+Q1*EDIT+Q2*EDIT**2+Q3*EDIT**3+Q4*EDIT**4+Q5*EDIT**5
      GO TO 201
  205 CRSEC=R0+R1*EDIT+R2*EDIT**2+R3*EDIT**3+R4*EDIT**4+R5*EDIT**5
  201 COFAC=1.38535*SQRT(EDIT*(EDIT+7.*Q/6.))
      PDIF=2./(3.*COFAC)
      TEMP=1./(PDIF*CRSEC)
C
C  CALCULATE NEUTRON FLUX AND ERRORS
C
      FLXL1(K)=-TEMP*SLOP1
      FLXL2(K)=-TEMP*SLOP2
      ERFL(K)=TEMP*ERSL*EDIT
      FLXMN(K)=PDIF*CRSEC*FLXL1(K)
      FLXMC(K)=PDIF*CRSEC*FLXL2(K)
      EDMN=(4.*ALI**2+2.*CLI-1.)*EDIT+4.*ALI*SQRT(EDIT*((ALI**2+CLI)
     1 *EDIT+BLI*Q))+(2.*BLI-1.)*Q
      B1LI=-2.*(-EDMN-2.*BLI*Q+Q)*(4.*ALI**2+2.*CLI-1.)-16.*BLI*Q*ALI**2
```

```
      C1LI=(-EDMN-2.*BLI*Q+C)**2
      EMIND=(-B1LI-SQRT(B1LI**2-4.*A1LI*C1LI))/(2.*A1LI)
      WRITE (6,401) K,FLXL2(K),EDIT,CRSEC
C
C  CONTRIBUTION FROM HIGH ENERGY NEUTRONS
C
      DO 211 I=1,K
      DUME=EDEN(I)*(RA+RB/SQRT(EDEN(I)))
      ELIMA=EDEN(I)+DUME
      ELIMI=EDEN(I)-DUME
      IF (EMIND .GT. ELIMA) GO TO 211
      IF (EMIND .LT. ELIMI) GO TO 211
      FLXL1(K)=FLXL1(K)-FLXMN(I)/(PDIF*CRSEC)
      FLXL2(K)=FLXL2(K)-FLXMC(I)/(PDIF*CRSEC)
      WRITE (6,402) I,FLXL2(K),EDEN(I),FLXL1(K)
  211 CONTINUE
      SUFLX=0.0
      SUFAC=0.0
C
C     CORRECTION FOR THE ANISOTROPIC OF THE REACTION IN THE C. OF M.
C
      DO 20 I=1,K
      EDDN=EDEN(I)
      CALL THETA1 (CRSEC,ALI,BLI,CLI,Q,EDDN,EDMN,FACTOR)
      IF (FACTOR .LT. 0.0) FACTOR=0.0786
      IF (FLXL1(I) .LT. 0.0) FLXL1(I)=0.0
      SUFAC=SUFAC+FACTOR*FLXL1(I)
      SUFLX=SUFLX+FLXL1(I)
   20 CONTINUE
      FACAVG=SUFAC/SUFLX
      FLXL1(K)=EDIT*FLXL1(K)*FACAVG
      FLXL2(K)=EDIT*FLXL2(K)
      WRITE (6,19) EDIT,FACAVG
   19 FORMAT (37X,'EDIT=',F8.3,2X,'FACAVG=',F7.4)
      IF (LASTMD-K) 28,28,604
C
```

```
C   NORMALIZE DATA TO AREA EQUAL TO ONE
C
   28 SUM=0.0
      DO 300 I=1,NED
      SUM=SUM+FLXL2(I)
  300 CONTINUE
      DO 301 I=1,NED
      BACKG(I)=FLXL2(I)/(EDEN(I)**1.5)
  301 CONTINUE
C
C   PRINT RESULTS
C
      WRITE (6,17)
      WRITE (6,18) (EN(I),SPECT(I),F(I),SIGMA(I),I=1,LASTMD)
      WRITE (6,14)
      WRITE (6,401) (I,FLXMN(I),EDEN(I),FLXMC(I),I=1,NED)
      WRITE (6,25)
      WRITE (6,400) (I,FLXL2(I),EDEN(I),FLXL1(I),ERFL(I),BACKG(I),
     1I=1,NED)
      STOP
      END
      SUBROUTINE THETA1 (CRSEC,ALI,BLI,CLI,Q,EDDN,EDMN,FACTOR)
      DOUBLE PRECISION ACLI,BCLI,COSAVG,B1L,B2L
      SL=SQRT(0.75)
      SM=7.0
      P=SM*(1.+SL**2)
      XO=SQRT(1.0/((1.+4780./EDDN)*7.0-1.0))
      ACLI=(P/EDDN)*XO/(2.*SL)
      BCLI=(1.+(SL*XO)**2)/(2.*SL*XO)
      CRSMB=CRSEC*1.0E 03/(4.*3.1416)
      RIMIT=0.5*(EDMN+EDDN +4780.)
      COSAVG=ACLI*RIMIT-BCLI
      IF(COSAVG.LT.-1.0.OR.COSAVG.GT.1.0)COSAVG=1.0
      B1L=0.0
      IF(EDDN.GT.500.) GO TO  3
      IF(EDDN.GT.230.) GO TO 2
```

```
      B1L=0.361637E 01+0.299759E 00*EDDN-0.332217E-02*EDDN**2
     X +0.123972E-04*EDDN**3+0.958966E-07*EDDN**4-0.369525E-09*EDDN**5
      GO TO 3
    2 B1L=-0.192129E 05+0.296034E 03*EDDN-0.17721E 01*EDDN**2
     X +0.517800E-02*EDDN**3-0.740771E-05*EDDN**4+0.415967E-08*EDDN**5
    3 CONTINUE
      B2L=0.0
      IF (EDDN.GT.250.) GO TO 4
      IF(EDDN.LT.20.) GO TC 5
      B2L=0.270083E 02-0.181831E 01*EDDN+0.449072E-01*EDDN**2
     X-0.456533E-03*EDDN**3+0.203892E-05*EDDN**4-0.315637E-08*EDDN**5
      GO TO 5
    4 B2L=0.187157E 04-0.142100E 02*EDDN +0.428408E-01*EDDN**2
     X-0.634674E-04*EDDN**3 +0.460910E-07*EDDN**4-0.131301E-10*EDDN**5
    5 CONTINUE
      FACTOR=CRSMB+B1L*COSAVG+0.5*B2L*(3.*COSAVG**2-1.0)
      FACTOR =FACTOR/(4.*3.1416*CRSMB)
      RETURN
      END
```

Appendix D

PSNS - A COMPUTER PROGRAM TO UNFOLD NEUTRON SPECTRA FROM PROTON SPECTRA

The Computer program listing in this Appendix is a version of the program written by Bennett (B5). It was re-written in Fortran IV language for the IBM 370 machine of the MIT computer center. The original PSNS was programed in CDC-3600 Fortran. Another important change in the program is consideration of the energy dependence of the ionization function W. The W variation reported in reference (B4) was incorporated in the program to correct the measured proton spectra. This is an improvement over the assumption that it is everywhere constant.

A detail description of the program is presented in reference (B5). Because of minor changes in the input data and for convenience of future users the input data format is included in Table D1.

TABLE D.1

PSNS Input Data

Card	Variable	Format	Description
1	PROB	18A4	Problem identification.
2	MN	I6	Total number of sets in the measurement (10).
	NMET	I6	Number of methane counter sets (3).
	NUC	I6	Number of sets precorrected for all response-function effects (1).
	RA	F6.0	Energy-independent slope-taking half-interval factor (0.05).
	RB	F6.0	Energy-dependent slope-taking half-interval factor (0.05).
	DINC	F6.0	Energy increment used to form an energy sequence with the fixed logarithmic spacing (0.10).
	ELIMIT	E12.5	Energy below which the response function for the methane counter is independent of energy (552.8 keV).
	NP	I6	Option to punch final energies, fluxes, and errors; enter 0 for punch; 1 for no punch.
3	F1	E12.5	Energy cut-off for proton ionization in the methane counter (4.0 keV).

TABLE D.1 (CONT'D)

PSNS Input Data

Card	Variable	Format	Description
	RC1	E12.5	Relative carbon-to-hydrogen atom ratio in the methane counter (0.24).
	RN1	E12.5	Relative nitrogen-to-hydrogen atom ratio for the methane counter (0.01).
	F2	E12.5	Energy cut-off for proton ionization in the hydrogen counter (0.290 keV).
	RC2	E12.5	Carbon-to-hydrogen ratio hydrogen counter (.010).
	RN2	E12.5	Nitrogen-to-hydrogen ratio, hydrogen counter (0.010).
4	CPFT(L,1)	4E16.5	Third-order polynomial coefficients which fit the energy variation of the Legendre amplitudes of the non-Gaussian response function (see Ref. E4).
5	CPFT(L,2)	4E16.5	
6	CPFT(L,3)	4E16.5	
7	CPFT(L,4)	4E16.5	
8	CLHYD(L)	4E16.5	Amplitudes of the four Legendre polynomials that parametrize the non-gaussian response function of the hydrogen counter.

TABLE D.1 (CONT'D)

PSNS Input Data

Card	Variable	Format	Description
9	EFB(I,J)	18A4	Set identifier, voltage, and counter type.
10	INCH(J)	I6	First data channel in the set to be used in the calculation.
	M(J)	I6	Number of data points in the set (50).
	A(J)	E12.E	Energy per channel (12.8 keV).
	C(J)	E12.5	Time (sec) multiplied by hydrogen atom number (units of 10^{24}). (eg. 164.).
11	RAPS(I,J)	10X,5F10.0	Experimental pulse-height spectrum; raw proton spectrum.

```
C      PROGRAM PSNS
C     REVISION OF AUGUST 1967
C     PROTON SPECTRUM TO NEUTRON SPECTRUM
       DIMENSION RAPS(200,11),PRAPS(200,11),CHEN(200,11),EFB(20,18),PROB
      1(18),INCH(20),M(20),A(20),C(20),F(20),RC(20),RN(20),HPCOR(500),
      2FLXL(2,500),ERFL(500),EDEN(500),MNOLL(20),CLHYD(6),CPFT(6,6),INCH
      3A(20)
       COMMON FLXL,ERFL
      1,CLEG(6)
    4 FORMAT(2I6,2E12.5)
  300 FORMAT(4E16.5)
  733 FORMAT(6E12.4)
    2 FORMAT(6E12.5)
   55 FORMAT(///18A4)
  200 FORMAT(1H I6,E17.5,E18.5,E20.5)
   58 FORMAT(3I6,3F6.0,E12.5,I6)
    5 FORMAT(18A4)
   21 FORMAT(1H1 10X28HANL-RP393X (PSNS)  AUG, 1967 )
   22 FORMAT(3(/),3X 48HPROGRAM TO PROCESS PROTON RECOIL DATA FROM
     2  /  3X56HPROPORTIONAL COUNTERS. VARIOUS CORRECTIONS ARE APPLIED
     2  /  3X56HTO REMOVE NON-IDEAL COUNTER RESPONSE EFFECTS AND THE
     1  /  3X46HINCIDENT NEUTRON FLUX SPECTRUM IS DERIVED.      )
   23 FORMAT(3(/),3X20HTHIS PROBLEM IS FOR  )
   24 FORMAT(3(/),3X11HA TOTAL OF I4,2X29HSETS OF DATA (INCLUDING BOTH
     1/ 3X58HVOLTAGE AND COUNTER CHANGES) WERE ACCUMULATED FOR THIS
     2/ 3X22HEXPERIMENT. THE FIRST I4,2X28HSETS REFER TO THE PREDOMINA-
     3/ 3X52HNTLY METHANE COUNTER COVERING THE HIGHER ENERGIES.      )
   25 FORMAT(3(/),3X I4,2X41HSETS (IN ORDER OF DECREASING ENERGY) HAVE
     1/ 3X55HBEEN PRE-CORRECTED FOR ALL NON-IDEAL RESPONSE EFFECTS.  )
  299 FORMAT(3(/),3X46HTHE SPECTRUM COMPUTATION INCREMENT WAS CHOSEN
     4/3X 6HTO BE      F6.3,2X15HLETHARGY UNITS. ///
     1/ 3X38HTHE SLOPE-TAKING HALF INTERVAL USED IS F6.3,2X 4HPLUS /
     6F8.3,2X53HTIMES THE RECIPROCAL SQUARE ROOT OF ENERGY (IN KEV ).
     3 4(/),3X23HA W CUT-OFF ENERGY OF  F6.3, 2X20HKEV  FOR THE METHANE
     1 / 3X13HCOUNTER AND  F6.3, 2X33HKEV  FOR THE HYDROGEN COUNTER HAS
     5 / 3X14HBEEN ASSUMED. /
```

```
     8 3(/),3X54HTHE RATIO OF CARBON TO HYDROGEN IN THE METHANE COUNTER
     7 / 3X 5HWAS  F6.4,2X41HAND THE RATIO OF NITROGEN TO HYDROGEN WAS
     9/3XF6.4,1X45H. THESE RATIOS FOR THE HYDROGEN COUNTER WERE F6.4,
     1 / 3X 5HAND  F6.4,2X13HRESPECTIVELY. )
  26 FORMAT(3(/),3X47HTHE ENERGY LIMIT FOR THE METHANE COUNTER BELOW
     1/ 3X57HWHICH THE RESPONSE FUNCTION IS NOT DEPENDENT UPON ENERGY
     2/3X 4HIS  E12.5,2X42HKEV. THE PREDOMINANTLY HYDROGEN COUNTER IS
     3/ 3X58HNOT USED AT ENERGIES SUFFICIENTLY HIGH TO PERMIT THE
     4/ 3X37HRESPONSE TO BECOME ENERGY DEPENDENT.  )
  27 FORMAT(3(/),3X47HTHE FOUR POLYNOMIAL TERMS USED TO EXPRESS THE
     1/ 3X57HENERGY DEPENDENCE OF THE AMPLITUDE OF THE FOUR LEGENDRE
     2/ 3X57HFUNCTIONS WHICH PARAMETRIZE THE ENERGY DEPENDENT RESPONSE
     3/ 3X37HFUNCTION FOR THE METHANE COUNTER ARE   / )
  16 FORMAT(3(/),3X47HTHE FOUR LEGENDRE FUNCTION AMPLITUDES USED TO
     1/ 3X57HPARAMETRIZE THE RESPONSE FUNCTION FOR THE PREDOMINANTLY
     2/ 3X27HHYDROGEN FILLED COUNTER ARE  / )
  17 FORMAT(6(/),3X33HA SUMMARY OF INPUT DATA FOLLOWS.  / )
 501 FORMAT(1(/),1H 11X28HA(ENERGY(KEV) PER CHANNEL) = 18XE12.3,/1H 11X
     146HC(TIME(SEC) X H-ATOM NO. (10 TO THE 24))     =  E12.3,/ )
 500 FORMAT(18H INITIAL CHANNEL =I4,10X14HFINAL CHANNEL=I4,//(10F10.0))
 100 FORMAT(6(/),3X31HPROGRAM OUTPUT IS LISTED BELOW. 4(/),3X8HCHAN.
     258HCHANNEL ENERGY   RAW PROTON DIST.   CORRECTED PROTON DIST. /)
 400 FORMAT(3(/),2X1HN2X13HRAW FLUX/LTY.2X11HEDIT ENERGY 3X 9HFLUX/LTY.
     13X10HFLUX ERROR 2X12HHEAVY RECOIL//(I4,5E13.4))
  59 FORMAT (10X,5F10.0)
  35 READ (5,5,END=36) (PROB(I),I=1,18)
  37 READ 59,MN,NMET,NUC,RA,RB,DINC,ELIMIT,NP
     READ 2,F1,RC1,RN1,F2,FC2,RN2
     READ 300,((CPFT(L,K),L=1,4),K=1,4)
     READ 300,(CLHYD(L),L=1,4)
     PRINT 21
     PRINT 22
     PRINT 23
     PRINT 5,(PROB(I),I=1,18)
     PRINT 24,MN,NMET
     PRINT 25,NUC
```

```
      PRINT 299,DINC,RA,RP,F1,F2,RC1,RN1,RC2,RN2
      PRINT 26,ELIMIT
      PRINT 27
      PRINT 300,((CPFT(L,K),L=1,4),K=1,4)
      PRINT 16
      PRINT 300,(CLHYD(L),L=1,4)
      PRINT 17
      DO 10 J=1,MN
      READ 5,(EFB(J,K),K=1,18)
      PRINT 55,(EFB(J,K),K=1,18)
      READ 4,INCH(J),M(J),A(J),C(J)
      PRINT 501,A(J),C(J)
      INCHA(J)=INCH(J)
      INCH(J)=1
      MAXCHA =M(J)
      INCHAN=INCH(J)
      READ 59,(RAPS(I,J),I=1,MAXCHA)
      MAXCHE=M(J)+INCHA(J)-1
      PRINT 500,INCHA(J),MAXCHE,(RAPS(I,J),I=INCHAN,MAXCHA)
C
C  FORM CHANNEL ENERGY AND PROTON ENERGY DISTRIBUTION
C
      AA=A(J)
      IF(J-NMET)409,409,411
  409 FF=F1
      GO TO 412
  411 FF=F2
  412 DO 10 I=1,MAXCHA
      CHEN(I,J)=AA*(I+INCHA(J)-1)+FF
      IF (CHEN(I,J) .GT. 10.) GO TO 11
      IF (CHEN(I,J) .LT.  1.) GO TO 11
      ENI=CHEN(I,J)
      W=1.20419 -.362375*ENI +.14061*ENI**2 -2.29243*.01*ENI**3 +1.71742
     X*.001*ENI**4 -4.89125*.00001*ENI**5
      GO TO 10
   11 W=1.0
```

```
   10 RAPS(I,J)=1.C/(C(J)*AA*W)*RAPS(I,J)
C
C    DEFINE MINIMUM  NON-OVERLAPPING LIMITS  (MNOLL(J)) FOR EACH SET
C
      J=1
   63 K=INCH(J)
      IF(J+1-MN)40,40,62
   40 IF(CHEN(K,J)-CHEN(M(J+1),J+1))67,68,68
   67 K=K+1
      IF(K-M(J))40,68,68
   68 MNOLL(J)=K
      J=J+1
      GO TO 63
   62 MNOLL(MN)=INCH(MN)
C
C  RESPONSE FUNCTION INTEGRATION FOR BOTH COUNTER
C  DEPENDENCE ON THE METHANE COUNTER AT HIGHER ENERGIES
C
      DO 170 I=1,MA
      KA=INCH(I)
      KO=M(I)
      DO 170 K=KA,KO
  170 PRAPS(K,I)=RAPS(K,I)
      I=1+NUC
   79 N=M(I)
   90 J=1
      X=0.0
   86 MNLL=MNOLL(J)
      L=M(J)-1
   88 ARG=CHEN(N,I)/CHEN(L,J)
      IF(I-NMET)191,191,192
  192 DO 193 KL=1,4
  193 CLEG(KL)=CLHYD(KL)
      GO TO 194
  191 IF(CHEN(L,J)-ELIMIT)97,98,98
   97 U=ELIMIT
```

```
      GO TO 95
   98 L=CHEN(L,J)
   95 DO 96 KL=1,4
   96 CLEG(KL)=CPFT(1,KL)+U*(CPFT(2,KL)+U*(CPFT(3,KL)+U*(CPFT(4,KL))))
  194 S=(CHEN(L+1,J)-CHEN(L,J))*0.5*(PRAPS(L,J)+PRAPS(L+1,J))/CHEN(L,J)
      DO 99 KL=1,4
   99 X=X+S*CLEG(KL)*PLEG(KL,ARG)
      L=L-1
      IF(I-1)80,93,80
   93 IF(N-M(1))80,84,80
   84 X=0.0
   80 IF(I-J)92,91,92
   92 IF(MNLL-L)88,88,81
   91 IF(N-L)88,88,89
   81 ARG=CHEN(N,I)/CHEN(M(J+1),J+1)
      IF(I-NMET)181,181,182
  182 DO 183 KL=1,4
  183 CLEG(KL)=CLHYD(KL)
      GO TO 184
  181 IF(CHEN(MNLL,J)-ELIMIT)76,83,83
   76 L=ELIMIT
      GO TO 78
   83 U=CHEN(MNLL,J)
   78 DO 71 KL=1,4
   71 CLEG(KL)=CPFT(1,KL)+L*(CPFT(2,KL)+U*(CPFT(3,KL)+U*(CPFT(4,KL))))
  184 S=0.5*(PRAPS(M(J+1),J+1)+PRAPS(MNLL,J))*(CHEN(MNLL,J)-CHEN(M(J+1),
     1J+1))/CHEN(M(J+1),J+1)
      DO 72 KL=1,4
   72 X=X+S*CLEG(KL)*PLEG(KL,ARG)
      J=J+1
      GO TO 86
   89 PRAPS(N,I)=(PAPS(N,I)-X)/(1.-CLEG(1))
      N=N-1
      IF(INCH(I)-N)90,90,77
   77 I=I+1
      IF(I-MN)79,79,14
```

```
C
C  FORM EDIT ENERGIES HAVING FIXED LOGARITHMIC SPACING
C
   14 EDEN(1)=CHEN(M(1),1)/(1.+(RA+RB/SQRT (CHEN(M(1),1)))*1.01)
      TEST=CHEN(INCH(MN),MN)
      DO 50 I=2,500
      EDEN(I)=EDEN(I-1)/(1.+DINC)
      ED=EDEN(I)
      IF(EC-ED*(RA+RB/SQRT (ED))*1.01-TEST)15,15,50
   50 CONTINUE
   15 NED=I-1
      DO 201 I=1,NED
      HPCOR(I)=0.0
      ERFL(I)=0.0
      FLXL(2,I)=0.0
  201 FLXL(1,I)=0.0
C
C  DEFINE RANGE OF DATA FOR SLOPE-TAKING
C
      J=1
  699 K=1
  601 IF(CHEN(M(J),J)-EDEN(K))602,602,603
  602 K=K+1
      GO TO 601
  604 K=K+1
  603 EDIT=EDEN(K)
      TEST1=EDIT+EDIT*(RA+RB/SQRT (EDIT))
      TEST2=EDIT-EDIT*(RA+RB/SQRT (EDIT))
      IF(CHEN(M(J),J)-TEST1)604,604,605
  605 IF(CHEN(INCH(J),J)-TEST2)606,28,28
  606 ITEST=M(J)
  623 IF(CHEN(ITEST,J)-TEST1)670,669,669
  669 ITEST=ITEST-1
      GO TO 623
  670 N2=ITEST+1
      ITEST=INCH(J)
```

```
  614 IF(CHEN(ITEST,J)-TEST2)615,615,616
  615 ITEST=ITEST+1
      GO TO 614
  616 N1=ITEST-1
C
C  DETERMINE SLOPES AND ERRORS
C
      L=N1
      T1=0.0
      T2=0.0
      T3=0.0
      T4=0.0
      TP1=0.0
      TP3=0.0
      TP5=0.0
  687 T1=T1+CHEN(L,J)*PRAPS(L,J)
      T2=T2+CHEN(L,J)
      T3=T3+PRAPS(L,J)
      T4=T4+CHEN(L,J)**2
      TP1=TP1+CHEN(L,J)*RAPS(L,J)
      TP3=TP3+RAPS(L,J)
      TP5=TP5+RAPS(L,J)*CHEN(L,J)**2
      L=L+1
      IF(N2-L)688,687,687
  688 T2SQ=T2**2
      V=N2-N1+1
      SLOP1=(T1*V-T2*T3)/(T4*V-T2SQ)
      SLOP2=(TP1*V-T2*TP3)/(T4*V-T2SQ)
      ERSL=SQRT ((TP5*V*V+TP3*T2SQ-2.*TP1*T2*V)/(C(J)*A(J)))/(T4*V-T2SQ)
     1*PRAPS(N1,J)/RAPS(N1,J)
      SIGE=11010./(EDIT+4041.)+2387./(EDIT+135.5)
      TEMP=EDIT**2/SIGE
C
C  STORE FLUXES AND ERRORS WITH REGARD TO OVERLAP
C
      IF(ERFL(K))38,39,38
```

```
   38 DEN=1./(ERFL(K)**2)+1./((TEMP*ERSL)**2)
      FLXL(1,K)=(FLXL(1,K)/(ERFL(K)**2)-TEMP*SLOP1/((TEMP*ERSL)**2))
     1/DEN
      FLXL(2,K)=(FLXL(2,K)/(ERFL(K)**2)-TEMP*SLOP2/((TEMP*ERSL)**2))
     1/DEN
      ERFL(K)=1./SQRT (DEN)
      GO TO 41
   39 FLXL(1,K)=-TEMP*SLOP1
      FLXL(2,K)=-TEMP*SLOP2
      ERFL(K)=TEMP*ERSL
C
C  CORRECT FOR CARBON AND NITROGEN RECOILS
C
   41 ET=5.*EDIT
      IF(ET-EDEN(1))101,102,102
  101 DO 70 I=1,NED
      IF(ET-EDEN(I))70,70,405
  405 IF(ERFL(I))105,105,401
  401 IF(ERFL(I-1))105,105,103
  103 FEE5=FLXL(1,I-1)+(ET-EDEN(I-1))/(EDEN(I)-EDEN(I-1))*(FLXL(1,I)
     1-FLXL(1,I-1))
      GO TO 105
   70 CONTINUE
  102 FEE5=0.0
  105 IF(J-NMET)402,402,403
  402 RC(1)=RC1
      RN(1)=RN1
      GO TO 404
  403 RC(1)=RC2
      RN(1)=RN2
  404 H=(RC(1)*(5520./(ET+1150.))+RN(1)*(1750./(ET+250.)))/SIGE
      FLXL(1,K)=FLXL(1,K)-H*FEE5
      IF(HPCOR(K))406,406,407
  406 HPCOR(K)=H*FEE5/FLXL(1,K)
      GO TO 604
  407 HPCOR(K)=.5*(HPCOR(K)+H*FEE5/FLXL(1,K))
```

```
      GO TO 604
   28 J=J+1
      IF(J-MN)699,699,29
C
C    DELETE EMPTY DATA LOCATIONS
C
   29 L=1
  506 IF(ERFL(L))503,504,503
  503 L=L+1
      IF(L-NED)506,506,505
  504 NED=NED-1
      DO 502 K=L,NED
      ERFL(K)=ERFL(K+1)
      FLXL(1,K)=FLXL(1,K+1)
      FLXL(2,K)=FLXL(2,K+1)
      HPCOR(K)=HPCOR(K+1)
  502 EDEN(K)=EDEN(K+1)
      GO TO 29
C
C    PRINT AND PUNCH RESULTS
C
  505 PRINT 100
      J=1
   33 I=M(J)
      III=M(J)+INCHA(J)-1
   31 PRINT 200,III,CHEN(I,J),RAPS(I,J),PRAPS(I,J)
      III=III-1
      I=I-1
      IF(I-INCH(J))32,31,31
   32 J=J+1
      IF(MN-J)34,33,33
   34 PRINT 400,(I,FLXL(2,I),EDEN(I),FLXL(1,I),ERFL(I),HPCOR(I),I=1,NED)
      IF(NP)73,73,35
   73 I=1
   74 PRINT 733,EDEN(I),FLXL(1,I),ERFL(I),EDEN(I+1),FLXL(1,I+1),ERFL(I+1
     1)
```

```
      I=I+2
      IF(I-NED)74,75,35
   75 PRINT 733,EDEN(I),FLXL(1,I),ERFL(I)
      GO TO 35
   36 CONTINUE
      END
      FUNCTION PLEG(N,ARG)
      GO TO (1,2,3,4),N
    1 PLEG=1.
      RETURN
    2 PLEG=(2.*ARG-1.)*1.73205
      RETURN
    3 PLEG=(-1.+ARG*(ARG-1.)+1.)*2.23607
      RETURN
    4 PLEG=(-1.+ARG*(12.-ARG*(30.-ARG*20.)))*2.64575
      RETURN
      END
```

Appendix E

REFERENCES

B1 Bame, S.J. and Cobitt, R.C., Phys. Rev. 114, No. 6 (1580-1583) 1959.

B2 Bennett, E.F., Nucl. Sci. and Eng. 27, 28-33 (1967).

B3 Bennett, E.F., Nucl. Sci. and Eng. 27, 16-27 (1967).

B4 Bennett, E.F., and T.J. Yule, ANL-7777, Argonne National Laboratory (1971).

B5 Bennett, E.F., R. Gold and I.K. Olson, ANL-7394, Argonne National Laboratory (1968).

B6 Berger, R. "Lithium 6 Fast Neutron Spectrometry" Center D'Etudes Nucleaires, EURFNR-781, 1969.

B7 Bishop, G.B. Nucl. Instr. and Meth. 62, 247-252 (1968).

B8 Bluhm H. and D. Stegemann, Nucl. Instr. and Meth. 70, 141-150 (1969).

B9 Bluhm H. and D. Stegemann, Nucl. Instr. and Meth. 70, 151-160 (1969).

B10 Brown, W.K., A.N. Ellis and D.D. Peterson, IEEE Trans. Nucl. Sci., 404-409, February, 1967.

B11 Brock and C.E. Anderson, Rev. Sci. Instr. 31, 1063 (1960).

D1 Davey, W.G. and Redman, W.C., "Techniques in Fast Reactor Critical Experiments," Argonne National Laboratory (Gordon and Breach Science Publisher), 1970.

D2 De Guarrini, F. and Malaroda R., Nucl. Instr. and Meth. 92, 277-284 (1971).

D3 Driscoll, M.J. and Leung, T.C., "A Simple Foil Method for LMFBR Spectrum Determination," Trans. Am. Nucl. Soc., Vol. 13, No. 2, November, 1971.

E1 Evans, R.D., "The Atomic Nucleus," McGraw-Hill Book Company, New York (1955).

F1 Forbes, I.A., "Design, Construction and Evaluation of of a Facility for the Simulation of Fast Reactor Blankets," MIT-4105-2, MITNE-110 (February, 1970).

F2 Fowler, J., and L. Marion, Fast Neutron Physics, Part I, Intersciences Pub., Inc., New York (1960).

F3 Furuta Y., S. Kinbara and K. Kaieda, Nucl. Instr. and Meth. 84, 269-274 (1970).

G1 Gold, R., "An Iterative Unfolding Method for Response Matrices," ANL-6984, December, 1964.

G2 Green, L., Nucl. Sci. Eng. 37, 232-242 (1969).

H1 Hodgman, C.D., "C.R.C. Standard Mathematical Tables," Twelfth Edition, 1959.

H2 Hukai, Y., N.C. Rasmussen and M.J. Driscoll, "Some Applications of Ge(Li) Gamma-Ray Spectroscopy to Fuel Element Assay," MITNE-113, MIT-3944-5 (April,1970).

H3 Ho, S.L., "Measurement of Fast and Epithermal Neutron Spectra Using Foil Activation Techniques," S.M. Thesis, Dept. of Nucl. Eng. MIT (January,1970).

I1 Instruction Manual 525 Neutron Spectrometer System, ORTEC.

J1 Jeter, R.T. and M.C. Kennison, IEEE Trans. Nucl. Sci., 422-427, February 1967.

K1 Kang, C.S., "Use of Gamma-Spectroscopy for Neutronic Analysis of LMFBR Blankets," MIT-4105-8, MITNE-130 (January, 1972).

K2 Kuo, Shan S., "Numerical Methods and Computers," Addison-Wesley, Inc. 1965.

L1 Leung, T.C., "Neutronics of an LMFBR Blanket Mockup," MIT-4105-9 MITNE-127, (January, 1972).

L2 LMFBR Blanket Physics Project Progress Report No. 1, MIT-4105-3, MITNE-116 (June, 1970).

M1 Mahaux, C. and Robaye, G., Nucl. Phys. 74, 165-171 (1965).

M2 Maroni, C., Russo, F. and Verondini, E., Nucl. Instr. and Meth. 74, 256-260 (1969).

M3 Meadows, J.W., Phys. Rev. 157, 1076 (1967).

N1 Nereson, N. and F. Reins; Rev. Sci. Instr. 21; 534 (1950).

P1 Price, W.J., Nuclear Radiation Detection, Second Edition McGraw-Hill Book Company, New York (1958).

P2 Passmann, N.A., "An Improved Foil Activation Method for Determination of Fast Neutron Spectra," S.M. Thesis, Dept. of Nucl. Eng., MIT (January, 1971).

R1 Rickard, I.C., Nucl. Instr. and Meth. 82, 287-288 (1970).

R2 Rickard, I.C., PhD Thesis, University of London (1971).

R3 Rogers, J.W., Nucl. Instr. and Meth. 80, 313-340 (1970).

R4 Rybakov and Sidorov, "Fast Neutron Spectroscopy," Consultants Bureau, Inc., New York (1960).

R5 Rydin, R.A., IEEE Trans. Nucl. Sci., 377-392, February, 1967.

S1 Schwartz, S., Stromberg, L.G. and Bergstrom, A., Nucl. Phys. 63, 593-609 (1965).

S2 Silk, M.G., AERE-R5183 (1966).

S3 Silk, M.G., Nucl. Instr. and Meth. 66, 93-101 (1968).

S4 Silk, M.G., and Windsor, M.E., J. Nucl. Eng. 21, 17-33 (1967).

T1 Terrel, J., Phys. Rev. 113, 527 (1959).

T2 Toms, M.E., Nucl. Instr. and Meth. 92, 61-70 (1971).

W1 Windsor, M.E. and Wright, S.B., J. Nucl. Eng. 20, 465 (1966).

W2 Winyard, R.A., Lutkin, J.E. and McBeth, Nucl. Instr. and Meth. 95, 141-153 (1971).

W3 Werle, H., Fieg, G. Seufert H., Stegemann, D., Nucl. Instr. and Meth. 72, 111 (1969).

Y1 Yule, T.J. and Bennett, B.F., Nucl. Sci. and Eng. 46, 236-243 (1971).